# THE INITIAL MASS FUNCTION FOR MASSIVE STARS IN THE MAGELLANIC CLOUDS. III. LUMINOSITY AND MASS FUNCTIONS FOR 14013 ASSOCIATIONS

Robert J. Hill[1,2]
Department of Astronomy
University of Toronto
60 St. George St.
Toronto, Ontario, Canada M5S IA]

Barry F'. Madore[2]
NASA/IPAC Extragalactic Database
Infrared Processing and Analysis Center
California institute of l'ethnology
Jet Propulsion Laboratory, MS 100-22
Pasadena, CA 91125

Wendy L. Freedman
The Observatories
Carnegie Institution of Washington
813 Santa Barbara St.
Pasadena, CA 91101

[1] Current address: The Observatories, Carnegie Institution of Washington, 813 Santa. Barbara St., Pasadena, CA 91101

2 Visiting Astronomer, Las Campanas Observatory, Carnegie Institution of Washington

## Abstract

We have used UBV photometry of 14 associations in the Large and Small Magellanic Clouds to derive luminosity and mass functions for the most massive stars in the associations. The main sequence luminosity functions for the associations are quite similar, having an average Slope of $s = 0.30$. The slopes of the mass functions for the associations span similar ranges in both the LMC and SMC and there is no strong evidence for a significant variation in the slopes from onc association to another. Metal abundance does not appear to have a strong effect on the IMF, at least for the range in metal abundances observed between the Magellanic Clouds. The average slope of the IMF for the Magellanic Cloud associations is $\Gamma = -2.0 \pm 0.5$ for $M > 9M_{\odot}$, while the individual associations span a range in slope of $-1.2 > \Gamma > -2.5$. 'he wide range in slopes is more likely due to the large uncertainties which are associated with the calculations of the mass functions, rather than to a real variation in the IMFs. There may be some evidence for a decrease in the slope of the IMF at masses below $9M_{\odot}$, but incompleteness and the larger photometric errors associated with the faintest stars make this change in slope uncertain.



Keywords: stars: OB associations – stars: photometry – stars: masses — galaxies: LMC and SMC

# 1. INTRODUCTION

The Vogt-Russell theorem states that, to first order, the initial mass of a star determines its structure and evolution. Therefore, a knowledge of the distribution of the initial masses of stars, or the initial mass function (IMF), is of great importance to many aspects of research into the structure and evolution of galaxies. The form of the IMF, along with the rate of star formation, will determine the distribution of stellar populations which exist in a galaxy at any given time. The IMF and star formation rate for massive stars is of further importance because of the influence of massive stars on the chemical and dynamical evolution of the interstellar medium. Massive stars control the energy input and the amount and composition of material returned to the interstellar medium through stellar winds and supernovae. Thus any study of the evolution of the ISM requires a knowledge of the massive star IMF as one of the input parameters.

We have undertaken an observational program with the goal of determining the IMF for massive stars in OB associations in the Magellanic Clouds. Even though the OB stars in the Magellanic Clouds are more distant, and hence fainter, than Galactic OB stars, there are several advantages to using a sample of Magellanic Cloud stars rather than Galactic stars. The most important advantage is that the amount of interstellar reddening and absorption toward massive stars in the Magellanic Clouds is much less than toward their Galactic counterparts. Since the derivation of luminosity and mass functions requires an accurate knowledge of the absolute magnitudes of stars, it follows that the amount of extinction towards each of these stars must first be reliably determined. The nearest Galactic O and B stars may suffer as much as a magnitude or more of absorption in the visual and the amount of absorption varies significantly for different lines-of-sight, making accurate determinations of the extinction difficult. On the

other hand, the Magellanic Clouds lie in directions well away from the Galactic plane ($b^{II} \sim$ –33° for the LMC and $b^{II} \sim$ –44° for the SMC) and hence the foreground extinction is low. The only appreciable gas and dust along the lines-of-sight to massive star forming regions in the Magellanic Clouds is associated with the star forming regions themselves.

The second reason for going to the Magellanic Clouds to determine the massive star IMF is that all of the stars in each galaxy can be considered to be at the same distance. Any errors in the assumed distances to the two galaxies will result only in a scale error in the derived IMF, with the shape of the IMF being unaffected. This will not be true, however, if Galactic O and B stars are used to determine the IMF for massive stars. In order to obtain a statistically significant sample of stars, it is necessary to include stars which are at distances ranging from a few hundred parsecs up to approximately 3 kpc. The uncertainties in the distances to individual stars can lead to significant errors in the derived Galactic IMF.

The distances to the Magellanic Clouds have been the subject of some controversy over the last two decades. Accurate knowledge of the distances to these galaxies is extremely important to the study of many extragalactic problems, primarily because the Magellanic Clouds are the first step outside our galaxy in establishing the extragalactic distance scale. Fortunately, most recent measurements of the distances to these galaxies are now in general agreement. Westerlund (1990) has summarized the recent results obtained from many different distance estimating techniques and has concluded that the most likely true distance moduli for the LMC and SMC are 18.5 and 18,9 mag, respectively. These distance moduli correspond to distances of 50 kpc for the LMC and 60 kpc for the SMC, and will be adopted here without further discussion.

A third reason for observing Magellanic Cloud stars is to investigate the sensitivity of the

IMF and the physics of star formation to metal abundance. The metallicities of the Magellanic Clouds are lower than the Galaxy and different from each other ($Z$ =0.01 and $Z$ = 0.002 for the LMC and SMC, respectively (Lequeux *et al.* 1979, Dufour *et al.* 1982, and Dufour 1984). Therefore any systematic differences between the forms of the IMF for the two galaxies may indicate a dependence on metal abundance, although other possibilities cannot be ruled out *a* priori.

For the above reasons, we have chosen to attempt to determine the form of the massive star IMF from observations of Magellanic Cloud OB associations. The U BV observational data for the 14 associations is presented in hill *et al. (1992a,* hereafter Paper 1). The first step in deriving the IMF from the data is to remove the effects of interstellar extinction (Hill *et al.* 1992b, hereafter Paper II). A full treatment of the procedures used to do this and the effects of the random and systematic errors associated with them is also given therein.

The UBV observational data, once corrected for reddening, can be used to derive a mass function in at least two different ways. The first method requires the construction of a main sequence luminosity function from the observed data. This luminosity function is then converted to a mass function by employing an adopted mass-luminosity relation. The steps involved and the sources of error associated with this techniquc have been thoroughly reviewed by Scalo (1986). The second method involves the transformation of the observational (V,(B-V)) data star by star to the theoretical ($M_{bol}$, log $T_{eff}$) plane, where the data can then be compared directly to theoretical evolutionary tracks to construct the mass function.

'J'here arc difficulties with each approach. In the first case, the construction of a main sequence luminosity function is straightforward, but the mass-luminosity relation must be constructed from theoretical evolutionary models. These models generally yield a bolomet-

ric luminosity and effective temperature for each stage of evolution. in order to construct the appropriate mass-luminosity relation, a bolometric correction must be applied to the theoretical luminosities. Also, the mass-luminosity relation will be a function of the age of the association, because of the evolution of stars near the top of the observed main sequence. Thus, if these evolved stars arc to be included in the analysis, a distinct mass-luminosity relation must be derived for each association. Finally, the most evolved stars in the associations are not near the main sequence at all and hence are not included in the luminosity function. These stars arc of importance because they are rare examples of (usually) the most massive members of the associations,

On the other hand, the second method requires the transformation of the individual stellar magnitudes and colors to the t heoretical plane. This in turn requires accurate color/effective temperature and effective temperature/bolometric correction relations. However, this method has at least three advantages. (1) The stars arc transformed individually to the theoretical plane. 'l'his in turn allows a more thorough investigation into how well the observational and theoretical planes map onto each other, since the positions of the individual stars in the theoretical 11 R diagram can be directly compared to the published evolutionary tracks. (2) The evolved stars can be included in the analysis, even though their assigned masses may be less certain than those of main sequence stars. This is important in cases such as the association LH 111, which has a large population of red supergiants. (3) No assumptions are made regarding the star formation history of the associations. The construction of a unique mass-luminosity relation for each association, which is necessary in employing the first method implicit] y assumes that star formation occured instantaneously in each association. This is almost certainly untrue. The second method makes no such assumption, and, in fact, the

positions of stars in the theoretical HR diagram may yield information concerning the duration of the star formation event. For these reasons, we have chosen to employ the second method in the construction of the mass functions for the Magellanic Cloud associations.

Nevertheless, the luminosity functions are still a useful tool for investigating the systematic of the stellar populations of the associations and for comparison with previous studies. Hence we present the luminosity functions for the associations in §II before deriving the equations used to transform the observational data to the theoretical plane in §III. The mass functions are derived in §IV. The properties of the individual associations are discussed in §V and we compare our results to previous work in §VI. The conclusions are presented in §VII.

## II. LUMINOSITY FUNCTIONS

The main sequence luminosity functions were constructed in a straightforward manner. The UBV data presented in Paper I were corrected for interstellar reddening and extinction according to the precepts outlined in Paper II to yield intrinsic magnitudes and colors. The main sequence stars were selected by including only stars with $(B-V)_o \leq 0.2$ msg. This limit was chosen to account for the broadening of the main sequence at faint magnitudes (due to the photometric errors), while still excluding the bulk of the field stars. These stars were then binned in 0.5 magnitude intervals. The luminosity functions are tabulated in Tables 1 and 2 and are displayed in Figures 1-14.

We may attempt to parameterize the luminosity functions by assuming that they can be represented by a power law. There is no justification for expecting the luminosity functions to conform to a power law, but the observational data do not require the adoption of a more complex parameterization. This parameterization also facilitates a comparison with previous

work. The luminosity function then takes the form

$$\log[\Phi(V_o)] = sV_o + b \quad (1)$$

where $\Phi(V_o)$ represents the number of main sequence stars found in the magnitude range $(V_o - 0.25) \leq V_o \leq (V_o + 0.25)$, and s is the slope of the luminosity function. The slope can be determined by a least-squares fit to the binned data.

The slopes of the V magnitude main sequence luminosity functions for the Magellanic Cloud associations are listed in Table 3. The magnitude ranges for which the slopes are calculated are found in column 2, and the slopes are listed in column 3. The slopes listed in column 4 are explained below. The tabulated errors are the formal errors from the least-squares fits. Each magnitude bin was weighted according to the square-root of the number of stars in the bin.

The luminosity functions for each association begin to turn over at fainter magnitudes where the data becomes incomplete. The effect of incompleteness in the fainter magnitude bins would be to decrease the slopes of the luminosity functions. No attempt has been made to make a completeness correction to the number of stars at faint magnitudes. However, the range over which the slopes were calculated was chosen in each case to avoid this part of the luminosity function.

Unresolved binary stars can have an affect on the luminosity function slopes. The typical seeing on any given night was $\sim$ 1", which, at the distance of the Magellanic Clouds, corresponds to a physical distance of $\sim$ 0.2 pc. Hence, any two or more stars which are closer than this separation will not be resolved by DAOPHOT. Therefore, most binary stars will not be identified as such and many of the "stars" observed may actually consist of two or more fainter

stars. 'There is no method of accurately accounting for the presence of unresolved binaries, unless the binary frequency and their magnitude distribution is known. However, in a case where a binary system has been identified as a single star, it should be replaced by two stars at fainter magnitudes. Thus, the effect of unresolved binaries is to replace two fainter stars with one brighter one. Therefore, the presence of unresolved binaries will result in the observed luminosity function having a smaller slope than the true luminosity function. This effect has been quantitatively verified by the numerical simulations of Freedman (1983). The mass functions which we present later (§ IV) will be affected in the same way by the presence of unresolved binaries.

This same resolution problem may also cause incompleteness in the data at brighter magnitudes in crowded regions. However, most of the associations observed in this study are loose, uncrowded systems. The two exceptions are LH 111 and NGC 376. The slopes of the luminosity functions for these two associations do not differ from those of the less compact objects.

The photometric errors are not a significant source of error in the slopes of the luminosity functions. In the case of the bright stars, the photometric errors are of the order 0.02 msg. Since the magnitude bins are 0.5 mag in width, very few bright stars will be placed in the wrong bins. The photometric errors are larger for the faintest stars ($\sim$ 0,2 mag), but the luminosity functions are affected by incompleteness before the errors become this large, and hence these stars fall into magnitude bins which were not used in the calculation of the slopes of the luminosity functions.

The color magnitude diagrams for the associations (see Paper 11) demonstrate that the main sequences of the associations extend to different limits at the bright end, indicating a spread in the ages of the associations. In order to make a proper comparison of the luminosity functions,

their slopes should be talc.ulatcd over the same range of magnitude in each case. This will ensure that the same types of stars are used to construct all of the luminosity functions. At the bright end, the limit is defined by those associations which have the faintest upper main sequences. An attempt was made to make the magnitude cut-off faint enough so that stars which have evolved significantly from the ZAMS were excluded. At the faint end, the limit is set by the completeness of the data. For the LMC, a suitable range in magnitude appears to be $14.5 < V_o \leq 17.5$ msg. Allowing for its greater distance, a similar range for the SMC associations is $15.0 \leq V_o \leq 18.0$ msg. The slopes of the main sequence luminosity functions, $s_{ms}$, calculated over these ranges have been tabulated in column 4 of q'able 3. The one exception is LH 111, for which the data are incomplete at magnitudes $V_o < 17.0$ mag, and therefore a value of $s_{ms}$ has not been calculated for this association. The formal errors associated with these slopes are much larger than in the previous case because the magnitude range is smaller.

The slopes for the LM C associations are remarkably similar, considering the uncertainties in the slopes. The average slope is (s) = 0.25 for the full range luminosity functions and $\langle s_{ms} \rangle$ = 0.29 for the limited range main sequence luminosity functions. There are, however, hints that the luminosity functions for LH 54 and 1,11 58 are flattening out, or perhaps even starting to turn over, at magnitudes fainter than $V_o \leq 16.5$ msg. The data are still complete at this magnitude, so this may reflect a real difference in the stellar populations of these associations, but this interpretation depends on only onc or two magnitude bins. Therefore, the significance of the flattening of the luminosity functions for these associations is uncertain. If wc recalculate the slopes of the luminosity functions for these two associations for the brighter stars only, wc obtain s = 0.32 ± 0.05 ($12.0 \leq V_o \leq 17.0$ mag) for LH 54 and s = 0.33 ± 0.08 ($13.0 \leq V_o \leq 17.5$ mag) for 1,11 58. These numbers arc not significantly different from the slopes obtained for the

other associations in the sample.

The slopes for the SMC associations arc also similar ((s) = 0.30, $\langle s_{ms} \rangle$ = 0.31), with the exception of N 24 and possibly NGC 249. N 24 is a very complex region containing more than onc center of H$\alpha$ emission (see Figure 1b of McCall *et al.* 1990) as well as a supernova remnant (Mathewson and Clarke 1973). It is possible that star formation in this association took place over an extended period with more than onc centre. This would result in a steeper luminosity function because some of the upper main sequence stars from the earliest star formation events would have evolved off the main sequence while all of the lower mass stars which were formed would still be on the main sequence. Thus, the brighter magnitude bins would be depleted relative to the fainter bins (this is essentially the same argument which Salpeter (1955) used to explain the change in slope of the luminosity function of the solar neighborhood at $M_V \sim +4.0$). In the case of NGC *249,* the calculated s1OPCS have larger associated errors because it is" the least populous of the associations and hence the luminosity function is more susceptible to small number statistics. Therefore, the larger slope obtained for this association is of dubious significance.

The differences in the slopes calculated over the two different magnitude ranges indicate that the value obtained for the s1OPC is very sensitive to the choice of the upper and lower magnitude limits. Even though the errors on the full range slopes in 'J'able 3 arc of the order of 10 – 15%, the calculated slopes can change by larger amounts depending on the upper and lower magnitude limits. Therefore, the formal errors given for the full range luminosity function slopes in column 3 of 'J'able 3 arc probably underestimates of the true uncertainties.

A comparison of the results obtained here with other work is difficult because most other investigators have sam pled a different range of 1 uminosi tics along the main sequen cc. '1'here is

no *a priori* reason to expect that the slope of the luminosity function should be constant over a wide range in magnitude; this must. be kept in mind when comparing the results of different studies. Moreover, in this study, associations of a single (or small range in) age have been observed, whereas most other studies have concentrated on field stars, which have a wide range in ages.

LH 111 is the only object in common between the associations studied here and those studied by Lee (1990). The luminosity function presented by Lee (1990) for this association has a slope of 0.364:0.04, over the range $12.5 < V_o \leq 17.0$ mag, calculated in the same way as the slopes given in Table 3. This agrees reasonably well with the value found here (0.294: 0.03, which is unchanged if we restrict our calculation of the slope to the same range used by Lee). Lucke (1974) also studied the luminosity functions of the system of LMC associations. A slope of s $\sim$ 0.3 is estimated from his Figure 10 for stars in the range $13.0 \leq V_o \leq 14.5$, again in agreement. with the results obtained here.

Lequeux *et* al. (1980) have constructed a luminosity function for the brightest blue stars in the LMC based on the catalogue of Rousseau *et al.* (1978). A weighted least-squares fit to their luminosity function yields a slope of 0.51 $\pm$ 0.03 over the range $-8.5 < M_v < -6.0$ msg. The main sequence luminosity functions presented here correspond to somewhat fainter magnitudes ($-4.0 < M_V < -1.0$ mag). Also, the Rousseau *et al.* catalogue contains a mixed population of objects, most of which are blue supergiants rather than main sequence stars, and hence a steeper slope is to be expected.

Freedman (1 985) has presented luminosity functions for 10 Local Group late-type spiral and irregular galaxies, including the LMC and SMC. The LMC data used in that study arc also those of Rousseau *et al.* *(1* 978), while the SMC data were taken from Ardeberg and

Maurice (1977). Freedman finds a slope of 0.67+ 0.02 for stars brighter than $M_V = -5.0$, with very little variation from galaxy to galaxy. The same caveats apply to this result as apply to those of Lequeux *et al.* (1 980), namely that the stars observed are brighter than those studied here and they belong to a mixed population. Freedman has also pointed out that the slope of the luminosity function must decrease somewhere in the range $-5.0 < M_V < +5$ msg. A luminosity function as steep as 0.67 would result in integrated luminosities brighter than the known luminosities of these galaxies.

Recently, Blaha and Humphreys (J 989) have compared the luminosity functions of the brightest stars in the Galaxy, the LMC and the SMC. They find that the slope of the luminosity function is $\sim 0.7$ in the range $-9 \leq M_V \leq -7$ and is similar in all three galaxies. This range in luminosity corresponds to the brightest, most massive supergiants. The value found for the slope agrees with that of Freedman (1 *985).*

A better comparison to these other studies can be made if the data from all the LMC associations are summed together (a similar data set can be created for the SMC). Unfortunately, even when the data are combined in this manner, there are still too few stars at the extremely bright magnitudes sampled by Lequeux *et al. (1 980),* Freedman ( 1985) and Blaha and Humphreys (1989) to make a meaningful comparison. The luminosity function for the summed LMC data has a slope ofs = 0.40+ 0.08 for $M_V \leq -4.5$, while the summed SMC data give a slope ofs = 0.52+ 0.08 for $M_V \leq -4.0$. However, these slopes are based on less than 100 stars in each case and about half of the stars fall into the lowest magnitude bin. Nevertheless, the trend is in the right direction.

Hardy *et al.* (1984) have studied the field star main sequence luminosity function of the LMC at fainter magnitudes. An unweighted fit to the luminosity function presented in their

Table 2 and Figure 7 yields a slope of $s \sim 0.6$ for $-1.3 \leq M_v \leq 1.4$. There is only marginal overlap between the luminosities of the stars studied by Hardy *et al.* and those studied here and, once again, the field stars form a mixed population. Butcher (1 977) has also investigated the field star luminosity function of the LMC in an effort to find the change in slope which should occur at the turn-off point of the oldest stars in the J, MC, which in turn yields the epoch of the earliest major burst of star formation in the galaxy. The luminosity function appears to change in slope at $M_v \sim +3.0$, but this result is sensitive to the estimated degree of completeness of the data. The luminosity function presented in Butcher's "1'able 1 gives a slope of s $\sim$ 0.45 for stars brighter than this turn-off point ($0.0 \leq M_V \leq 3.0$).

In summary, the main sequence luminosity functions of the Magellanic Cloud associations are quite similar. Despite the fact that there arc hints that there may be differences in a fcw cases, the significance of these variations is questionable. There appears to be no clear evidence to suggest that the main sequence luminosity functions differ from one association to another. The average slope of the main sequence luminosity functions is s = 0.30, which agrees with previous results obtained for stars of similar luminosities. The larger slopes obtained by other investigators for brighter stars may reflect a true difference relative to the fainter stars, or may be due to the inclusion of a mixed population including many blue supergiants.

## HI. CONVERSION FROM THE OBSERVATIONAL TO THE THEORETICAL PLANE

in order to construct mass functions, the observational data must be compared with theoretical models of stellar evolution. The stellar parameters calculated in these models arc usually bolometric magnitude and effective temperature. Therefore, in order to effect a comparison, the observational data must be transformed from $(V_o, (B-V)_o)$ plane to the theoretical

$(M_{bol}, \log(T_{eff}))$ plane.

This transformation to the theoretical plane is made in three steps. The first step is to calculate the stellar effective temperatures from the individual colors, the second is to apply the bolometric correction to the $V_o$ magnitudes, and finally the distance modulus is used to convert the bolometric magnitudes to absolute bolometric magnitudes.

The most common means of determining effective temperat u res from photometric data is to usc a calibration of $(B-V)_o$ colors versus effective temperatures. Böhm-Vitense (1981) has comprehensively reviewed the effective temperature scale and the difficulties associated with measuring stellar effective temperatures.

The $(B-V)_o$ colors of hot stars become degenerate for stars earlier than approximately 09, and hence the (B – $V)_o$ colors alone are not sufficient to yield accurate effective temperatures for the hottest stars in the associations. However, the $(U-B)_o$ colors provide a better discrimination among the hotter stars. Therefore we have chosen to make usc of both the $(U-B)_o$ and $(B-V)_o$ colors in determining the effective temperatures of the hottest stars. The reddening free parameter, Q, provides a useful combination of the two colors for use in calculating effective temperatures. The advantage of using Q is that any errors in the individual values of $E(B-V)$ and $A_v$ which were used to deredden each star will not affect the effective temperature calibration, provided, of course, that the correct reddening law was used.

The calibration of Q versus effective temperature was derived by using the intrinsic. colors of Schmidt-Kaler (1982) combined with the color/effective temperature relationofIJlower(1977). Since the U observations do not extend to magnitudes as faint as do the B and V observations, some of the fainter main sequence stars will have either very large photometric errors in U (while still having relatively small B and V errors) or no U observation at all. For these stars,

we have no choice but to use the $(B - V)$ colors alone to determine the effective temperatures. The bolometric corrections were derived from Flower's (1 977) effective temperature-bolometric correction relations. Tables 4 and 5 display the resulting color/effective temperature and effective temperature-bolometric correction relations, respectively, for different ranges of intrinsic $(B - V)_o$ color.

It should be noted that Conti *et al.* 1986 and Garmany *et al.* 1987 have recently suggested that the intrinsic colors of LMC and SMC O and B stars may be different from those of Galactic stars. This would not be surprising, since the metal abundances of LMC and SMC stars are less than Galactic stars, and this might be expected to influence the energy distribution of the emergent flux. If the intrinsic colors are different, then the application of a Galactic. color/effective temperature calibration would lead to systematic errors in the assigned effective temperatures. However, these same authors (Conti *et al.* 1986 and Massey *et al.* 1989b) have also pointed out that the apparent discrepancy between the intrinsic colors of Galactic and Magellanic Cloud OB stars may be due to errors in the Galactic calibration. The intrinsic colors used by Massey and co-workers are those of Fitzgerald (1 970). The intrinsic colors used here (Schmidt- Kaler 1982) are based in part on the work of FitzGerald.

The final step in the transformation to the theoretical plane is to apply the correction for the distance modulus. The final bolometric magnitude for each star is given by

$$M_{bol} = V_o - (m - M) + BC, \tag{2}$$

where $(m - M)$ is the distance modulus (18.5 mag for the LMC and 18.9 mag for the SMC).

Figure 15 shows the theoretical HR diagram for NGC 465 after applying the effective tem-

perature and bolometric correction conversions of Tables 4 and 5. The main sequence is quite evident in the plot.

The faint stars which are not on the main sequence are not supergiants, and therefore the bolometric corrections derived for these stars will not be correct. These stars will be primarily giant stars. The difference between the supergiant and giant effective temperature-bolometric correction relations is typically about 0.1 mag, in the sense that the corrections applied here are too small. The bolometric magnitudes for these stars should therefore be about 0.1 mag brighter. However, these stars are not included in the determination of the mass functions and thus any error made here will have no influence on the derived mass functions.

A much more significant error can arise from the strong dependence of bolometric correction on the effecti ve temperature for hot stars. When combined with the strong dependence of the effective temperature on the intrinsic stellar colors, and the degeneracy of these colors for the hot test stars, it is possible to make large errors in assigning bolometri c corrections to these stars. For example, the bright stars have colors which are accurate to better than $\pm 0.03$ msg. Errors of this size result in errors of $\pm 0.05$ in $\log T_{eff}$ and $\pm 0.25$ mag in $BC$. The problem is more serious for the fainter lower main sequence stars, which have larger errors. A typical lower main sequence star might have $(B-V)_o = -0.10 \pm 0.10$ msg. The equations in Tables 4 and 5 give $\log T_{eff} = 4.07$ and $BC = -0.63$ msg. If the true color of the star is $(B-V)_o = -0.20$ mag, then the errors will be +0.20 in $\log T_{eff}$ and – 1.19 mag in $BC$, respectively. On the other hand, if the true color is $(B-V)_o = 0.0$, then the errors will be –0.09 in $\log T_{eff}$ and +0.38 m ag in $BC$, respective] y. The errors arc not symmet ri c; much larger errors are made when t he observationally determined stellar colors arc bluer than the true colors than when the observed colors are too red. If the $(B-V)_o$ error is as large as --0.20 mag, the errors will be +0.44 in

log $T_{eff}$ and –2.60 mag in $BC$. Errors of this size can strongly affect the mass function which is derived from the data (see §IVc).

## IV. MASS FUNCTIONS

### a) *Definitions*

Before deriving the mass functions for the associations, it is useful to introduce some definitions which will help to avoid confusion when comparing the results presented here with other work. The observed data can be used to construct a present day mass function (PDMF) which is related to the IMF by the star formation rate. If we define the PDMF, $N(M)$, as the number of stars observed per unit mass in a given volume, then the PDMF can be expressed as

$$N(M) = \int_{max[0,\tau-\tau_l(M)]}^{\tau} \xi(M,Z,t,\ldots)\Psi(t)dt, \tag{3}$$

where $\xi(M,Z,t,\ldots)$, the initial mass function, is the number of stars formed per unit mass per unit time in a given volume. $\Psi(t)$ is the star formation rate, which is the number of stars formed per unit time in a given volume, $\tau$ is the time elapsed since the formation of the first stars, and $\tau_l(M)$ is the lifetime of a star of mass $M$.

in general, $\xi$ may be a function of mass, metal abundance, time and other parameters representing the physical conditions in a star-forming region. However, in most applications it is assumed that the IMF is independent of metal abundance, time and other parameters, and is a function of mass only. These assumptions may come close to being satisfied in an isolated region, such as a star formation event in a single molecular cloud. Under these conditions, equation 3 becomes

$$N(M) = \xi(M) \int \Psi(t)dt. \tag{4}$$

Finally, if we make the further assumption that all of the stars formed at the same time, we have

$$N(M) = \xi(M)\Psi, \tag{5}$$

where $\Psi$ is now a scale factor representing the total number of stars which formed in the event. Although the assumption of instantaneous star formation cannot be strictly true, it may be valid if the duration of the star formation event is short compared to stellar lifetimes. Under these assumptions, the PDMF is proportional to the IMF over the range in mass spanned by the observed stars. Of course, the PDMF can give no information concerning the IMF for stars more massive than the most massive remaining stars.

Although the IMF may be a function of metal abundance, all of the stars in a given association will have formed from one molecular cloud (or perhaps two if star formation was precipitated by a collision between two clouds). Therefore, the metallicity of the stars should be close to uniform, provided that star formation had ended by the time the most massive stars evolved to become supernovae. Despite this, the possibility of a non-coeval population must be considered in the interpretation of the mass functions.

Many previous studies yield the slope of the IMF as a major result. This slope refers to a power law parametrization of the IMF. With this parameterization

$$\xi(M) = AM^{\gamma} \tag{6}$$

Recently, it has become common to adopt the notation of Scalo (1986), and to employ a logarithmic IMF of the form

$$\xi(\log M) \propto M^{\Gamma}, \tag{7}$$

where $\xi(\log M)$ is the number of stars formed per unit time per unit logarithmic mass interval $d\log M$ in a given volume. With this parameterization, the slope of the IMF is

$$\Gamma = \frac{d\log \xi(\log M)}{d\log M} \quad (8)$$

We will adopt this form and slope for the IMF in the discussions to follow. The two representations of the IMF are related by the scale factor $M\ln 10$ and hence the two slopes are related by $\gamma = \Gamma - 1$. Using this notation, the classical Salpeter (1955) IMF has a slope of $\Gamma = -1.35$.

*b) Evolutionary Tracks*

In order to construct the PDMF, the positions of stars in the theoretical HR diagram must be compared with evolutionary tracks derived from theoretical models of stellar evolution.

Many different sets of models exist in the literature. However, until recently, most models did not include the effects of convective overshoot and mass loss. The importance of including convective overshoot in the calculation of models of intermediate and high mass stars has been demonstrated recently in many observational and theoretical studies (Meylan and Maeder 1982, Maeder and Meynet 1982, 1987, 1989, Bertelli *et al.* 1984, 1985, Chiosi *et al.* 1986). Chiosi and Pigatto (1986) and de Loore (1988) discuss the practical differences between classical models and those which include overshoot. The effects of mass loss on the evolution of massive stars and the difference between classical models and those which include mass loss are fully reviewed in Chiosi and Maeder (1986).

We have chosen to use the evolutionary tracks of Maeder and Meynet (1987,1988) because they are the only homogeneous set of tracks covering the range of masses of interest to this study which includes both the effects of convective overshoot and mass loss. These tracks are shown

in Figure 16. The distance of convective overshoot used in these models is $d = 0.25H_p$, where $H_p$ is the pressure scale height of the classical core. The mass loss rates used are taken from the parameterizations of de Jager *et al.* (1986,1988). Unfortunately, the models are computed for stars with abundances of (X, Y, $Z$) = (0.70,0.28, 0.02), which are appropriate to Population 1 stars in the Galaxy. More appropriate values for the metal abundances of the LMC and SMC are $Z$ = 0.01 and $Z$ = 0.002, respectively (Lequeux *et al.* 1979, Dufour *et al.* 1982, Dufour 1984). Brunish and Truran (1982) have shown that the effect of a decreased metal abundance is to shift the evolutionary tracks to higher temperatures and slightly higher luminosities at a given stage of evolution. However, their models did not include the effects of convective overshoot.

Figures 17-30 show the theoretical HR diagrams of the associations observed in this study with the theoretical evolutionary tracks of Maeder and Meynet (1987, 1988) superposed. The filled circles denote stars with the best photometry ($\sigma = \sqrt{\sigma_V^2 + \sigma_{BV}^2} \leq 0.05$ mag), open circles for stars with intermediate precision ($0.05 < \sigma < 0.10$ mag), and plus signs for stars with the largest photometric errors ($\sigma > 0.10$ mag). The dashed lines which extend from the blue end of each evolutionary track to higher effective temperatures demonstrate the effect, in the theoretical plane, of decreasing the $(B-V)_o$ color of a star while keeping the $V_o$ magnitude constant. These lines will prove useful in constructing the mass functions (see §IVc below). The dashed curves near the bottom of each figure, extending across the entire range of $\log(T_{eff})$, are drawn parallel to the completeness limits of the data. They are, in fact, the transformation to the theoretical plane of the dashed lines at the bottoms of the color-magnitude diagrams presented in Papers 1 and 11. There is, in general, very good agreement between the location of the main sequence defined by the data and the evolutionary tracks, which implies that the

transformations used to map the data from the observational to theoretical planes are reasonably accurate.

c) *Mass Functions For Magellanic Cloud Associations*

*The* ideal method of constructing the PDMF from the data would be to assign a mass to each star based on its position in the theoretical HR diagram. In practice, the assigned masses may not be very meaningful because of the observational errors, uncertainties in the transformation to the theoretical plane, and uncertainties in the accuracy of the theoretical models used to produce the evolutionary tracks.

In practice, a more reliable method is to bin the data in mass bins defined by the evolutionary tracks. All stars lying between two given evolutionary tracks are assigned to the bin corresponding to the range in masses spanned by the tracks. in this way, small errors in the placement of stars in the theoretical HR diagram have very little effect on the derived mass functions. Errors in the location of stars arc only important when they result in stars being assigned to the wrong mass bin.

We have constructed the PDMFs by counting the number of stars between each pair of evolutionary tracks, and dividing by the quantity $\log(M_U/M_L)$, where $M_U$ and $M_L$ arc the masses correspon ding to the higher and lower mass evolutionary tracks, respectivel y. To give a direct comparison of the different associations, it is also necessary to divide by the volume containing the observed stars. Since the volumes are unknown, this scale factor is not included. However, it will still be possible to compare the slopes of the mass functions, since the differing scale factors do not affect the slopes.

Many of the stars in the theoretical HR diagrams lie outside the regions which arc covered by the evolutionary tracks, and it is important to include these stars in the appropriate mass bins.

in particular, many stars fall to the blue of the ZAMS, presumably due to the combination of photometric errors, errors in the color excess, and errors in the transformation to the theoretical plane. Most of these stars arcs tars which have relatively large photometric errors (represented by plus signs in the plots). Therefore, it seems reasonable to assume that they fall to the blue of the ZAMS because of photometric errors in V or $B$ (recall that the $U$ magnitudes are not used in the transformation to the theoretical plane when the U errors arc large; scc Table 4).

Stars will appear to the blue of the ZAMS when the stellar $(B - V)_o$ colors are bluer than the $(B - V)$ color of the ZAMS at the same $V_o$ magnitude. These stars will be assigned a value of $\log(T_{eff})$ and a bolometric correction which arc too large, resulting in a displacement parallel to the dashed lines on the plots. As discussed in §III, an error in $(B-V)_o$ of -0.10 mag can result in an error in the bolometric correction of –1 .19 msg. On the other hand, an error in $V_o$ propagates directly into an error of the same size in $M_{bol}$, according to Equation 2. Thus, errors in $(B-V)_o$ are much more important in the transformation from the observational to theoretical planes. Also, since the evolutionary tracks used to define the mass bins are 1 –2 magnitudes apart, errors in $V_o$ alone will not result in many stars being placed in the wrong mass bin. Therefore, in order to assign stars to the blue of the ZAMS to a mass bin, wc will assume that these stars suffer only from errors in $(B-V)_o$. With this assumption, the dashed 1 incs which extend from the blue end of each evolutionary track can be used as "extensions" of the evolutionary tracks for the purposes of constructing the mass funcions. Stars which lie to the blue of the ZAMS arc placed in mass bins appropriate to the pair of evolutionary track "exten sions" they fall between.

Many of the faintest, lower mass stars arc evolved stars which arc either foreground Galactic st ars or belong to the background population of the LMC or SMC. Non-main sequence stars

with $M_{bol} > -5.0$ and $\log(T_{eff}) \leq 3.9$ are almost certainly not members of the associations being studied. Therefore, these stars are not included in the mass functions.

This still leaves some bright non-main sequence stars which might be either foreground Galactic stars, or supergiant stars which are in fact members of the associations. The most striking case is LH111, which contains a large number of red supergiants (see Figure 23). These stars are certainly members of the association and should therefore be included in the construction of the mass function. in order to discriminate between foreground Galactic stars and association members on a case-by-case basis, it would be necessary to obtain spectra of these stars to estimate their luminosities, or assign radial velocities. In the absence of these data, it is still possible to determine whether or not these stars are likely to be foreground Galactic stars, by using the foreground contamination predictions of Ratnatunga and Bahcall (1985). These predictions indicate that almost all of the stars with $(B-V)_o \geq 1.3$ mag are likely to be association members (i. e., red supergiants), while most of the stars with colors in the range $0.0 \leq (B-V)_o < 1.3$ mag are foreground stars. These stars have been included or excluded from the mass functions accordingly. Many of the red supergiants lie beyond the extent of the evolutionary tracks (i. e., they have effective temperatures cooler han predicted by any of the evolutionary tracks). These stars were assigned to mass bins by extending the horizontal parts of the evolutionary tracks to cooler effective temperatures.

The mass functions are displayed in Figures 31-44 and are tabulated in Tables 6 and 7. The error bars represent $\sqrt{N}$ where N is the number of stars in a given mass bin. The lines in the plots represent least-squares fits to the data over the range in masses spanned by the lines.

An examination of the mass functions indicates that a simple power law may not be a suitable parameterization. Most of the mass functions appear to change in slope at about

$10M_{\odot}$; the mass functions are steeper at high masses than at low masses. The slopes of the mass functions have therefore been calculated for two different ranges in mass, and are presented in Table 8. The slopes for the most massive stars ($M > 9M_{\odot}$) are listed in column 2, while column 3 gives the mass function slope over the larger ranges in mass listed in column 4. The errors in the slopes are the formal errors derived from the weighted least-squares fits. We discuss below the issue of whether the apparent change in slope at $M \sim 10M_{\odot}$ is real or an artifact of the data.

'1'here are many factors which may result in errors in the slopes of the mass functions. Such errors will result whenever stars are assigned to incorrect mass bins. However, any symmetric error which merely exchanges equal numbers of stars between bins will not affect the calculated slopes. The slopes will only be affected if errors result in a systematic shifting of stars among bins. The nature of the transformation from the observational to theoretical planes is such that random errors (e.g. photometric errors) can result in a systematic error in the manner in which stars are assigned to mass bins.

It was demonstrated in §III that the photometric errors associated with the bright stars should result in errors of no more than $\pm 0.05$ in $\log(T_{eff})$ and $\pm 0.25$ mag in the bolometric correction, and hence also in $M_{bol}$. Since the evolutionary tracks which define the mass bins are 1–2 magnitudes apart, these errors should not result in many stars being assigned to the wrong bin. However, Massey *et al.* (1989a,b) have claimed that the colors of the earliest-type stars cannot be used to accurately determine effective temperatures and bolometric corrections for these stars. In their study of NGC 346 in the SMC (Massey *et* al. 1989 b), they found that when photometry alone was used in the transformation to the theoretical plane, the slope of the IMF was increased to $\Gamma$ = –2.5 from the value of –1 .8. The latter value was obtained by

using spectroscopy to position the hottest stars on the theoretical HR diagram. The increase in slope is due to the incorrect placement of many of the most massive ($M > 25M_{\odot}$) stars into the $15 - 25M_{\odot}$ bin. This does not appear to be the case here. Two pieces of evidence support this claim. A look through the mass functions shows that there appears to be no systematic excess of stars in the $15 — 25M_{\odot}$ bin. The numbers of stars in this bin seem to reflect the statistical fluctuations expected and the $15 - 25M_{\odot}$ points lie approximately where they are expected from the linear parameterizations of the upper main sequence mass functions. Secondly, the effect claimed by Massey *et al.* resulted in a steepening of the slope of the IMF by $\Delta\Gamma \sim -0.7$. Therefore, the slopes calculated here should be systematically too steep by this amount. On the contrary, the slopes found here agree well with results obtained by other investigators for both the Galaxy and the Magellanic Clouds using a variety of methods (see §V). Therefore, we find no evidence for a steepening of the slope of the IMF due to a systematic underestimation of the effective temperatures and bolometric corrections of the hottest stars; the values of $M_{bol}$ appear reliable to within the estimated uncertainties.

The photometric errors associated with the faint stars are much larger and hence the errors in $\log(T_{eff})$ and BC are also larger. In §III, it was shown that these errors are largest when the measured colors are bluer than the true colors, with the result that these stars are shifted along trajectories parallel to the blue "extensions" of the evolutionary tracks marked on Figures 17–30. In turn, this shift can move the stars with the largest photometric errors from their true mass bins to higher mass bins. This in turn will result in a flattening of the mass functions and may, in part, explain the change in slope of the mass functions at $\sim 10M_{\odot}$. However, this effect cannot be entirely responsible for this flattening of the mass functions. Only the faintest stars will have photometric errors large enough to result in a significant shift of stars to higher mass

bins. These stars are designated by plus signs in Figures 17-30. The figures show that most of these stars fall into the $2.5 - 3M_{\odot}$ and $3 - 5M_{\odot}$ bins. Therefore, only these bins, and to a lesser extent, the $5 - 7M_{\odot}$ bin should be affected, while the number of stars in the $7 - 9M_{\odot}$ bin should be a true reflection of the number of stars in this mass range. Thus, the flattening of the mass function at $\sim 10M_{\odot}$ appears to be real. However, the slopes listed in column 3 of Table 8 will be affected by the large photometric errors associated with the faint (i. e., low mass) stars. Since the low mass bins are given the most weight in the calculation of the slope, these slopes should be viewed skeptically, given the uncertainty in the placement of stars in these bins.

It has already been shown that an extended period of star formation will result in a PDMF which is steeper than the IMF. Under these circumstances, the PDMF for massive stars should be steep and should become flatter at a mass corresponding to stars with main sequence lifetimes equal to the time elapsed since the beginning of the period of star formation. There is some evidence that star formation did not occur instantaneously in the associations studied here. The red supergiants found in several of the associations are not always the most massive stars in the associations. This implies that either (1) star formation has occurred over an extended period or in multiple episodes, (2) the bolometric corrections for the red supergiants are systematically too small, or (3) the evolutionary tracks at advanced stages of evolution are systematically too bright. The most compelling reason to believe that the first hypothesis is correct is that the red supergiants are sometimes the most massive stars in the associations, while in other cases they are not. in some associations (e.g. LH 111), the red supergiants span a range in initial mass from $\sim 12M_{\odot}$ up to almost $40M_{\odot}$. There are also stars which are slightly evolved off the main sequence spanning the same range in mass. Therefore, it seems very likely that star formation in LH 111 occured over an extended period. Also, the second and third hypotheses

would require very large errors in either the bolometric corrections or the calculation of the evolutionary tracks (some of the red supergiants lie as much as 2 mag below the evolutionary tracks of the most massive main sequence stars in the associations). It seems unnecessary to invoke such large errors given the likelihood that star formation has, in fact, taken place over an extended period.

Can extended star formation explain the change in the slope of the PDMF at $\sim 10 M_{\odot}$ which is seen in many of the associations? The problem with this hypothesis is that it would require that star formation commenced at the same time in all of these associations. This is very unlikely. If extended periods of star formation were responsible for the changes in slope, we would expect to find this change occurring at different masses, depending on how long ago star formation began in each association.

The population of the lowest mass bins is somewhat uncertain, due to incompleteness and errors in the transformation from the observational to theoretical planes. However, these uncertainties should not have a large effect on the $5 - 7 M_{\odot}$ and $7 - 9 M_{\odot}$ mass bins, and hence the reality of the change in slope at $\sim 10 M_{\odot}$ seems likely. As mentioned above, the uncertainties in the numbers of stars in the lowest mass bins make the slopes calculated using these bins very uncertain. Therefore, in the discussions to follow, all references to mass functions will apply to masses greater than $10 M_{\odot}$.

The slopes of the mass functions for the LMC associations range from -1.2 to -2.5, with an average of $\Gamma = -1.84 \pm 0.5$. The SMC slopes cover a wider range, but this is due to the very steep slopes found for N 24 and NGC 376. As discussed in §II, N 24 is a complex region which has probably undergone star formation over an extended period. If the duration of star formation is comparable to the age of the association, then the PDMF will not be equivalent

to the IMF. Furthermore, it is not possible to derive the IMF from the PDMF under these circumstances without making assumptions about the star formation history of the association. NGC 376 is the oldest of the associations studied and, hence, the PDMF slope calculated for $M > 9 M_{\odot}$ is based on only three mass bins. Furthermore, the steep value for the slope depends heavily on the low number of stars in the most massive ($15 < M < 25 M_{\odot}$) bin. Therefore, the calculated slope for this association should be considered to be very uncertain. If we ignore these two associations, the average slope of the mass function for the SMC associations is $\Gamma = -2.26 \pm 0.3$, with a range of -1.8 to --2.5.

These slopes apply strictly to the PDMFs and not to the IMF. in order to derive the IMF from the PDMF, it is necessary to either assume that star formation occured instantaneously (or, in practical terms, over a short period compared to the ages of the associations) or to make assumptions concerning the star formation history of the associations. It is clear that the assumption of instantaneous star formation cannot be true. However, making ad hoc assumptions about the history and rate of star formation would seem to be even more risky. We are therefore left with no simple means of converting the PDMF to the IMF. However, in calculating the slope of the PDMF, the largest weights are assigned to the lowest mass bins, where the effects of an extended period of star formation should be smallest. Therefore, we tentatively equate the IMF to the PDMF, with the understanding that the slope of the IMF may be slightly shallower than that of the PDMF. Note, however, that the presence of an unknown number of binaries and unresolved stars will tend to make the observed PDMF (and hence IMF) shallower than the true PDMF. These two effects operate in opposite directions.

Given the large uncertainties in the calculation of the slopes of the mass functions, there is apparently no strong evidence that the slope of the IMF varies from one association to another.

Also, there does not appear to be a significant difference between the slopes of the IMFs of associations in the LMC and those in the SMC. Therefore, it appears that metallicity does not have a strong effect on the slope of the IMF, at least over the range in metal abundances of the associations ($0.002 \leq Z \leq 0.03$). The overall average slope of the IMF for the LMC and SMC associations is $\Gamma = -2.0 \pm 0.5$ for $M > 9 M_{\odot}$.

## V. THE INDIVIDUAL ASSOCIATIONS

We consider here the properties of the individual associations before comparing our results to previous studies in §VI.

*LH 4.*—LH 4 is a rather isolated association in the northwestern part of the LMC. The CM diagram for LH 4 (see Figure 16 of Paper 11) shows a prominent main sequence with no bright evolved stars. The number of red stars found with $(B - V) > 0.5$ mag is consistent with the predictions of Ratnatunga and Bahcall (1985) for the number of Galactic foreground stars. The fainter red stars are likely part of the LMC field population. The theoretical }]]{. diagram (Figure 17) shows that the most massive star in the association has a mass between 60 and 85 $M_{\odot}$. 'J'he existence of such a massive star implies that the association is only 3--4 M yr old.

*LH 54.*—LH 54 is located in a region containing several 11 11 regions and star-forming complexes in the northern part of the I, MC. The association lies within the filamentary H 11 shell N 51 D, which in turn lies on the edge of the supergiant shell LMC 4 (Goudis and Meaburn 1978). Chu and MacLow (1990) and Wang and Helfand (1991) have studied the x-ray emission which is centered on the association and find that models of wind driven bubbles filled with hot gas cannot reproduce the observed x-ray luminosity. Instead, it is likely that the association contains an unseen supernova remnant which is responsible for tile x-rays. If this is the case, then the true IMF for the association should include at least one star more massive titan those

presently observed.

The bright yellow star at $(B - V) \sim 0.65$ mag in the CM diagram (see Figure 17 of Paper 11) is probably a Galactic foreground star and hence has not been included in the calculation of the mass function. The most massive stars in the association are $\sim 40 M_{\odot}$ (Figure 18) and hence the association is less than 5 Myr old,

*LH 58.*—LH 58 is located in a complex region containing several II II regions and other associations (LH 61 and LH 64 arc nearby). The CM diagram for this association (see Figure 18 of Paper 11) shows a well-defined main sequence. The bright yellow star with V $\sim 11.2$ mag and $(B$ — V) $\sim$ 0.6 mag is probably a member of the association but the somewhat fainter star at $V \sim$ 13.1 mag and $(B - V) \sim 0.5$ mag may be a Galactic foreground star. The latter star has therefore been excluded from the calculation of the slope of the IMF. 'l'his exclusion makes no difference to the calculated slope, since the star would have been placed in the 7 — $9 M_{\odot}$ bin (see Figure 4.19).

*LH* 83. —1,}1 83 (NGC 2030) is onc of the northernmost associations in the LMC and is located in an II II region, part of which is even visible in the V image of the association (see Figure 1 d of Paper J). The CM diagram for LH 83 (see Figure 19 of Paper 11) shows a well-defined main sequence. Lucke and Hodge (1970) classified this association as doubtful, but the CM diagram definitely confirms it as a young object containing massive stars. The most, massive stars in the association arc close to $60 M_{\odot}$ (Figure 20), which implies an age of less than 4 Myr. Also, the supernova remnant SNR 0530 -66.0 is located within the boundaries of the association. Shull (1983) finds an age of 0.5–2.0x10$^4$yr for the remnant, depending on the expansion speed and geometry.

1,1187.--1,11 87 (NGC 2048) is located to the southeast of the star cloud LH 96 in a region

containing several other associations. The 1111 region N 154 encloses both LH87 and the nearby association LH81. The optical appearance of the association (see Figure 1 c of Paper I) suggests a ring-like structure, which was noted by Lucke (1974). A study of the reddening of the stars in the association shows that differential reddening is not the cause of the ring-shaped morphology (Paper II).

Despite being rather sparsely populated, the CM diagram (see Figure 20 of Paper 11) shows a strong main sequence. The theoretical HR diagram (Figure 21) shows several stars above 40 $M_{\odot}$. Since there arc no evolved stars, this must be a very young object ($\leq 3$ Myr).

*LH* 93.—1,11 93 (NGC 2050) is part of a much larger star-forming complex (LH 96) in the eastern regions of the I, MC. The V image of the association (see Figure If of Paper 1) shows it to be very densely populated, although not concentrated into a tight cluster. The supernova remnant SNR 0543 -68.9 is located nearby but is probably not part of the association.

The very tight main sequence seen in the CM diagram (see Figure 17 of Paper I), before the effects of reddening have been removed, demonst rates that differential reddening is unimportant, even though the total amount of reddening is among the largest of all the associations in the sample. The theoretical HR diagram (Figure 22) shows a large number of stars extending to above 60$M_{\odot}$. however, there arc 3 red supergiants which appear to be about 25$M_{\odot}$. Their existence, combined with ages determined from the evolutionary tracks of M aeder and Meylan (1988), implies that the star formation process must have occured over a timescale of at least 2-5 Myr. This is not surprising since the association is part of a larger star-forming complex.

*LH 111.*— *1,11 111* is one of the bright blue globular clusters in the I, MC. It lies to the southeast of 30 Dor within the supergiant shell LMC 2 (Goudis and Meaburn 1978). The stellar density at the centre of the object is such that the photometry becomes incomplete

at magnitudes fainter than V $\sim$ 16.5, a much brighter limit than is achieved for the other associations studied here.

The CM diagram for LH 111 (see Figure 22 of Paper II) shows a rich main sequence and 20 red supergiants. This is a much larger population of red supergiants than is observed for any of the other associations. The theoretical HR diagram (Figure 23) shows most of these stars have masses in the range 15–25$M_{\odot}$. There are also several stars of similar masses which are currently evolving off the main sequence. The evolutionary models of Maeder and Meynet (1988) indicate that these stars have ages of 7-15 Myr. It is therefore likely that star formation has occured continuously over 8–10 Myr rather than in one or two discrete bursts. This hypothesis is in disagreement with Lee (1990), who favours two star formation episodes, at epochs 8 $\pm$ 3 and 18 $\pm$ 10 Myr ago, based on fits to theoretical isochrones. McGregor and Hyland (1984) also deduce an age spread of $\sim$ 8 Myr, based on the spread in the luminosities of the red supergiants.

*N* 24. —N 24 is in a complex region which contains more than one centre of HII emission (see Figure 1a of McCall *et al.* 1990), and there is at least one supernove remnant contained within the association (Matthewson and Clarke 1973).

The CM diagram (see Figure 23 of Paper 11) is qualitatively somewhat different from the other associations. Although there is a well-defined main sequence, there are many more stars with $0.0 \leq (B - V) \leq 1.0$ mag and $V \sim 15$ mag than there are in other associations. 'There are more stars in this range of colour and at this magnitude than predicted from estimates of the Galactic foreground population (Ratnatunga and Bahcall 1985). The theoretical 11 R diagram (Figure 24) shows that these stars have masses in the range $7 - 10 M_{\odot}$, provided they are legitimate SMC stars. These stars, as well as the red supergiant with $M_{bol} \sim$ –6.4 mag and $\log T_{eff} \sim 3.6$, have been included in the construction of the mass function. The most massive

main sequence stars arc $\sim 25 M_{\odot}$, and hence have ages of $\leq 8$ Myr, while the evolved stars are 30--50 Myr old. Thus, the region clearly has a complicated star formation history.

NGC *249 and NGC* 261.-- NGC 249 and NGC 261 are located in the southwestern part of the SMC, approximately 5 arcmin apart.

The main sequence of NGC 249 is not as prominent as in most of the other associations (see Figure 24 of Paper 11), but there arc two bright supergiants, which arc likely members of the association. The theoretical HR diagram (Figure 25) suggests that these stars have masses of 12--1514., indicating an age of 12–18 Myr. The two most massive main sequence stars have masses $M > 25 M_{\odot}$ and therefore have ages of less than 8 Myr. This may indicate more than one episode of star formation, but there are very few stars in the association, which makes it difficult to draw any firm conclusions.

The CM diagram for NGC 261 (see Figure 25 of Paper 11) shows that the association is more populous than its neighbour, and there is one red supergiant among the association membership. The theoretical HR diagram (Figure 26) indicates that this star has a mass of $\sim 25 M_{\odot}$, although this is somewhat uncertain because its $(B-V)_o$ colour is redder than the limits of the colour/effective temperature calibration, thus making the inferred bolometric correct ion very uncertain. The most massive main sequence stars are $\sim 40 M_{\odot}$, whit]] indicates that the association is <5 Myr in age.

*NGC* 376.—NGC 376 is a '(blue globular" cluster, similar in structure to LH 111 in the I, MC, although not quite as rich. The main sequence (see Figure 26 of Paper II) extends to $V \sim 14.9$ which is a fainter limit than the other associations. However, the association is comparative] y rich in su pergiants. 'J'here are 9 stars brighter than the tip of the main sequence. The theoretical HR diagram (Figure 27) shows that tile association is probably coeval, since

the supergiants are similar in mass to the most massive main sequence stars. The age of the association is approximately 10 M yr.

*NGC* 456, NGC 460 *and NGC 465.*---NGC 456, 460 and 465 form a star-forming complex southeast of the main body of the SMC. 'J'ester and Lortet (1987) and Lortet and Tester (1 988) have suggested that NGC 456,460 and 465 arc an example of sequential star formation, with NGC 456 being the youngest in the sequence. This hypothesis is based primarily on the increasing amount of nebulosity and stellar density in going from NGC 465 to NGC 460 to NGC 456.

The colour excesses for the three associations increase with the increasing nebulosity from NGC 465 to NGC 456, but the CM diagrams (see Figure 27–29 of Paper 11) and the theoretical HR diagrams (Figures 28–30) do not necessarily support the sequential star formation hypothesis. There are two evolved supergiants in NGC 456 which apparently have masses of 12–15$M_{\odot}$. These stars are less massive than the most massive main sequence stars in all three associations (all three contain stars in the 25–40$M_{\odot}$ mass range). It seems more likely that star formation has occurred simultaneously in each region.

## VI. COMPARISON WITH OTHER WORK

### *a) The Magellanic Clouds*

Early investigations of the IMF of the Magellanic Clouds were made by Lequeux (1 979a), Lequeux *et al. (1980),* Dennefeld and Tammann (1980), Vangioni-Flam (1980) and Humphreys and McElroy (1984). Scalo (1986, 1987) has comprehensively reviewed the status of our knowledge of the IMF up to 1985. The primary result of these studies is that the IMF for the most massive stars in the Magellanic Clouds is similar to the Galactic massive star IMF. However, these studies were limited to only the very brightest stars (based primarily on the surveys of

Sanduleak (1968,1969), Azzopardi and Vigneau (1975,1977), Fehrenbach *et al.* (1976), Martin *et al.* (1976), and Rousseau *et al.* (1978)). Most of these stars are supergiant and hence he uncertainties in the masses of these stars are large. It is also very difficult o interpret he PDMFs obtained in these studies, due to the effects of evolution.

More recently, several investigators have attempted to derive the slope of the IMF by studying individual clusters and associations in the Magellanic Clouds. The interpretation of the PDMFs is much simpler in these cases, if still somewhat uncertain. The mass range studied is also greater because the observations extend to fainter (lower mass) stars.

Mateo (1988) has used UBV photometry of six young clusters in the Magellanic Clouds to derive luminosity functions and subsequently mass functions. The luminosity functions were converted to mass functions using mass-luminosity relations derived from theoretical evolutionary models. Mateo finds that the IMFs of all six clusters arc similar and the average slope is $\Gamma = -2.52 \pm 0.16$ for $0.9 M_{\odot} \leq M \leq 10.5 A4_{0}$. He also found some evidence that the slope of the IMF is shallower at the high mass end, ranging from -1.6 to -2.1 for $M > 3 M_{\odot}$. Although this slope is similar to the value obtained here for $M \geq 9 M_{\odot}$, there is evidence that the slope of the IMF decreases at lower masses, in conflict with Mateo's result. Further study is required to resolve this issue.

Lee (1990) has followed Mateo's work by deriving the IMF for 15 Magellanic Cloud 1111 regions and young clusters. The method employed is the same as that used by Mateo (1988). Lee finds that the slopes of the individual IMFs vary from $\Gamma = -1.0$ to $\Gamma = -2.8$. The average value of the IMF for the objects studied is $\Gamma = -1.7 \pm 0.5$ over the range $3 M_{\odot} \leq M \leq 100 M_{\odot}$. This result agrees well with the IMF slope obtained here, despite the fact that very different methods were used to derive the mass functions.

Cayrel *et al.* (1988) have derived the IMF of the compact young cluster NGC 330 in the SMC. This cluster is the brightest of the "blue globular" clusters in the SMC, and was also included in the objects studied by Mateo (1988) and Lee (1990). Cayrel *et al.* find $\Gamma = -1.2$ for stars in the magnitude range $15.0 < V < 18.0$ (this should correspond to a mass range of approximately $5 - 12 M_{\odot}$). In contrast, Mateo finds $\Gamma = -2.4 \pm 0.7$ for $2.5 M_{\odot} < M < 11 M_{\odot}$, while Lee finds $\Gamma = -2.1 \pm 0.5$ for the range $6 M_{\odot} < M < 10 M_{\odot}$. All three studies used a mass-luminosity relation to derive the mass functions, although different evolutionary models were used in each case. The wide range of slopes found is a reflection of the large uncertainties which are associated with the calculations and interpretations of the data.

Massey and collaborators (Conti *et al. 1986,* Garmany *et al. 1987,* Massey *et al.* 1989a,b, Parker *et al.* 1992) have recently undertaken a large scale study of the most massive stars in the Magellanic Clouds with the ultimate goal of determining the shape of the IMF. These authors have obtained spectra of the brightest stars in order to place them in the theoretical HR diagram, while using photometry for the fainter stars. The IMF was derived by using the evolutionary tracks (Maeder and Meynet 1988) which were used here. They find that the slope of the IMF is $\Gamma = -1.8 \pm 0.1$ for the combined data for two LMC associations (LH 117 and LH 118, Massey *et al.* 1989a), $\Gamma = -1.8 \pm 0.2$ for NGC 346 in the SMC (Massey *et al.* 1989b), and $\Gamma = -1.6 \pm 0.1$ and $\Gamma = -1.1 \pm 0.1$ for the two adjacent associations LH 9 and 10, respectively, in the LMC (Parker *et al.* 1992). These slopes apply to stellar masses $M > 9 M_{\odot}$. The range of slopes found for the associations studied by Massey and collaborators fall within the range of slopes found in this study.

### *b) The Galaxy*

The work of Salpeter (1955) was the first effort to derive the IMF for field stars in the solar

neighbourhood. The 1 M F for massive stars in the solar neighbourhood has since been studied by Miller and Scalo (1979), Lequeux (1979b), Claudius and Grosbøl (1980), Garmany *et al.* (1982), Tarrab (1982), Humphreys and McElroy (1984), Vanbeveren (1984) and Van Buren (1985), among others. Some investigators have attempted to derive the IMF from studies of field stars, while others have studied young open clusters and associations. The results of all these studies have been thoroughly reviewed by Scalo (1986). Scalo concludes that the results are consistent with an IMF slope of $\Gamma \sim -1.7$ for $2M_{\odot} < M < 10M_{\odot}$. The slope at higher masses is very uncertain, and although it probably lies within the range $-2.4 \leq \Gamma \leq -1.3$, there is no reason to prefer any particular value within this range. The results obtained here ($\Gamma = -2.0 \pm 0.5$) imply that the IMF for massive stars in the Magellanic Clouds is indistinguishable from that in the Galaxy.

More recently, Rana (1987) has derived the IMF for the solar neighbourhood using a luminosity function formed from the data of Gilmore and Reid (1983), Eaton *et al.* (1984), Gilmore *et al.* (1985), and Robin and Crézé (1986) and scale heights for main sequence disk stars. Rana finds a slope of $\Gamma = -1.8$ for $M > 1.5M_{\odot}$, in good agreement with our result.

As discussed in §II, Blaha and Humphreys (1989) have compared the luminosity functions of the Galaxy, the LMC, and SMC. These investigators have also used these data to derive the IMF for the most massive stars in the three galaxies. The evolutionary tracks of Maeder and Meynet (1987) were used to generate the mass functions. Blaha and Humphreys find the slope of the IMF to be $\Gamma = -2.2 \pm 0.5$ for the Galaxy, $\Gamma = -1.9 \pm 0.5$ for the LMC, and $\Gamma = -2.0 \pm 0.9$ for the SMC. These slopes apply to masses in the range $25M_{\odot} < M < 85M_{\odot}$. They also found that, if data from the 30 Dor region of the LMC were included, the slope of the IMF decreased to $\Gamma = -1.5 \pm 0.4$. However, this result is questionable, due to possible incompleteness of the

lower mass stars in the 30 Dor region.

## VII. CONCLUSIONS

We have used UBV photometry of OB associations in the LMC and SM C to derive luminosity and mass functions for the most massive stars in the associations. Our major conclusions arc:

(1) The slope of the main sequence *luminosity function* appears to be universal in the range $-4.0 \leq M_V \leq -1.0$ mag, having a value of $s_{ms} = 0.30$ over this range in luminosity, with very little variation among associations. Furthermore, the luminosity functions for the sets of LMC and SMC associations arc similar, indicating that this part of the luminosity function can only be weakly dependent on metal abundance, which differs between these two galaxies.

(2) The slope of the main sequence luminosity *function* in the range $-4.0 \leq M_V \leq -1.0$ mag is significantly shallower than the luminosity function at higher luminosities. The slope of $s_{ms} = 0.30$ is much smaller than the value ofs $\sim 0.7$ found by Freedman (1985) and Blaha and Humphreys (1989) for brighter stars ($M_V < -5$ mag). The most likely reason for this difference is that the brighter stars consist primarily of a mixed and more highly evolved population.

(3) The slope of the IMF is 1' = -2.0+ 0.5 for masses $M > 9 M_\odot$. The IMFs were derived by comparing the positions of stars in the $(M_{bol}, \log(T_{eff}))$ plane with the theoretical evolutionary tracks of Maeder and Meynet (1988). There is no significant evidence for any variation of the IMF among the associations. The slope of the IMF is similar in both the LMC and SMC associations, and hence the IMF for massive stars ($9 \leq M \leq 60 M_\odot$) is also not strongly dependent on metallicity. The slope of the IMF found here agrees wc]] with other recent determinations of IMF slope in both the Galaxy and the Magellanic Clouds.

(4) '1'here is some evidence that the slope of tile IMF is flatter for $M < 10 M_\odot$ than it is

for higher mass tars. The slope of the IMF appears to change at $M \sim 10 M_{\odot}$ for many of the associations. The evidence indicates that the data should not be suffering from incompleteness until much lower masses and that systematic errors which tend to flatten the derived mass functions are not significant for the stars above $\sim 5 M_{\odot}$. Unfortunately, this leaves only a small range in mass on which to base this apparent decrease in the IMF slope. Further work will be necessary to verify this change in slope one way or the other.

BFM was supported in part by the Jet l'repulsion laboratory, California institute of Technology, under the sponsorship of the Astrophysics Division of *NASA's* Office of Space Science and Applications. WLF's research is supported in part by NSF Grant AST 87-13889.

Table 1

Luminosity Functions for LMC Associations

| | $\log(\Phi_V)$ | | | | | | |
|---|---|---|---|---|---|---|---|
| $V$ | LH 4 | LH 54 | 1.1158 | LH 83 | 1.1187 | 1.1193 | LH 111 |
| *10.25* | ... | ... | 0.00 | ... | ... | 0.00 | ... |
| *10.75* | 0.00 | ... | ... | ... | ... | ... | 0.00 |
| *11.25* | ... | 0.00 | ... | ... | ... | ... | 0.30 |
| 11.75 | ... | ... | 0.00 | 0.00 | 0.30 | 0.48 | 0.48 |
| 12.25 | 0.00 | 0.00 | 0.00 | ... | 0.00 | 0.48 | 0.30 |
| 12.75 | 0.30 | 0.30 | ... | 0.30 | 0.00 | 0.78 | 0.85 |
| 13.25 | 0.30 | 0.30 | 0.60 | 0.48 | 0.48 | 0.60 | 0.60 |
| 13.75 | 0.48 | 0.48 | 0.48 | 0.60 | 0.95 | 0.90 | 1.04 |
| 14.25 | 0.48 | 0.48 | 0.85 | 0.30 | 0.85 | 1.20 | 1.30 |
| 14.75 | 0.78 | 0.85 | 0.48 | 0.60 | 0.85 | 1.00 | 1.59 |
| 15.25 | 0.85 | 0.85' | 1.08 | 0.90 | 0.95 | 1.26 | 1.67 |
| 15.75 | 1.11 | 1.30 | 1.34 | 1.04 | 1.04 | 1.46 | 1.71 |
| 16.25 | 1.08 | 1.15 | 1.65 | 1.15 | 1.34 | 1.59 | 1.76 |
| 16.75 | 1.45 | 1.43 | 1.59 | 1.18 | 1.41 | 1.54 | 1.93 |
| 17.25 | 1.36 | 1.38 | 1.70 | 1.45 | 1.60 | 1.77 | 1.64 |
| 17.75 | 1.62 | 1.43 | 1.66 | 1.45 | 1.63 | 1.85 | 1.28 |
| 18.25 | 1.58 | 1.49 | 1.77 | 1.62 | 1.91 | 1.76 | 0.00 |
| 18.75 | 1.80 | 1.46 | 1.90 | 1.52 | 1.69 | 1.28 | ... |
| 19.25 | 1.68 | 1.54 | 1.84 | 1.51 | 0.48 | 0.00 | ... |
| 19.75 | 1.08 | 1.36 | 1.34 | 0.78 | ... | ... | ... |
| 20.25 | 0.48 | 0.70 | 0.78 | 0.00 | ... | ... | ... |

Table 2

Luminosity Functions for SMC Associations

| | $\log(\Phi_V)$ | | | | | | |
|---|---|---|---|---|---|---|---|
| $V$ | N 24 | NGC 249 | NGC 261 | NGC 376 | NGC 456 | NGC 460 | NGC 465 |
| 11.75 | ... | ... | 0.00 | ... | ... | ... | 0.30 |
| 12.25 | ... | 0,00 | ... | 0.00 | 0.00 | 0.00 | ... |
| 12.75 | ... | ... | 0.00 | 0.00 | 0.00 | ... | 0.00 |
| 13.25 | 0.00 | ... | 0.30 | ... | ... | ... | 0.30 |
| 13.75 | ... | 0.30 | 0.30 | ... | 0.00 | ... | 0,00 |
| 14.25 | 0.85 | 0.00 | 0.00 | 0.30 | 0.70 | 0.60 | 0.85 |
| 14.75 | 0.60 | 0.48 | 0.70 | 1.00 | 0.48 | 0.90 | 1.04 |
| 15.25 | 0.90 | 0.90 | 0.78 | 0.85 | 0.30 | 0.85 | 1.00 |
| 15.75 | 0.85 | 0.78 | 1.15 | 1.23 | 0.95 | 1.18 | 1.18 |
| 16.25 | 1.43 | 1.08 | 1.36 | 1.36 | 1.04 | 0.90 | 1.23 |
| 16.75 | 1.48 | 1.45 | 1.40 | 1.52 | 1.20 | 1.41 | 1.34 |
| 17.25 | 1.68 | 1.45 | 1.48 | 1.60 | 1.20 | I ,34 | 1.38 |
| 17.75 | 1.99 | 1.64 | 1.61 | 1.76 | 1.30 | 1.40 | 1.69 |
| 18.25 | 2.03 | 1.71 | 1.90 | 1.82 | 1.45 | 1.56 | 1.58 |
| 18.75 | 1.46 | 0.30 | 1.79 | 1.87 | 1.45 | 1.76 | 1.69 |
| 19.25 | 0.48 | 0.30 | 1.11 | 1.52 | 1.36 | 1.81 | 1.85 |
| 19.75 | ... | ... | ... | 0.30 | 0.85 | 1.54 | 1.72 |
| 20.25 | ... | ... | ... | ... | ... | 0.85 | 1.18 |
| 20.75 | ... | ... | ... | ... | ... | ... | 0.30 |

Table 3

Luminosity Function Slopes

| | Range | s | $s_{ms}$ |
|---|---|---|---|
| LMC LH 4 | $12.0 < V_o \leq 19.0$ | 0.25+ 0.04 | 0.31 ± 0.22 |
| 1,1154 | $12.0 < V_o \leq 18.5$ | 0.213, 0.03 | 0.21 ± 0.16 |
| 1,1158 | $13.0 < V_o \leq 19.0$ | 0.24 ± 0.04 | 0.32+ 0.20 |
| 1,1183 | $12.5 < V_o \leq 18.5$ | 0.26 ± 0.04 | 0.26 ± 0.19 |
| LH 87 | $12.0 < V_o \leq 18.5$ | 0.29+ 0.03 | 0.34 ± 0.16 |
| LH 93 | $11.5 < V_o \leq 18.0$ | 0.23+ 0.03 | 0.30+ 0.14 |
| 1,11111 | $10.5 < V_o \leq 17.0$ | 0.29+ 0.03 | |
| SMC N 24 | $14.0 < V_o \leq 18.0$ | 0.40 ± 0.05 | 0.394,0.12 |
| NGC 249 | $13.5 < V_o \leq 18.0$ | 0.38 ± 0.11 | 0.38 ± 0.33 |
| NGC 261 | $12.5 < V_o \leq 18.5$ | 0.35+ 0.04 | 0.23+ 0.23 |
| NGC 376 | $14.0 < V_o \leq 18.5$ | 0.30 ± 0.06 | 0.33 ± 0.11 |
| NGC 456 | $13.5 < V_o \leq 19.0$ | 0.24+ 0.04 | 0.34+ 0.14 |
| NGC 460 | $14.0 < V_o \leq 19.0$ | 0.25+ 0.05 | 0.22 ± 0.14 |
| NGC 465 | $12.5 < V_o \leq 19.5$ | 0.20+ 0.03 | 0.25+ 0.24 |

Table 4

Color/Effective Temperature Conversions

| | |
|---|---|
| $\log(T_{eff}) = 3.991 - 0.324Q + 0.294Q^2$ | $(B - V)_o < 0.00,\ \sigma_U \leq 0.10$ |
| $\log(T_{eff}) = 3.832 - 2.204(B - V)_o$ | $(B - V)_o < -0.12,\ \sigma_U > 0.10$ |
| $\log(T_{eff}) = 3.983 - 0.654(B - V)_o + 2.472\ (B - V)_o^2$ | $-0.12 < (B - V)_o \leq 0.00, \sigma_U > 0.10$ |
| $\log(T_{eff}) = 3.992 - 0.732(B - V)_o + 1.177\ (D - V)_o^2$ | $0.00 < (B - V)_o \leq 0.20$ |
| $\log(T_{eff}) = 3.948 - 0.331(B - V)_o + 0.064(B - V)_o^2$ | $0.20 < (B - V)_o \leq 1.60$ |
| $\log(T_{eff}) = 4.691 - 0.687(B - V)_o$ | $1.60 < (B - V)_o \leq 1.80$ |
| $\log(T_{eff}) = 3.45$ | $(B - V)_o > 1.80$ |

Table 5

Effective Temperature-Bolometric Correction Conversions

| | |
|---|---|
| $BC = 23.39 - 5.901 \log(T_{eff})$ | $\log(T_{eff}) \geq 4.00$ |
| $BC = 18.01 - 4.587 \log(T_{eff})$ | $3.9 < \log(T_{eff}) < 4.00$ |
| $BC = -137.1 + 70.88 \log(T_{eff}) - 9.150(\log(T_{eff}))^2$ | $3.72 < \log(T_{eff}) \leq 3.90$ |
| $BC = -564.9 + 303.3 \log(T_{eff}) - 40.73 (\log(T_{eff}))^2$ | $\log(T_{eff}) \leq 3.72$ |

'1'able 6

Mass Functions for LMC Associations

| Mass Range | $\log(\xi(\log M))$ | | | | | | |
|---|---|---|---|---|---|---|---|
| *(MO)* | LH 4 | 1,1154 | LH 58 | 1,1183 | 1,1187 | LH 93 | LH 111 |
| 2.5-3 | 2.74 | 2.68 | 2.85 | 2.50 | 2.73 | 2.55 | ... |
| 3-5 | 2.62 | 2.45 | 2.77 | 2.45 | 2.67 | 2.53 | 2.31 |
| 5-7 | 2.44 | 2.35 | 2.71 | 2.31 | 2.48 | 2.74 | 2.62 |
| 7-9 | 2.38 | 2.39 | 2.62 | 2.19 | 2.38 | 2.52 | 2.76 |
| 9-12 | 2.35 | 2.33 | 2.51 | 1.94 | 2.32 | 2.51 | 2.89 |
| 12-15 | 1.86 | 2.16 | 2.16 | 2.06 | 1.86 | 2.46 | 2.66 |
| 15-25 | 1.26 | 1.65 | 1.88 | 1.65 | 2.03 | 2.20 | 2.37 |
| 25-40 | 1.29 | 0.69 | 1.17 | 1.39 | 1.64 | 1.99 | 1.92 |
| 40-60 | . . . | 1.06 | 0.75 | 1.23 | 1.36 | 1.60 | 1.06 |
| 60-85 | 0.82 | ... | ... | ... | 0.82 | 1.52 | ... |

'l'able 7

Mass Functions for SMC Associations

| Mass Range | $\log(\xi(\log M))$ | | | | | | |
|---|---|---|---|---|---|---|---|
| $(M_\odot)$ | *N 24* | NGC 249 | NGC 261 | NGC 376 | NGC 456 | NGC 460 | NGC 46.5 |
| 2.5-3 | 2.48 | 2.22 | 2.67 | 2.78 | 2.33 | 2.84 | 2.80 |
| 3-5 | 2.65 | 2.45 | 2.71 | 2.69 | 2.32 | 2.65 | 2.71 |
| 5-7 | 2.87 | 2.43 | 2.59 | 2.72 | 2.30 | 2.39 | 2.67 |
| 7-9 | 2.62 | 2.22 | 2.14 | 2.56 | 2.04 | 2.42 | 2.54 |
| 9-12 | 2.47 | 2.28 | 2.38 | 2.46 | 2.18 | 2.30 | 2.43 |
| 12-15 | 2.19 | 1.97 | 2.13 | 2.34 | 1.92 | 2.24 | 2.19 |
| 15-25 | 1.65 | 1.70 | 1.80 | 1.50 | 1.80 | 1.70 | 1.73 |
| 25-40 | 0.69 | 0.69 | 1.39 | ... | ... | 0.69 | 1.39 |
| *40-00* | ... | *0.75* | *0.75* | ... | *0.75* | *0.75* | *0.75* |

"J'able 8

Mass Function Slopes

| | | 1'(M > 9$M_\odot$) | I'1 | Mass Range($M_\odot$) |
|---|---|---|---|---|
| LMC | LH 4 | *–2.07 ± 0.31* | –1.26 ± 0.13 | $3 \leq M \leq 85$ |
| | LH 54 | *–2.50 ± 0.38* | –0.93 ± 0.14 | $3 \leq M \leq 60$ |
| | LH 58 | –2.47 ± 0.31 | –1.193-0.11 | $3 \leq M \leq 60$ |
| | 1,1183 | --1.234.0.36 | --1.0940.13 | $3 \leq M \leq 60$ |
| | 1,1187 | --1.413 0.23 | –1.10 ± 0.09 | $3 \leq M \leq 85$ |
| | 1,1193 | --1.21 ± 0.17 | --1.0630.10 | $3 \leq M \leq 85$ |
| | LH 111 | –2.00 ± 0.19 | –2.00 ± 0.19 | $9 \leq M \leq 60$ |
| SMC | N 24 | –3.21 :1:0.44 | –2.22 ± 0.19 | $5 \leq M \leq 40$ |
| | NGC 249 | –2.44 ± 0.35 | –1.16 ± 0.14 | $3 \leq M \leq 60$ |
| | NGC 261 | --2.174:0.31 | –1.30 ± 0.11 | $3 \leq M \leq 60$ |
| | NGC 376 | –2.96± 0.63 | –0.84 ± 0.14 | $3 \leq M \leq 25$ |
| | NGC 456 | –1.79 ± 0.39 | –0.87 4:0.15 | $3 \leq M \leq 60$ |
| | NGC 460 | -2.533:0.35 | –1.24 4:0.12 | $3 \leq M \leq 60$ |
| | NGC 465 | --2.364:0.31 | –1.21 ± 0.11 | $3 \leq M \leq 60$ |

## REFERENCES


Ardeberg, A., & Maurice, E. 1977, A & AS, 30,261

Azzopardi, M., & Vigneau, J. 1975, A & AS, 22,285

Azzopardi, M., & Vigneau, J. 1977, A & A, 56, 151

Bertelli, G., Bressan, A. G., & Chiosi, C. 1984, A & A, 130, 279

Bertelli, G., Bressan, A. G., & Chiosi, C. 1985, A & A, 150, 33

Blaha, C., & Humphreys, R. M. 1989, AJ, 98, 1598

Böhm-Vitense, E. 1981, ARAA,19, 295

Brunish, W. M., & Truran, J. W. 1982, ApJS, 49, 447

Butcher, 11.1977, ApJ, 216, 372

Cayrel, R., Tarrab, 1., & Richtler, 'J'. 1988, *ESO* Messenger, No. 54, 29.

Claudius, M., & Grosbøl, I'. J. 1980, A & A, 87, 339

Chiosi, C., Bertelli, G., Bressan, A. G., & Nasi, E. 1986, A & A, 165,84

Chiosi, C., & Maeder, A. 1986, ARAA,24, 329

Chiosi, C., & Pigatto, L. 1986, ApJ, 308, 1

Chu, Y.-11., & Mac Low, M.-M. 1990, ApJ, 365, 510

Conti, 1'. S., Garmany, C. D., & Massey, 1'.1986, AJ, 92, *48*

de Jager, C., Niewenhuijzen, H., & van der Hucht, K. A. 1986, in *IAU Symp. No. 116, Luminous Stars and Associations In Galaxies,* cd. C. W.H.de Loore, A. J. Willis, & P.Laskarides, Dordrecht: Reidel, p 90.

de Jager, C., Niewenhuijzen, 11., & van der Hucht, K. A. 1988, A & AS, 72, 2.59

de Loore, C. 1988, A & A, 203, 71

Dennefeld, M., & Tammann, G. A. 1980, A & A, 83, 275

Dufour, R. J., Shields, G. A., & Talbot, R. J. 1982, ApJ, 225, 461

Dufour, R. J. 1984, in *IA U Symp. No. 108, Structure And Evolution of the Magellanic Clouds,* cd. S. van den Bergh, & K. S. de Boer, Dordrecht:Reidel, p 353.

Eaton, N., Adam, D. J., & Gilts, A. 11.1984, MNRAS, 208, 241

Fehrenbach, Ch., Duflot, M., & Acker, A. 1976, A & AS, 24, 379

FitzGerald, M. 1'.1970, A & A, 4, 234

Flower, 1'. J. 1977, A & A, 54, 31

Freedman, W. 1,. 1983, in *IA U Coil. No. 76, The Nearby Stars And The Stellar Luminosity Function,* cd. A. G. Davis Philip & A. R. Upgren, I,. Davis Press, Inc., p 191.

Freedman, W. J,. 1985, ApJ, 299, 74

Garmany, C. D., Conti, I'. S., & Chiosi, C. 1982, ApJ, 263, 777

Garmany, C. D., Conti, P. S., & Massey, P. 1987, AJ, 93, 1070

Gilmore, G., & Reid, N. 1983, MNRAS, 202, 1025

Gilmore, G., Reid, N., & Hewett, 1'.1985, MNRAS, 213,257

Hardy, E., Buonanno, R., Corsi, C. E., Janes, K. A., & Schommer, R. A. 1984, ApJ, 278, 592

Hill, R., Madore, 13. 1'., & Freedman, W. J,. 1993a, ApJ, submitted (Paper 1)

Hill, R., Madore, B. 1'., & Freedman, W. L. 1993b, ApJ, submitted (Paper II)

Humphreys, R. M., & McElroy, D. B. 1984, ApJ, 284, 565

Lee, M. G. 1990, *Ph.* I). Thesis, University of Washington.

Lequeux, J. 1979a, A & A, 71, 1

Lequeux, J. 1979b, A & A, 80, 35

Lequeux, J., Martin, N., Prévot, 1,., Prévot-Burnichon, M. 1,., Rebeirot, E., & Rousseau, J. 1980, A & A, 85, 305

Lequeux, J., Peimbert, M., Rayo, J. II'., Serrano, A., & Torres-Peimbert, S. 1979, A & A, 80, 155

Lucke, P. 11.1974, ApJS, 28, 73

Maeder, A., & Meynet, G.1982, A & A, 108, 148

Maeder, A., & Meynet, G. 1987, A & A, 182,243

Maeder, A., & Meynet, G. 1988, A & AS, 76, 411

Maeder, A., & Meynct, G. 1989, A & A, 210, 155

Martin, N., Prévot, 1,., Rebeirot, E., & Rousseau, J., 1976, A & A, 51, 31

Massey, 1'., Garmany, C. l)., Silkey, M, & Degioia-Eastwood, I<. 1989a, AJ, 97, 107

Massey, 1'., Parker, J. W., & Garmany, C. D.1989b, AJ, 98, 1305

Mateo, M. 1988, ApJ, 331,261

Mathewson, D. S., & Clarke, J. N. 1973, ApJ, 182, 697

McCall, M. L., Hill, R., & English, J. 1990, AJ, 100, 193

Meylan, G., & Maeder, A. 1982, A & A, 108, 148

Miller, G. E., & Scale, J. M. 1979, ApJS, 41, 513

Parker, J. W., Garmany, C. D., Massey, 1'., & Walborn, N. R. 1992, AJ, 103, 1205

Rana, *N. C.* 1987, A & A, 184, 104

Ratnatunga, K. V., & Bahcall, J. 11.1985, ApJS, 59,63

Robin, A., & Crézé, M. 1986, A & A, 157, 71

Rousseau, J., Martin, N., Prévot, 1,., Rebeirot, E., Robin, A., & Brunet, J. 1'., & 1978, A & AS, 31, 243

Sanduleak, N. 1968, AJ, 73, 246

Sanduleak, N. 1969, AJ, 74, 877

Salpeter, E. E. 1955, ApJ, 121, 161

Scale, J. M. 1986, Fund. Cos. I'hys.,11, 1

Scale, J. M. 1987, in *Starbursts And Galaxy Evolution*, cd. T. T. Thuan, T. Montmerle & J. TranThanh Van, Editions Frontières, p. 445.

Schmidt-Kaler, Th. 1982, in *Landolt-Bornstein, Vol. 2b*, cd. 1{. Schaifers, & 11.11. Vogt, p. 14.

Shull, 1'.1983, ApJ, 275, 592

Tarrab, I. 1982, A & A, 109, 285

Vanbeveren, D. ]984, A & A, ] 39, 545

VanBuren, D. 1985, ApJ, 294,567

Vangioni-Flam, E., Lequeux, J., Maucherat-Joubert, M., & Rocca-Volmerange, B. 1980, A & A, 90, 73

Wang, Q., & Helfand, D. J. 1991, ApJ, 373,497

Westerlund, B. E. 1990, A & A Rev, 2,29

## FI GURE CAPTI ONS

Fig. 1 Luminosity Function for LH 4. The error bars represent $\sqrt{N}$ where $N$ is the number of stars in a given magnitude interval.

Fig. 2- luminosity Function for 1,11 54.

Fig. 3- Luminosity Function for 1,1158.

Fig. 4- Luminosity Function for 1.1183.

Fig. 5 - luminosity Function for 1,1187.

Fig. 6 - luminosity Function for LH 93.

Fig. 7- luminosity Function for LH 111.

Fig. 8-- Luminosity Function for N 24.

Fig. 9-- Luminosity Function for NGC 249.

Fig. 10 – luminosity Function for NGC 261.

Fig. 1– Luminosity Function for NGC 376.

Fig. 2-- luminosity Function for NGC 456.

Fig. 3- Luminosity Function for NGC 460.

Fig. 14- luminosity Function for NGC 465.

Fig. 15-- Theoretical 11 R Diagram for NGC *465*. Filled circles denote stars with the highest quality photometry, open circles represent stars with intermediate precision photometry and plus signs denote stars with the least precise photometry. 'The stars with the best photometry clearly define the main sequence while the stars with poor photometry show the effects of errors in the transformation to the theoretic.al plane (see text for details).

Fig. 16- Theoretical evolutionary tracks of Maeder and Meynet (1 988).

Fig. 17- Theoretical HR Diagram for 1,11 4. The evolutionary tracks shown (from bottom to

top) arc for 2.5, 3, 5, 7, 9, 12,15,25,40,60 and $85 M_{\odot}$. See the text for an explanation of the dashed lines.

Fig. 18 – Theoretical HR Diagram for LH *54*. The evolutionary tracks shown (from bottom to top) arc for 2.5,3,5,7,9,12, 15,25,40,00 and $85 M_{\odot}$. See the text for an explanation of the dashed lines.

Fig. 19 – Theoretical HR Diagram for LH 58. The evolutionary tracks shown (from bottom to top) are for 2.5,3,5, 7,9, ]2, 15,25,40,00 and $85 M_{\odot}$. See the text for an explan nation of the dashed lines.

Fig. 20 – Theoretical HR Diagram for LH 83. The evolutionary tracks shown (from bottom to top) arc for 2.5,3,5,7,9,12, 15,25,40,60 and $85 M_{\odot}$. See the text for an explanation of the dashed lines.

Fig. 21 – Theoretical HR Diagram for LH 87. The evolutionary tracks shown (from bottom to top) arc for 2.5,3,5,7,9,12, 15,25,40,60 and $85 M_{\odot}$. See the text for an explanation of the dashed lines.

Fig. 22 – Theoretical HR Diagram for LH 93. The evolutionary tracks shown (from bottom to top) arc for 2.5,3,5,7,9,12, 15,25,40,60 and $85 M_{\odot}$. See the text for an explan ation of the dashed lines.

Fig. 23- Theoretical HR Diagram for LH 111. The evolutionary tracks shown (from bottom to top) are for 2.5,3,5,7,9,12,15,25,40,,60 and $85 M_{\odot}$. See the text for an explanation of the dashed lines.

Fig. 24- Theoretical HR Diagram for N 24. The evolutionary tracks shown (from bottom to top) arc for 2.5,3,5,7,9,12, 15,25,40,60 and $85 M_{\odot}$. See the text for an explanation of the dashed lines.

Fig. 25- Theoretical HR Diagram for NGC 249. The evolutionary tracks shown (from bottom to top) are for 2.5,3,5,7,9,12, 15,25,40,60 and 85$M_{\odot}$. See the text for an explanation of the dashed lines.

Fig. 26- Theoretical 11 R Diagram for NGC 261. The evolutionary tracks shown (from bottom to top) are for *2.5,3,5, 7,9,12, 15,25,40,60* and 85$M_{\odot}$. See the text for an explanation of the dashed lines.

Fig. 27- Theoretical HR Diagram for NGC 376. The evolutionary tracks shown (from bottom to top) are for 2.5,3,5,7,9,12, 15,25,40,60 and 85 $M_{\odot}$. See the text for an explanation of the dashed lines.

Fig. 28- Theoretical HR Diagram for NGC 456. The evolutionary tracks shown (from bottom to top) are for 2.5,3,5,7,9,12, 15,25,40,60 and 85$M_{\odot}$. See the text for an explanation of the dashed lines.

Fig. 29 – Theoretical HR Diagram for NGC 460. The evolutionary tracks shown (from bottom to top) arc for 2.5,3,5,7,9,12, 15,25,40,60 and 85$M_{\odot}$. See the text for an explanation of the dashed lines.

Fig. 30- Theoretical HR Diagram for NGC 465. The evolutionary tracks shown (from bottom to top) are for 2.5,3,5, 7,9,12, 15,25,40,60 and 85 $M_{\odot}$. See the text for an explanation of the dashed lines.

Fig. 31 - Mass Function for LH 4. The error bars represent $\sqrt{N}$ where $N$ is the number of stars in a given mass bin. The line represents a lca.st-squares fit to the data over the range in masses spanned by the line.

Fig. 32- Mass Function for LH 54.

Fig. 33- Mass Function for 1,1158.

Fig. 34 - Mass Function for 1,11 83.

Fig. 35 - Mass Function for 1,1187.

Fig. 36 – Mass Function for 1,1193.

Fig. 37- Mass Function for 1,11 111.

Fig. 38- Mass Function for N *24*.

Fig. 39- Mass Function for NGC 249.

Fig. 40- Mass Function for NGC 261.

Fig. 41- Mass Function for NGC 376.

Fig. 42- Mass Function for NGC 456.

Fig. 43- Mass Function for NGC 460.

Fig. 44 – Mass Function for NGC 465.

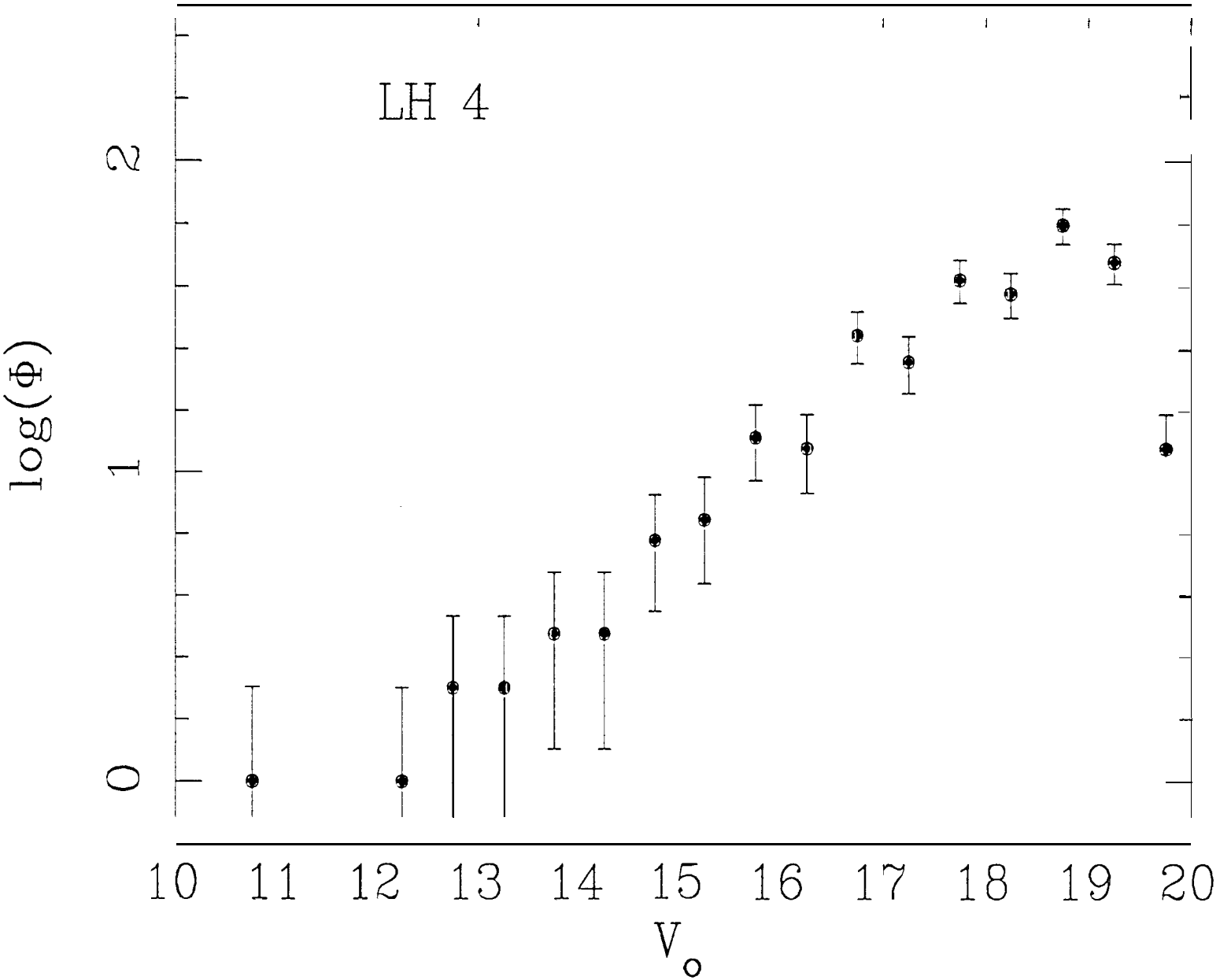
LH 4
log(Φ)
0
1
2
10
11
12
13
14
15
16
17
18
19
20
V_o

Figure 2

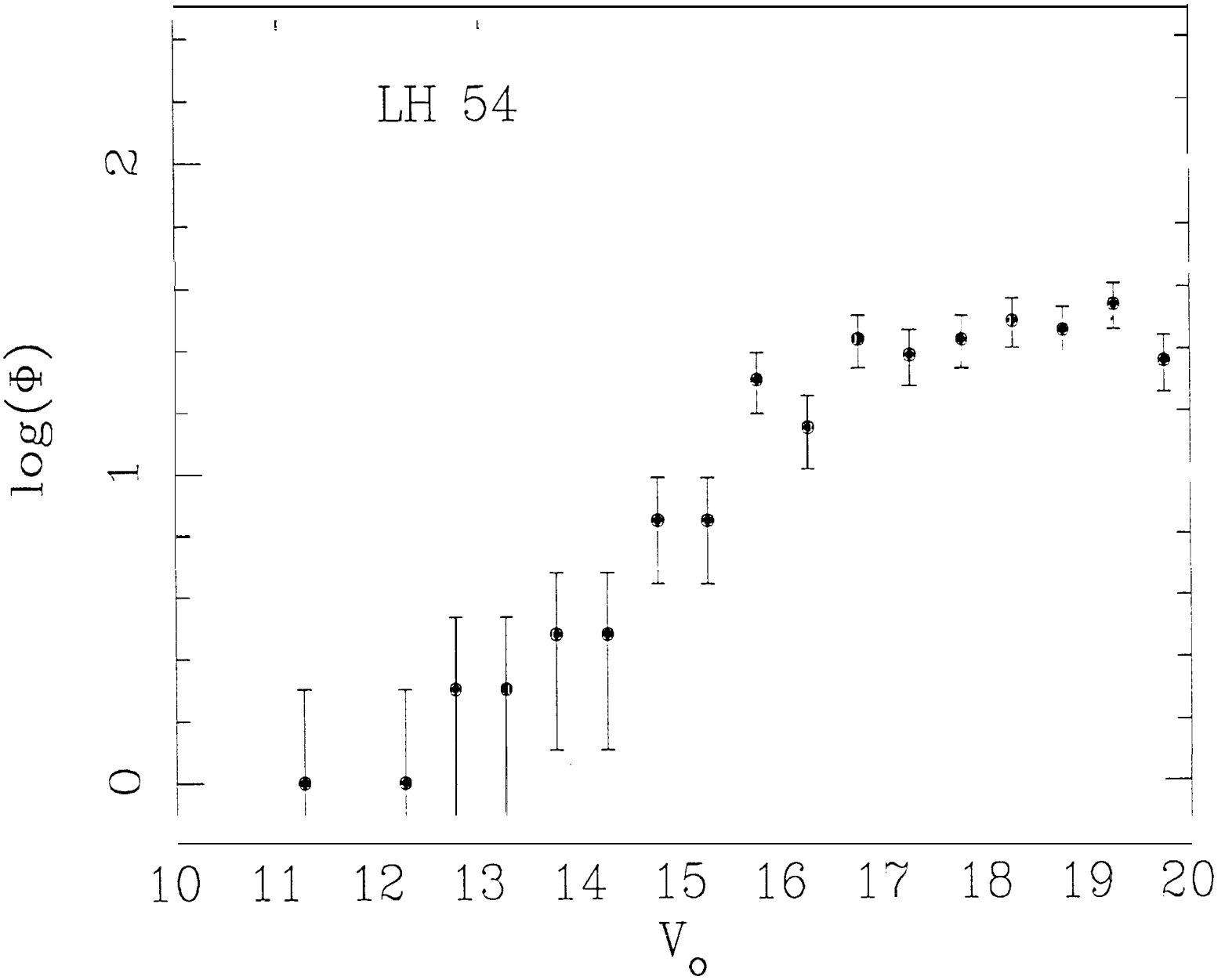

Figure 3

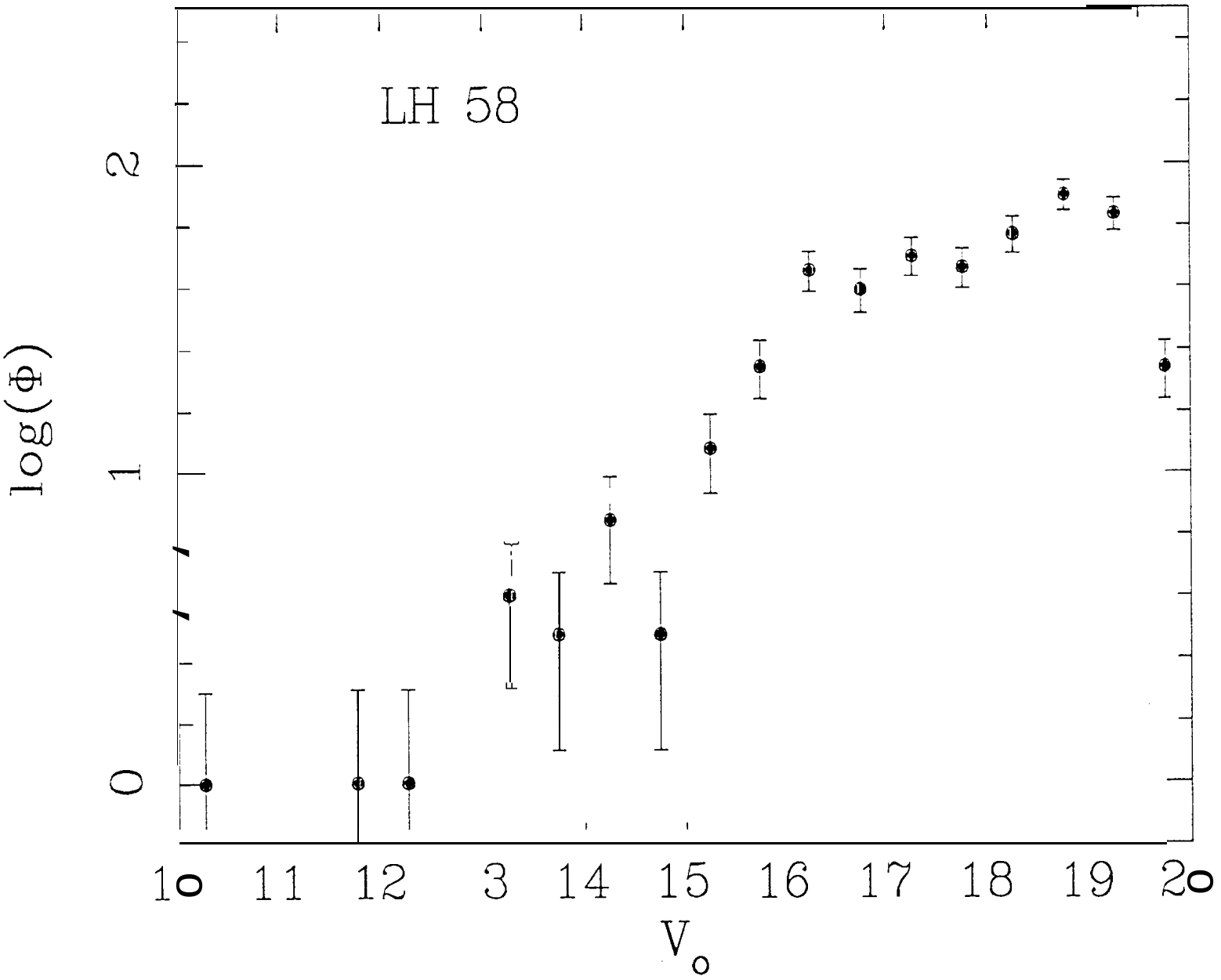

Figure 4

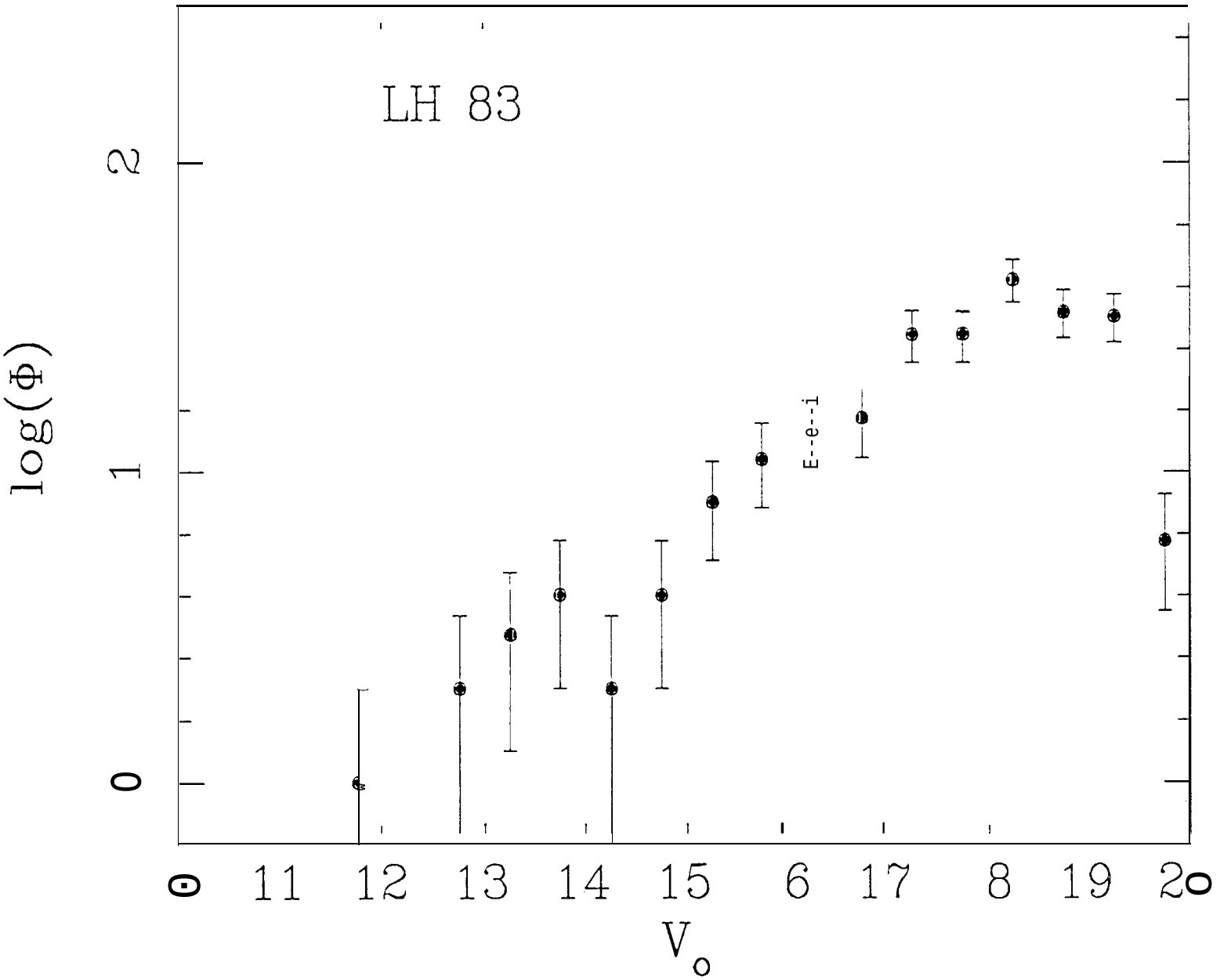

Figure 5

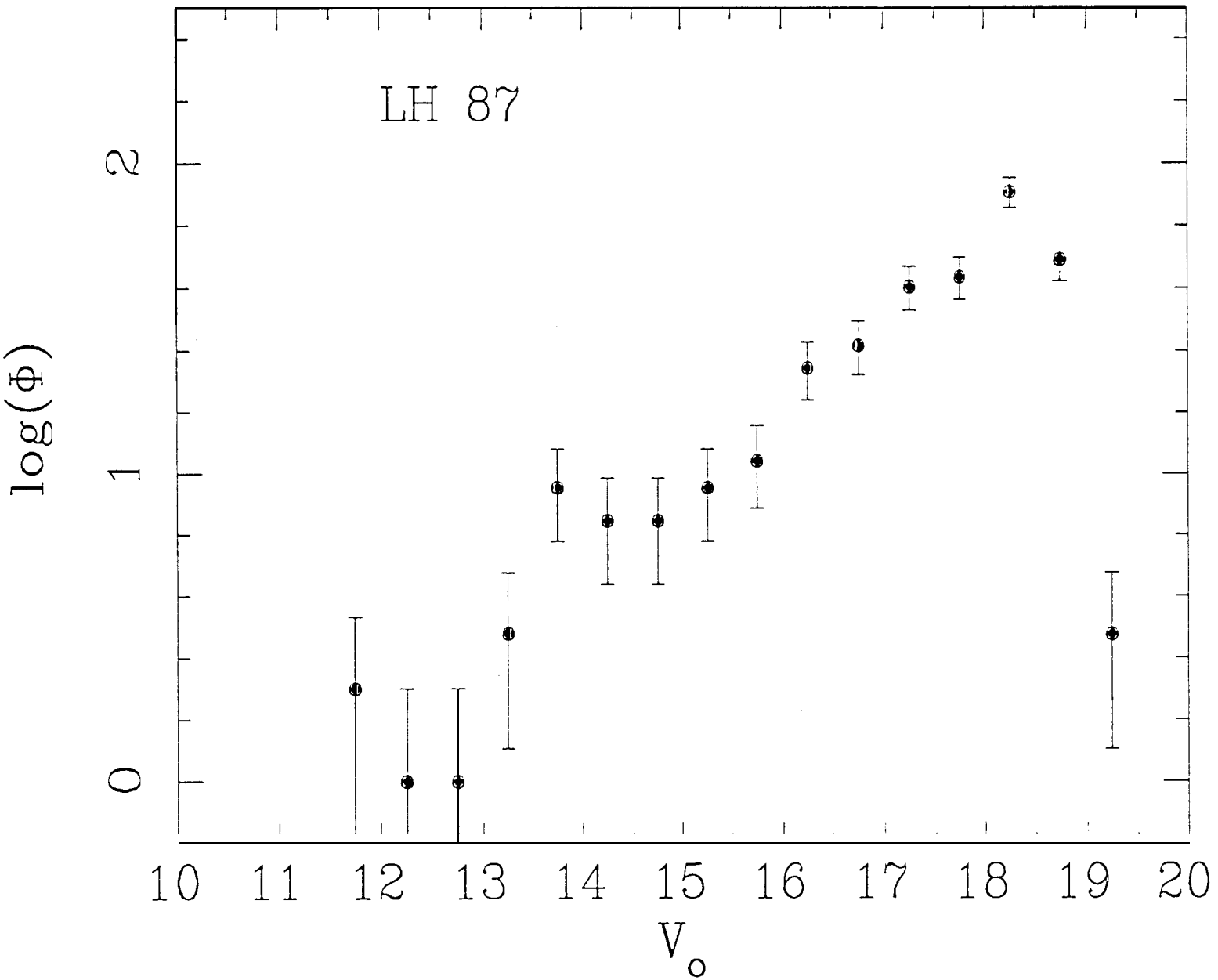

Figure 6

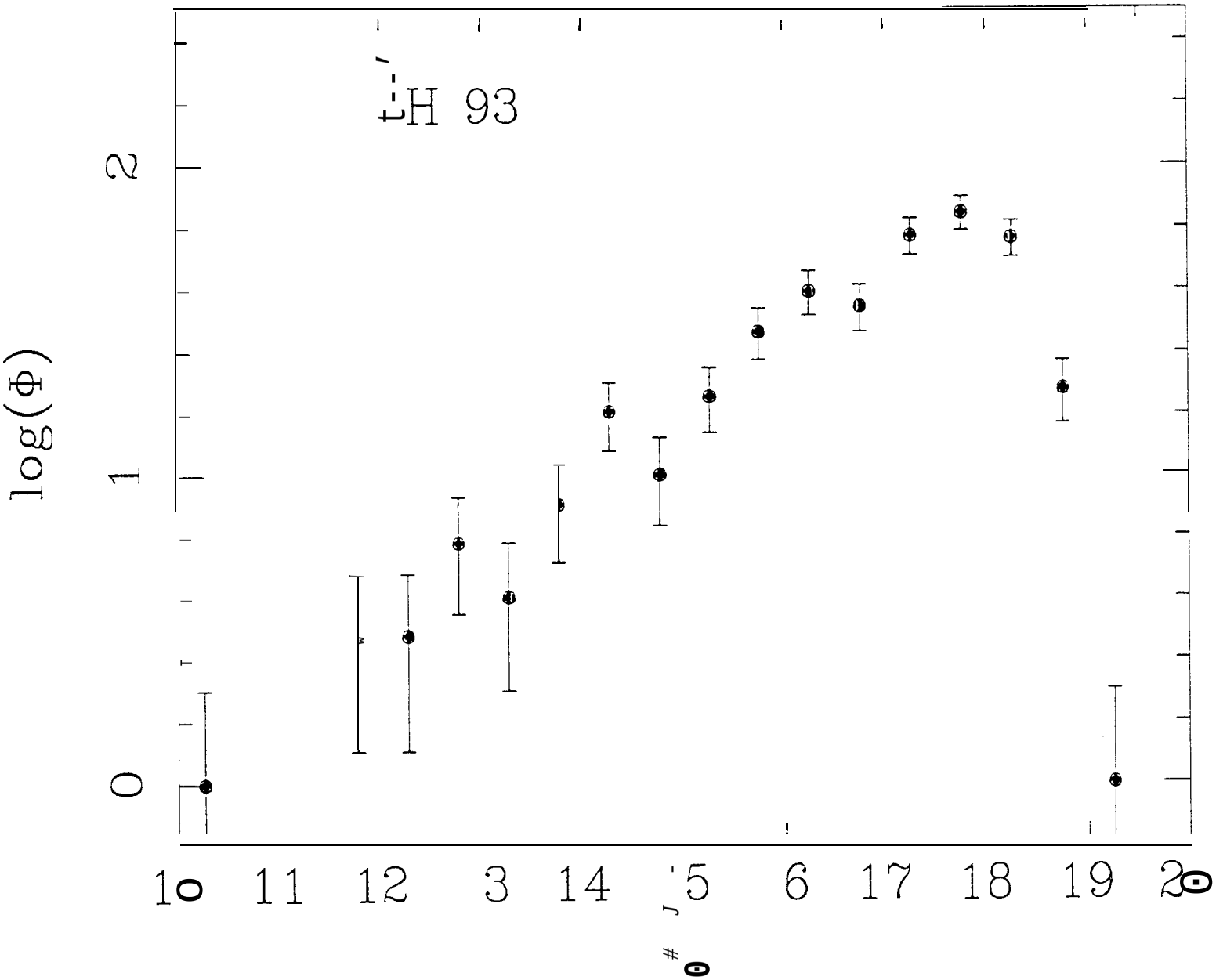

Figure 7

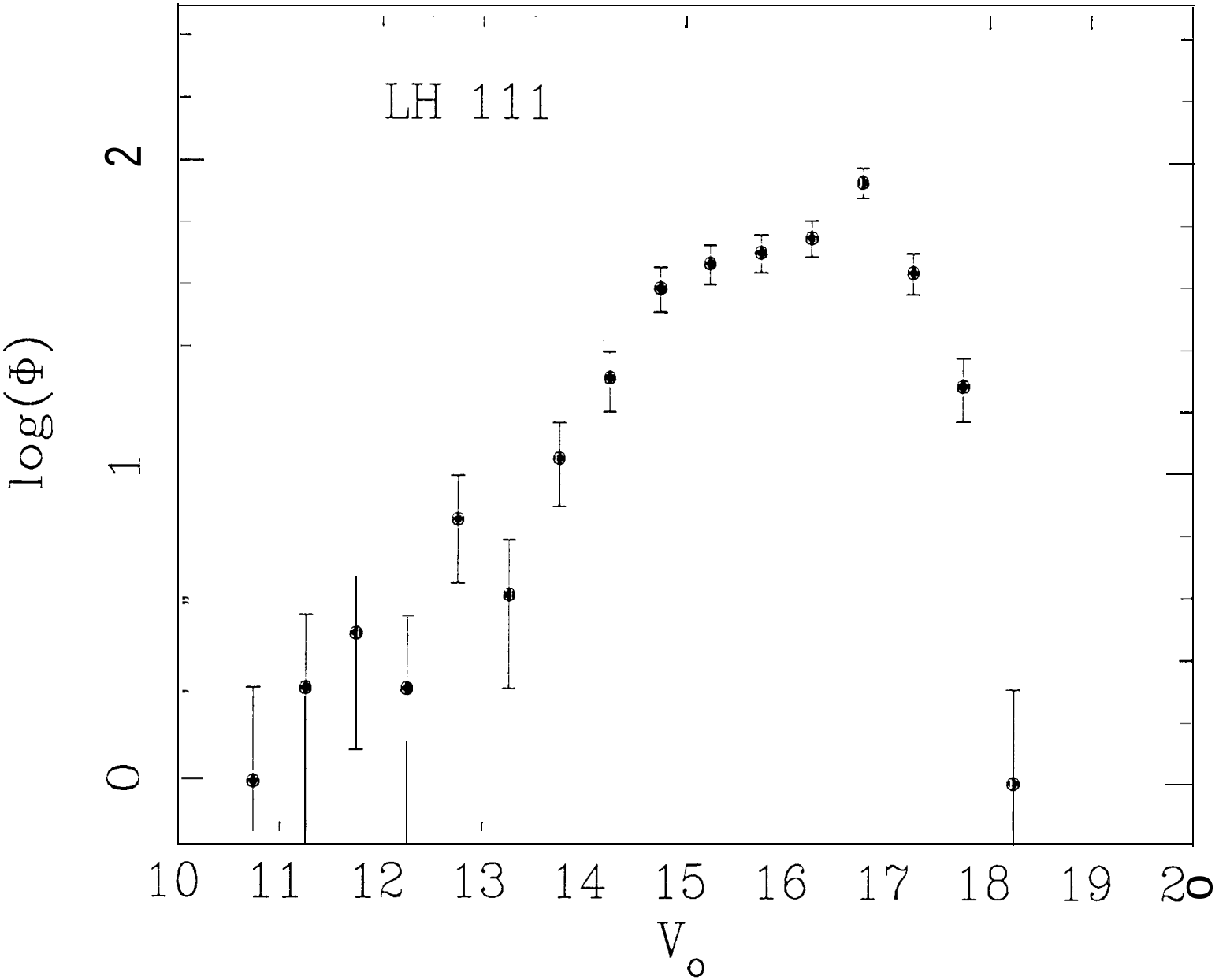

Figure 8

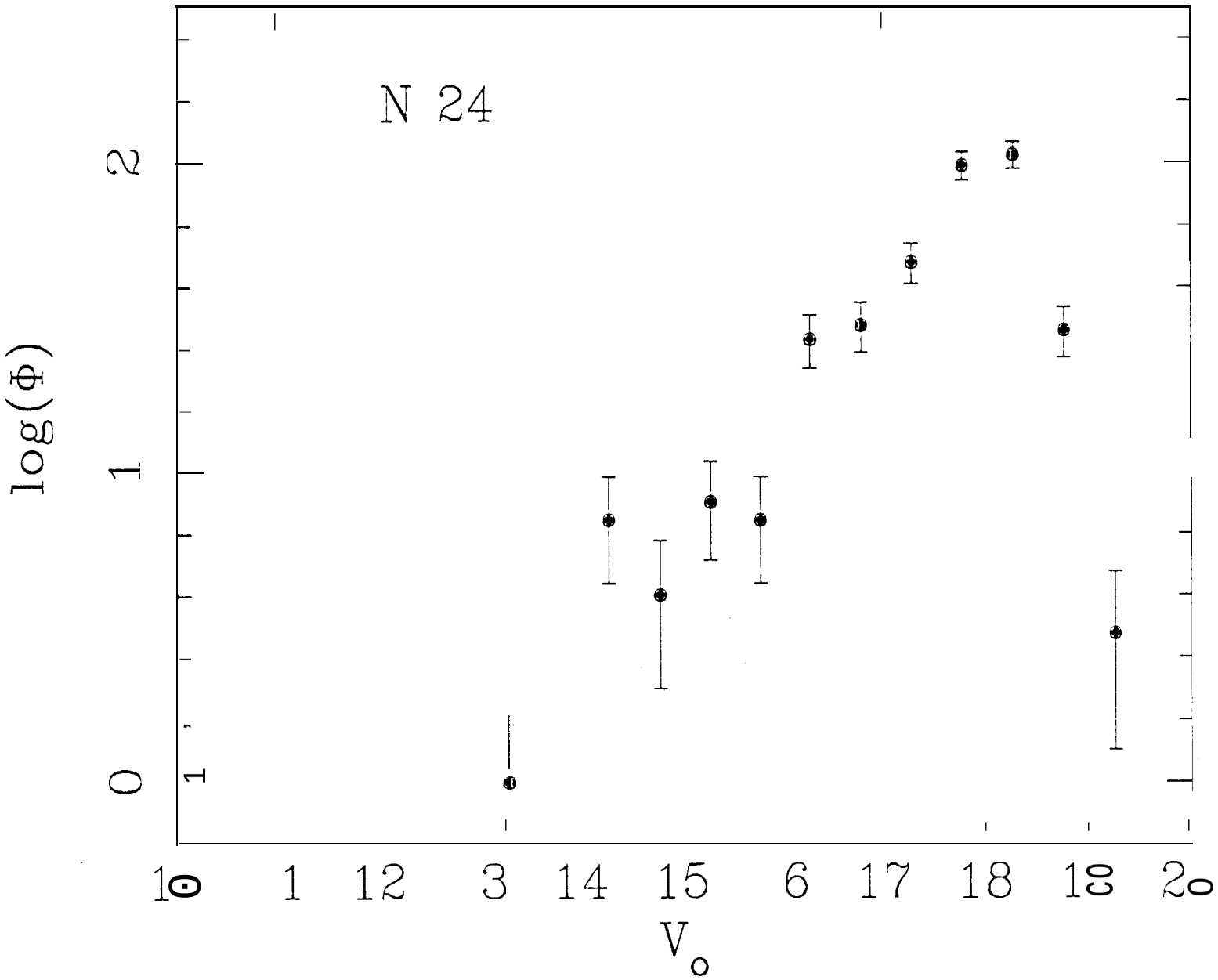

Figure 9

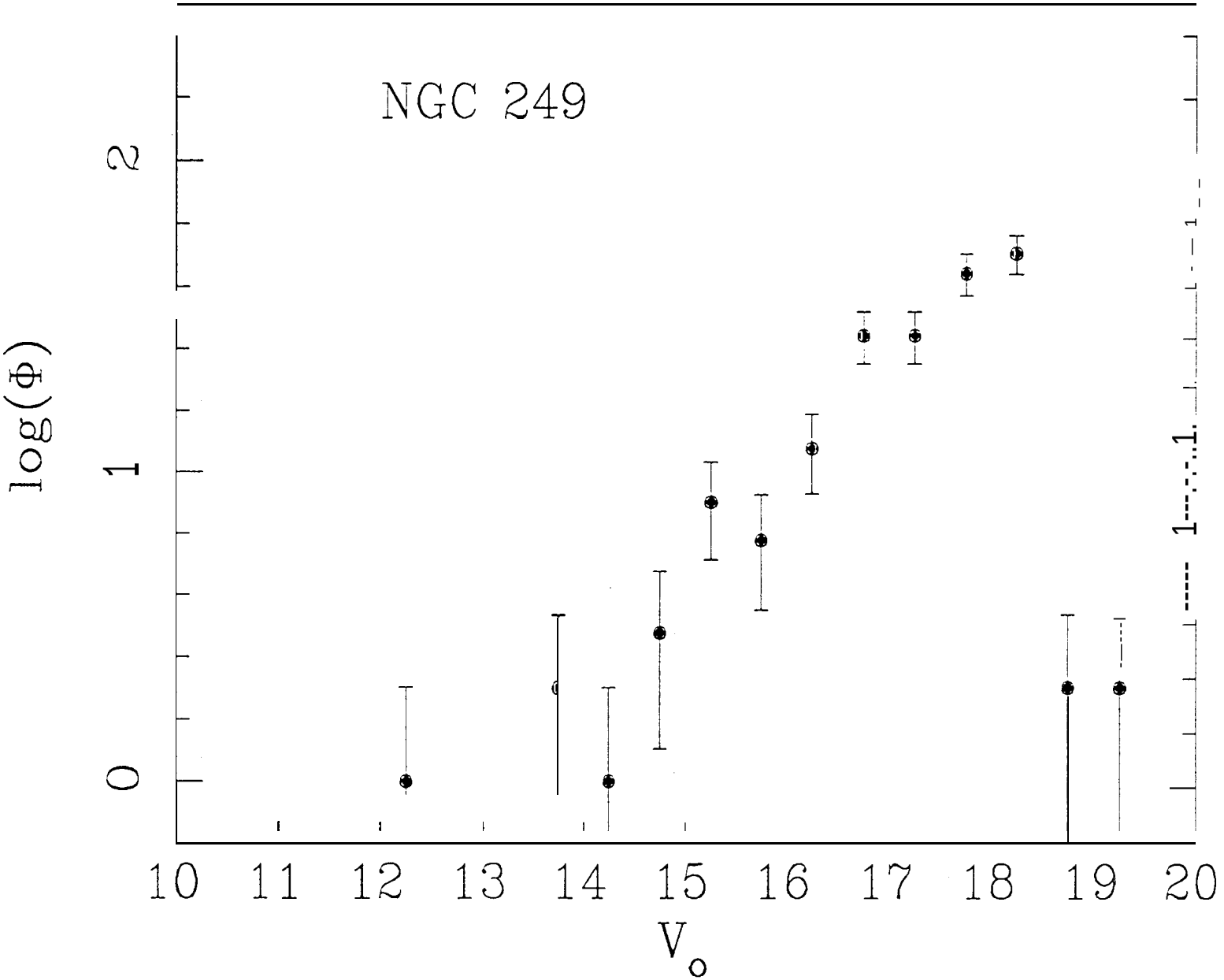

Figure 10

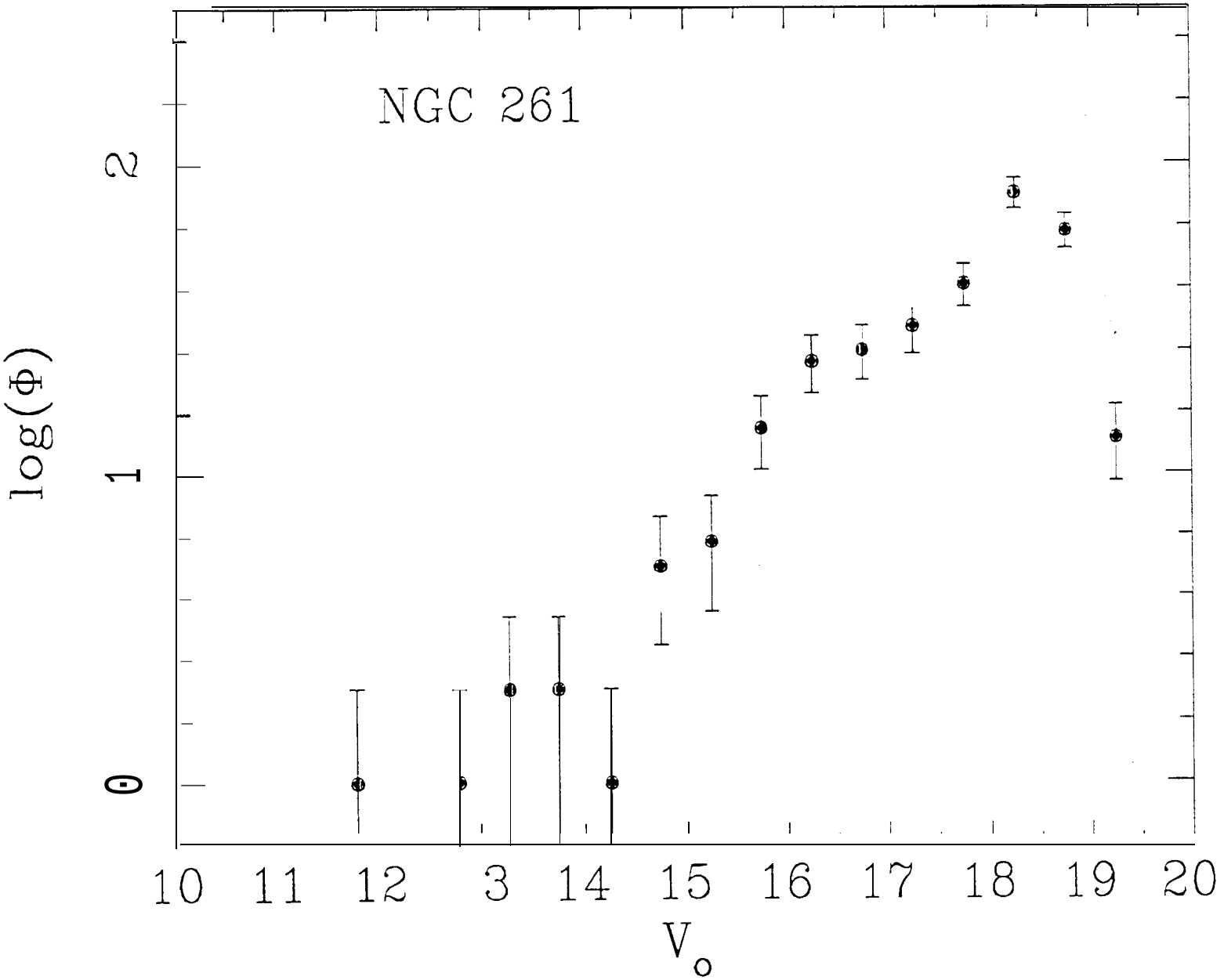

Figure 1

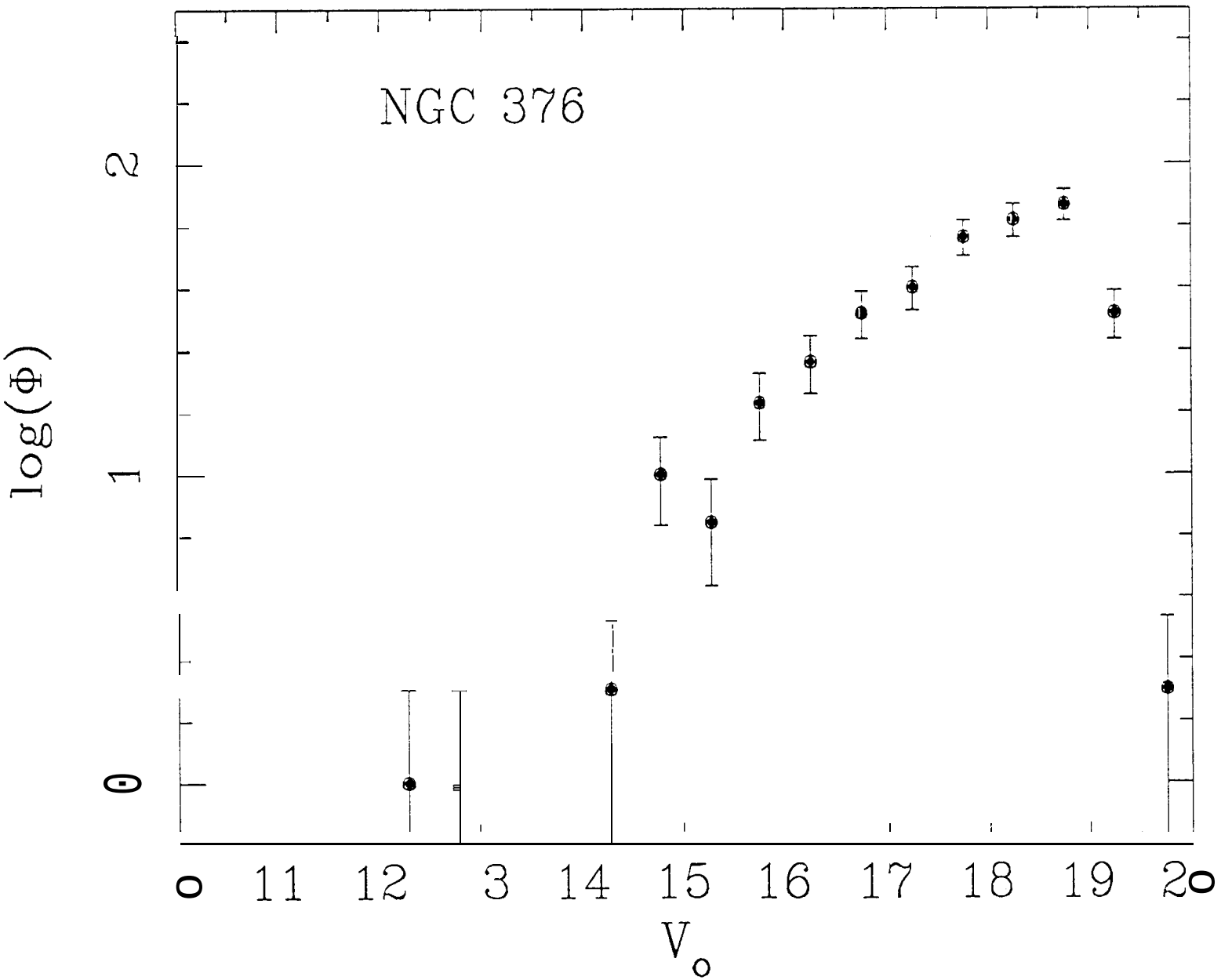

Figure 12

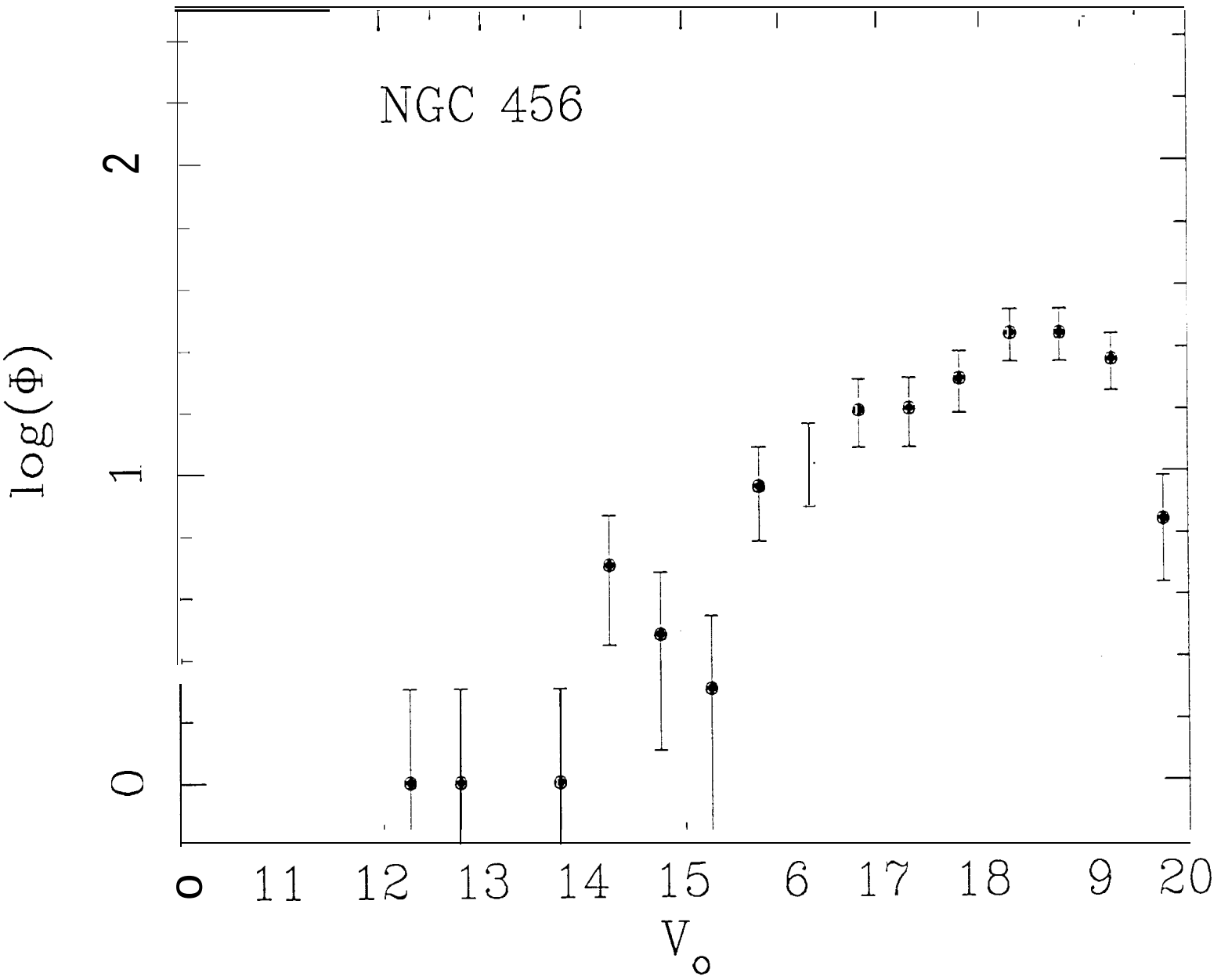

Figure 13

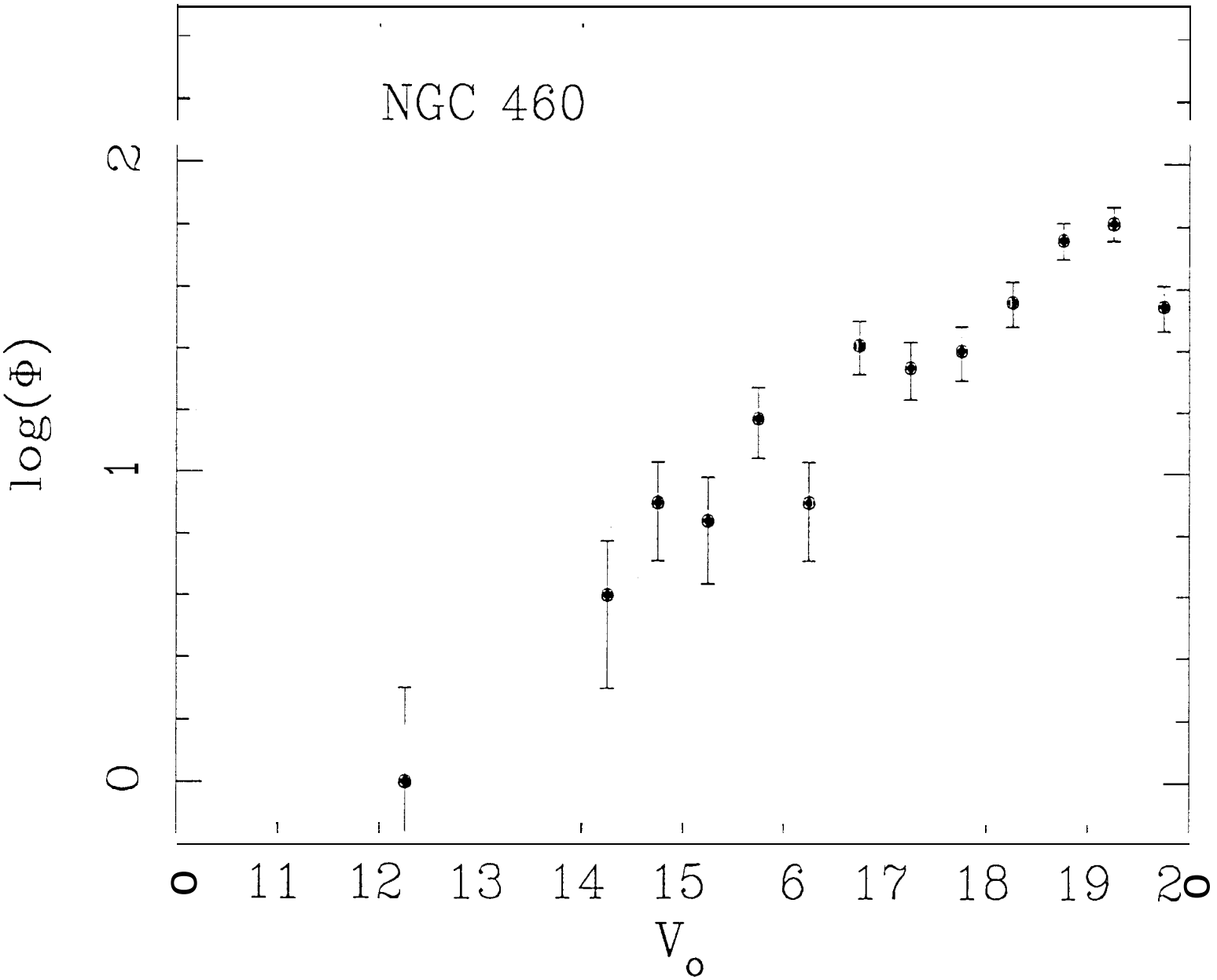

Figure 4

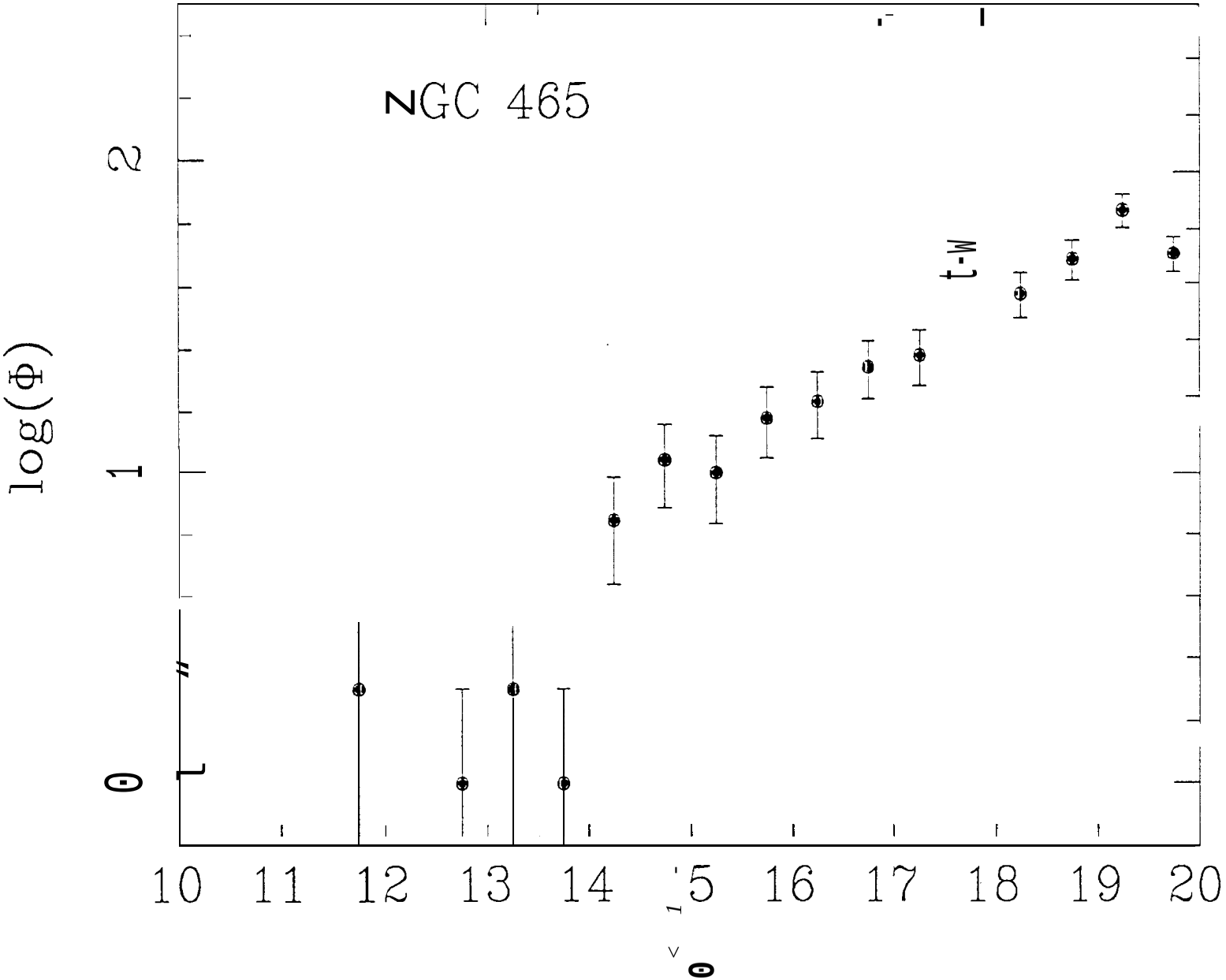

Figure 15

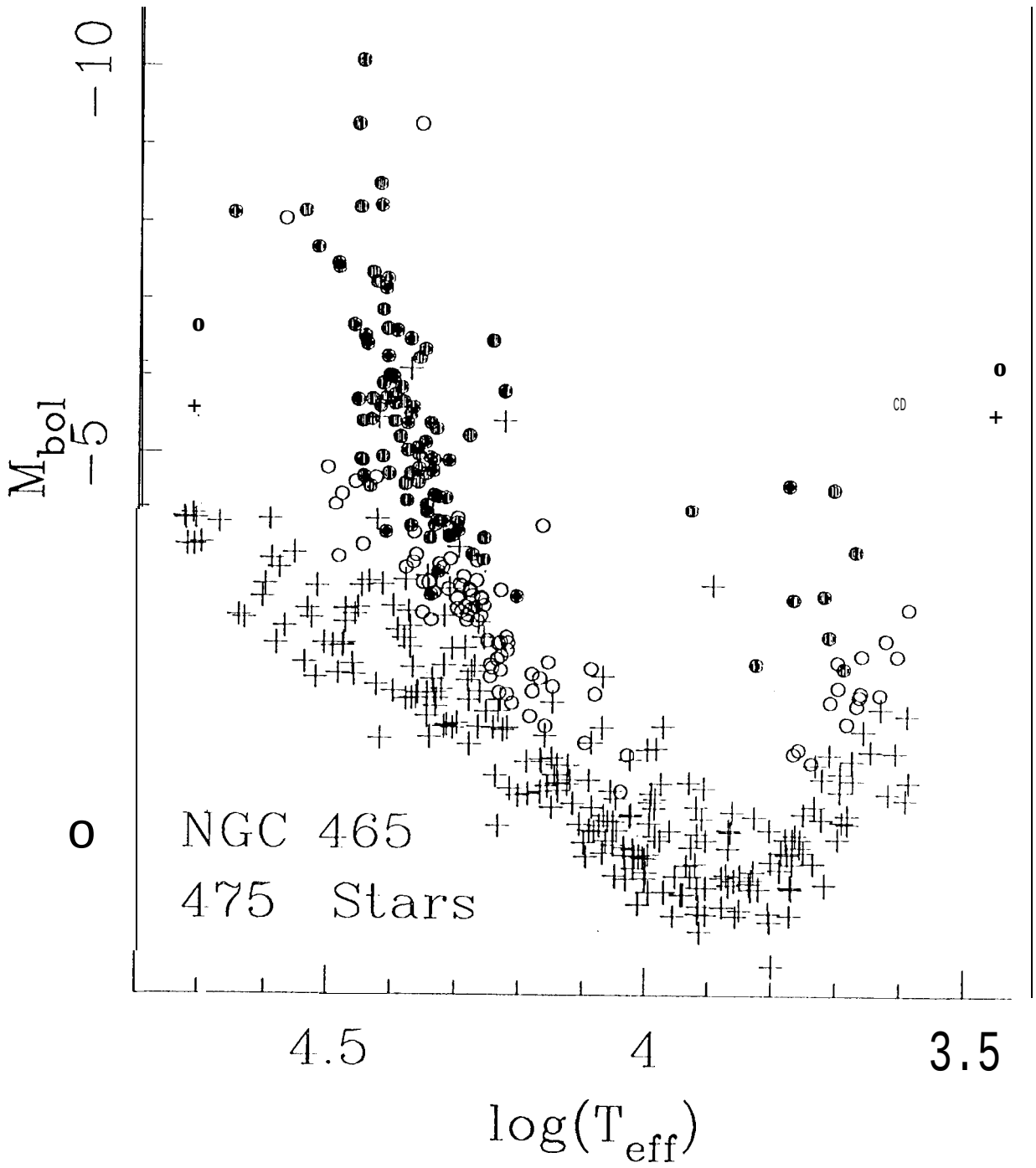

Figure 16

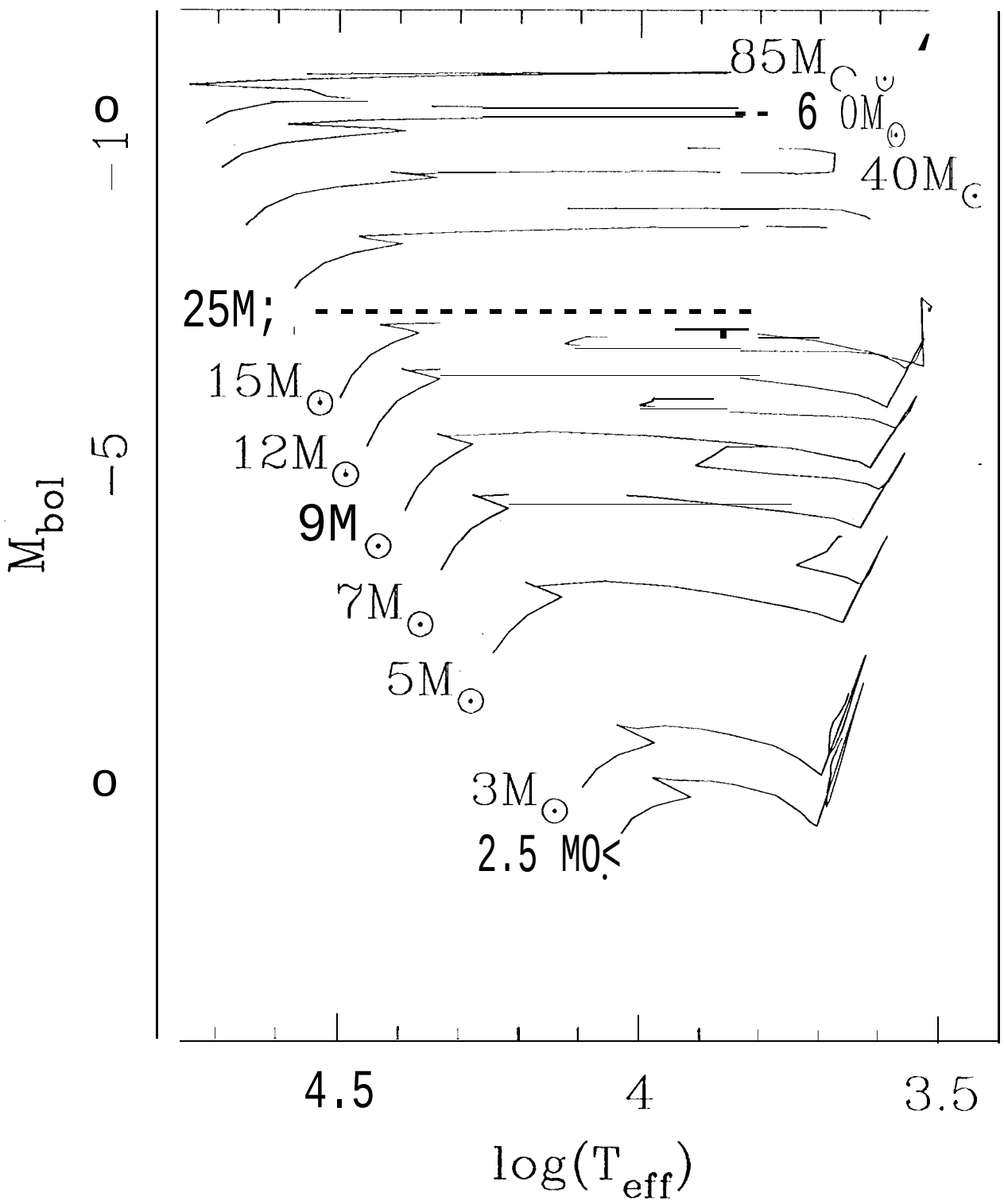

Figure 17

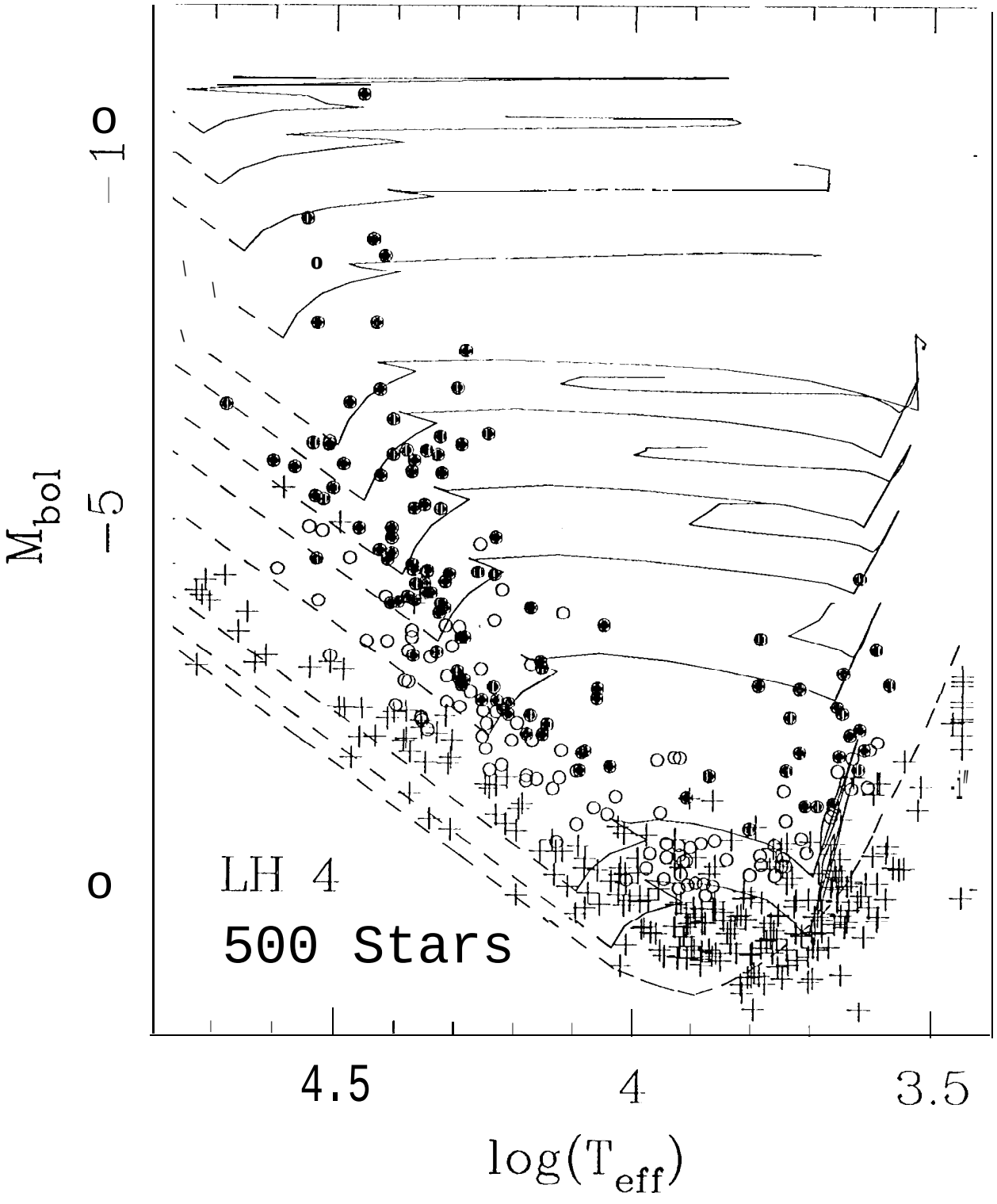

Figure 18

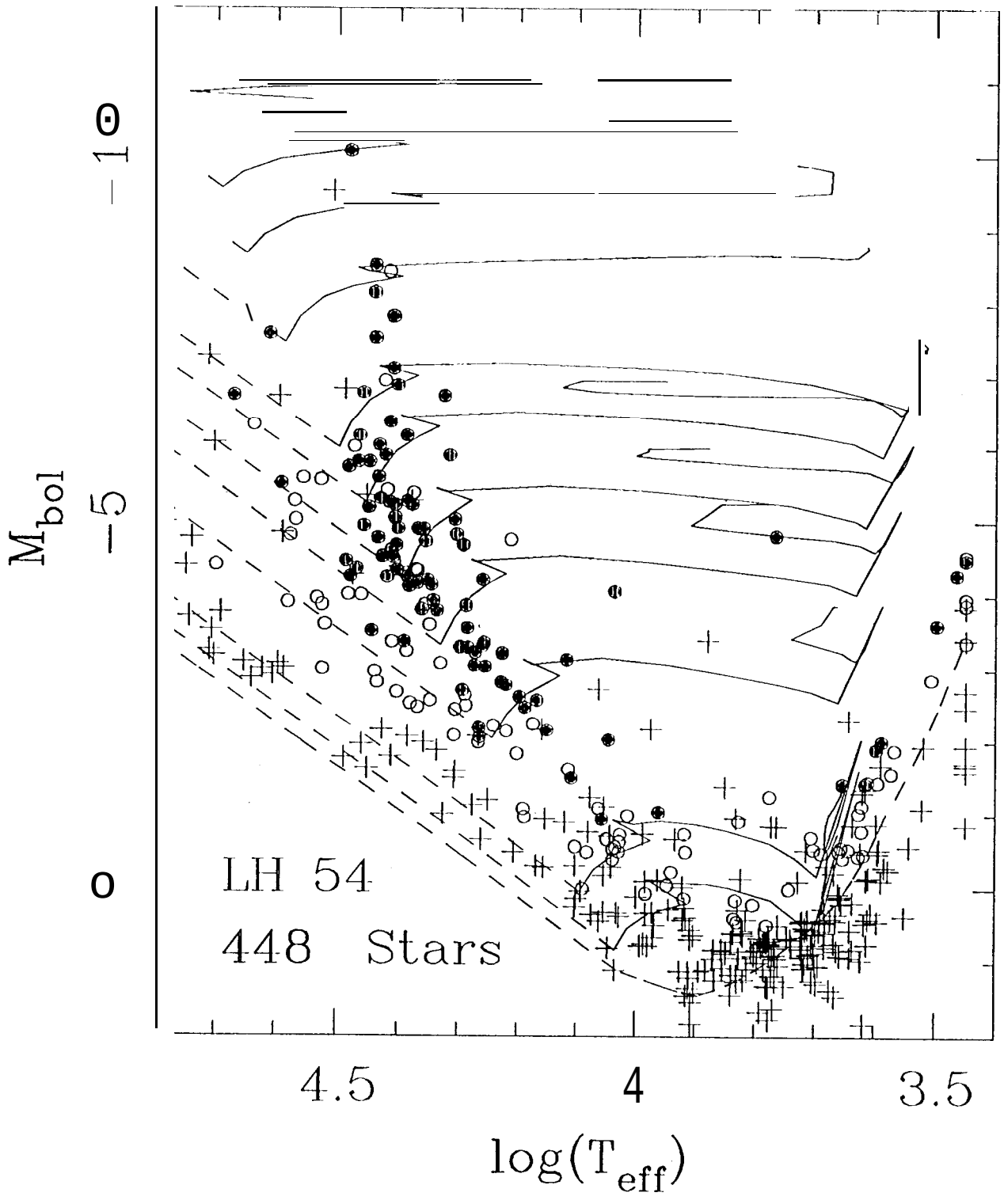

Figure 19

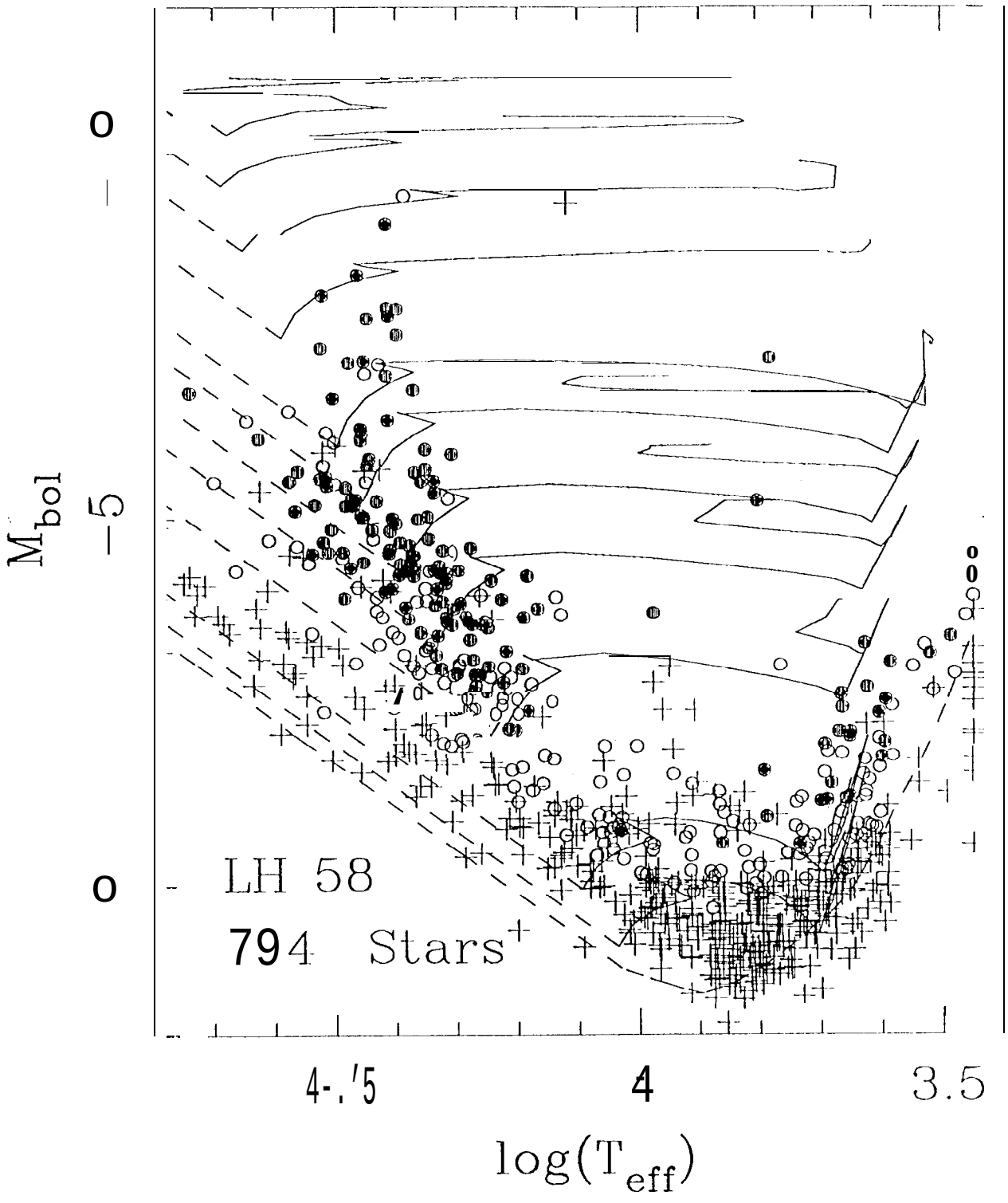

Figure 20

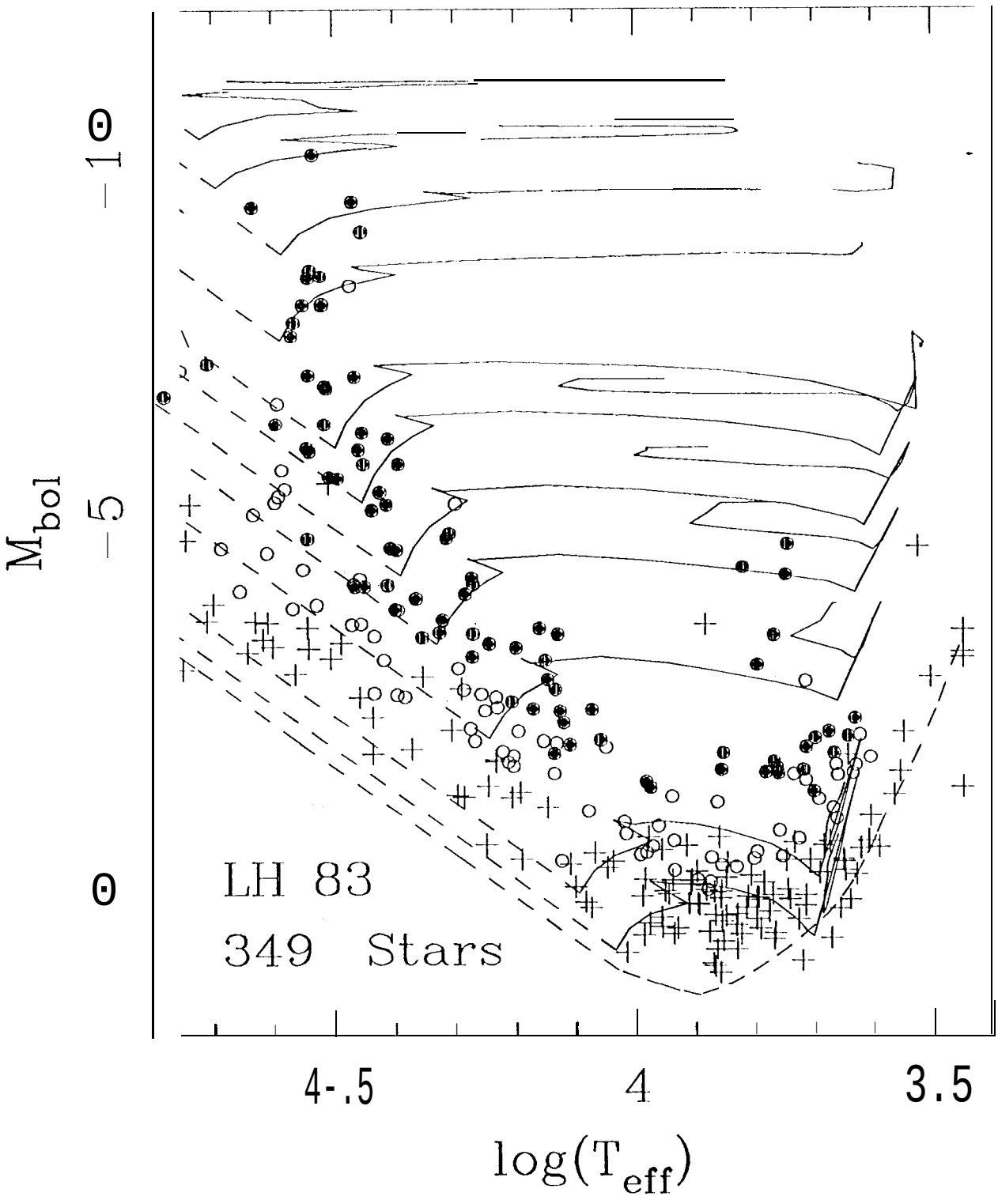

Figure 21

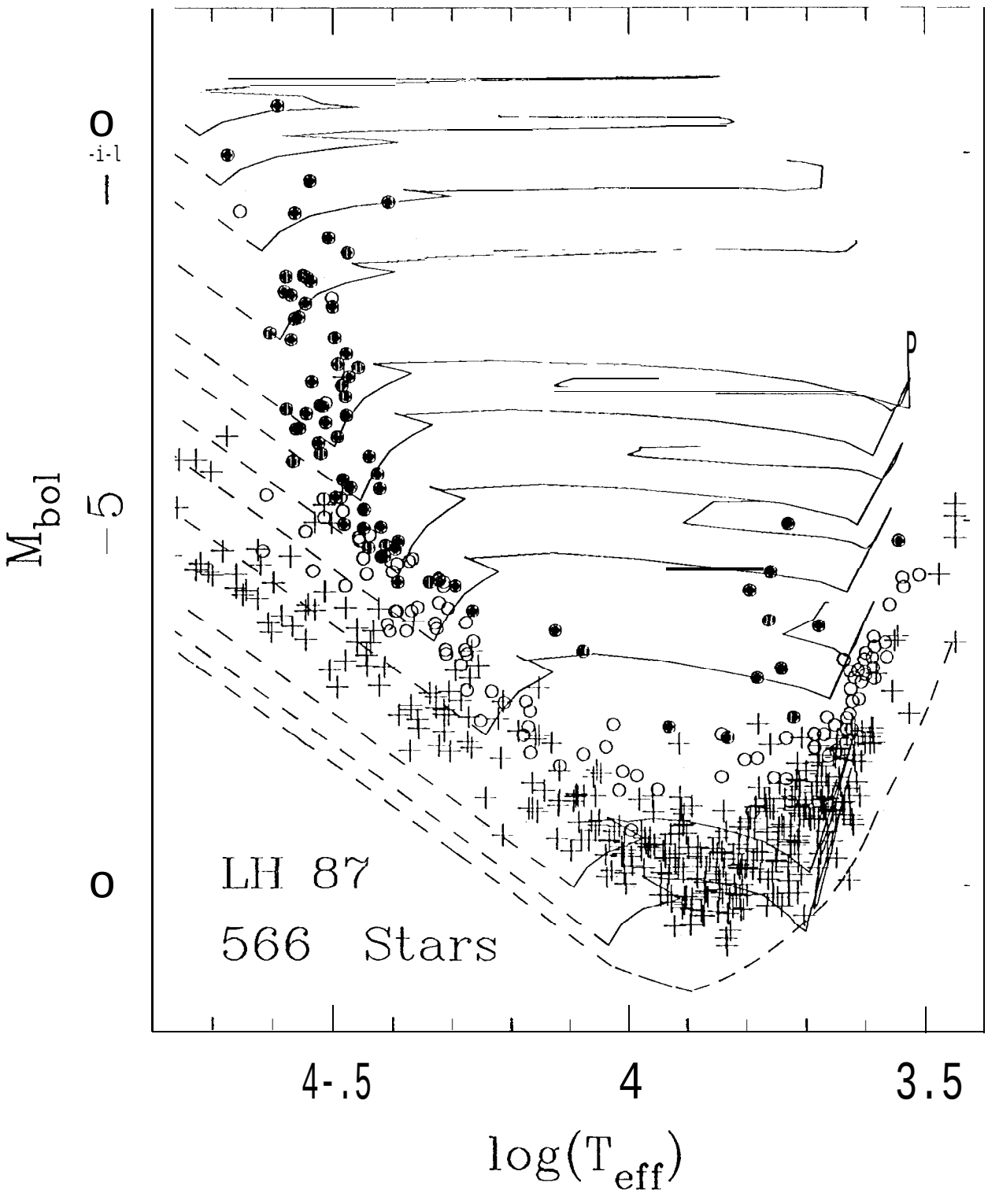

Figure 22

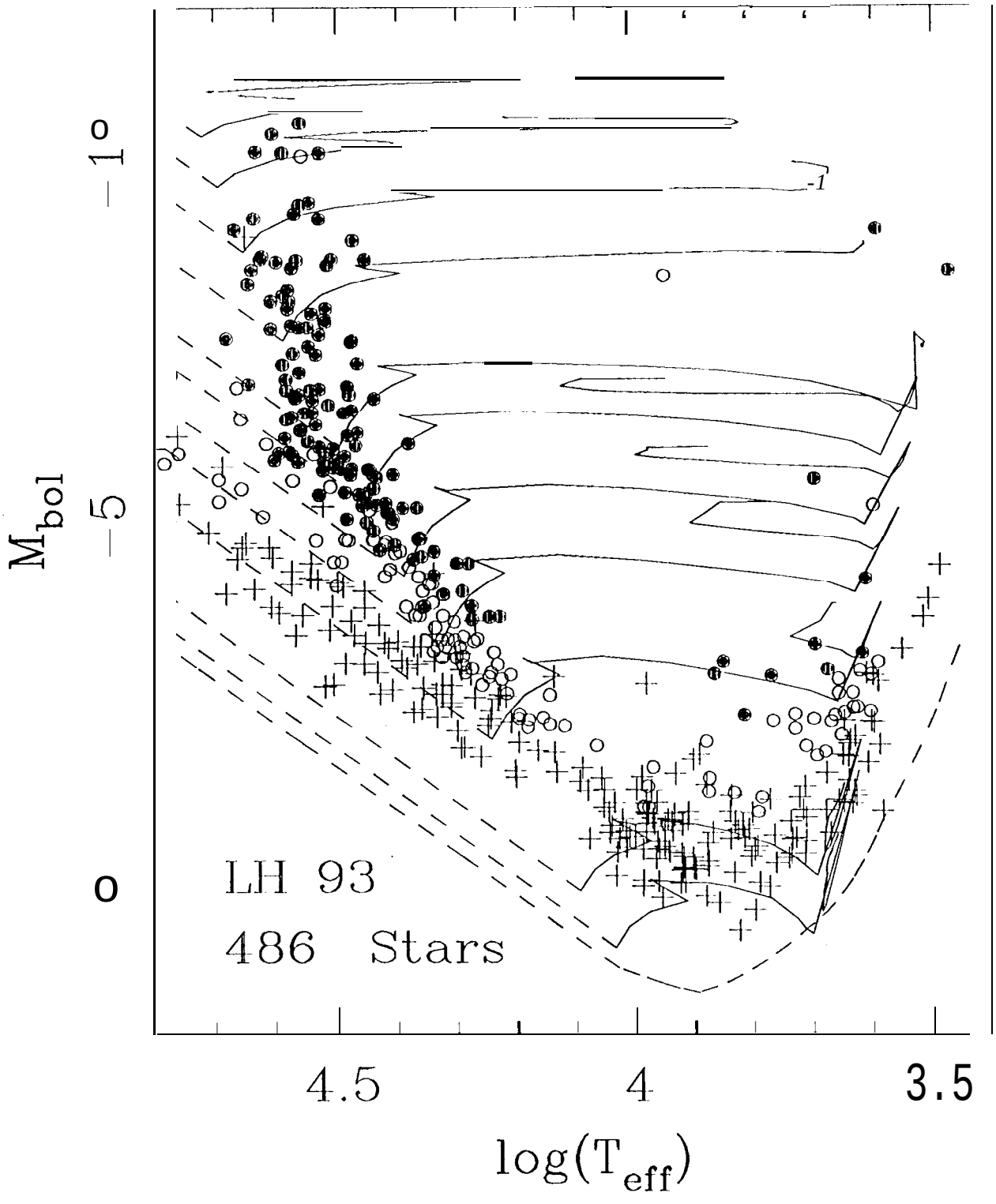

Figure 23

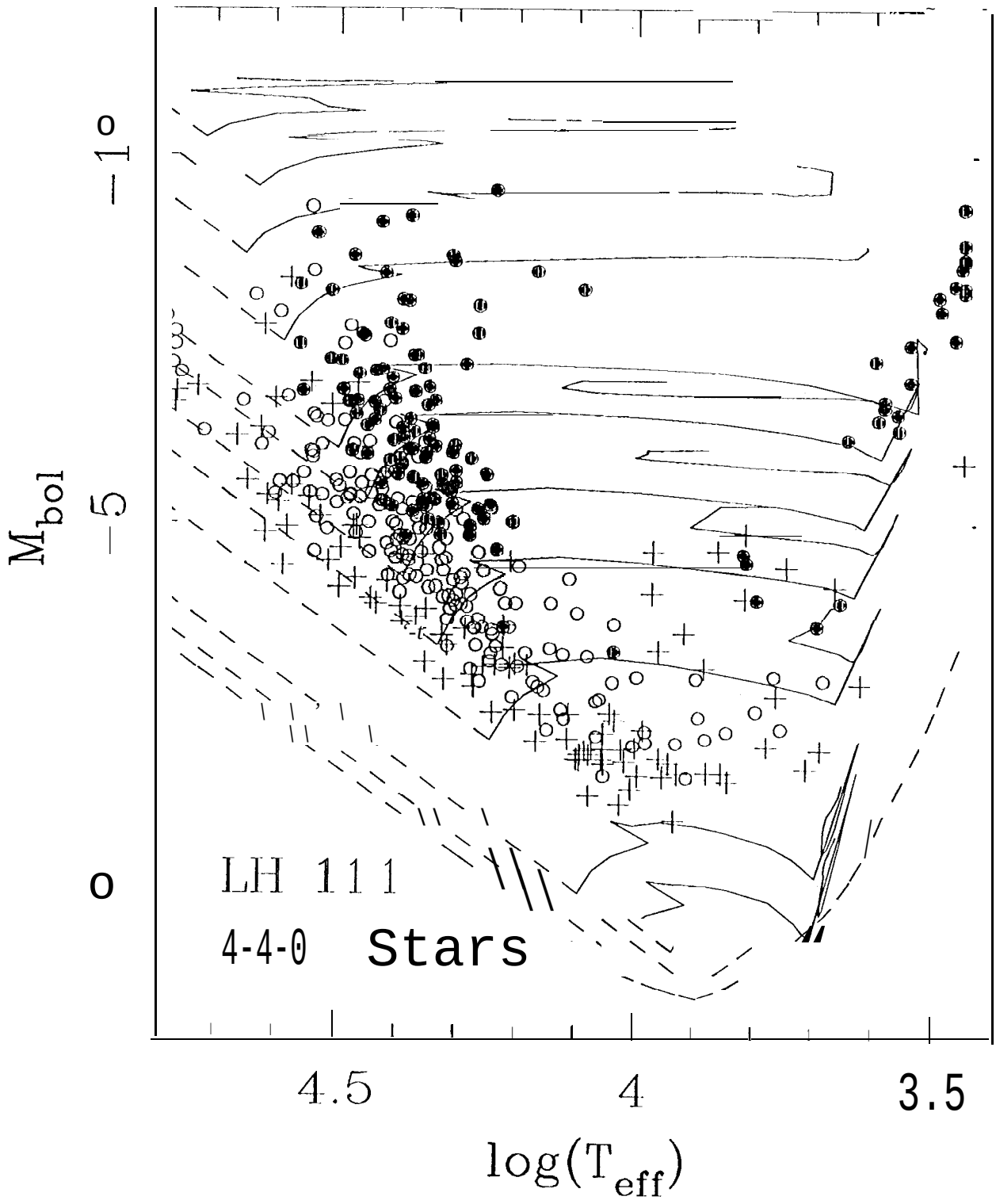

Figure 24

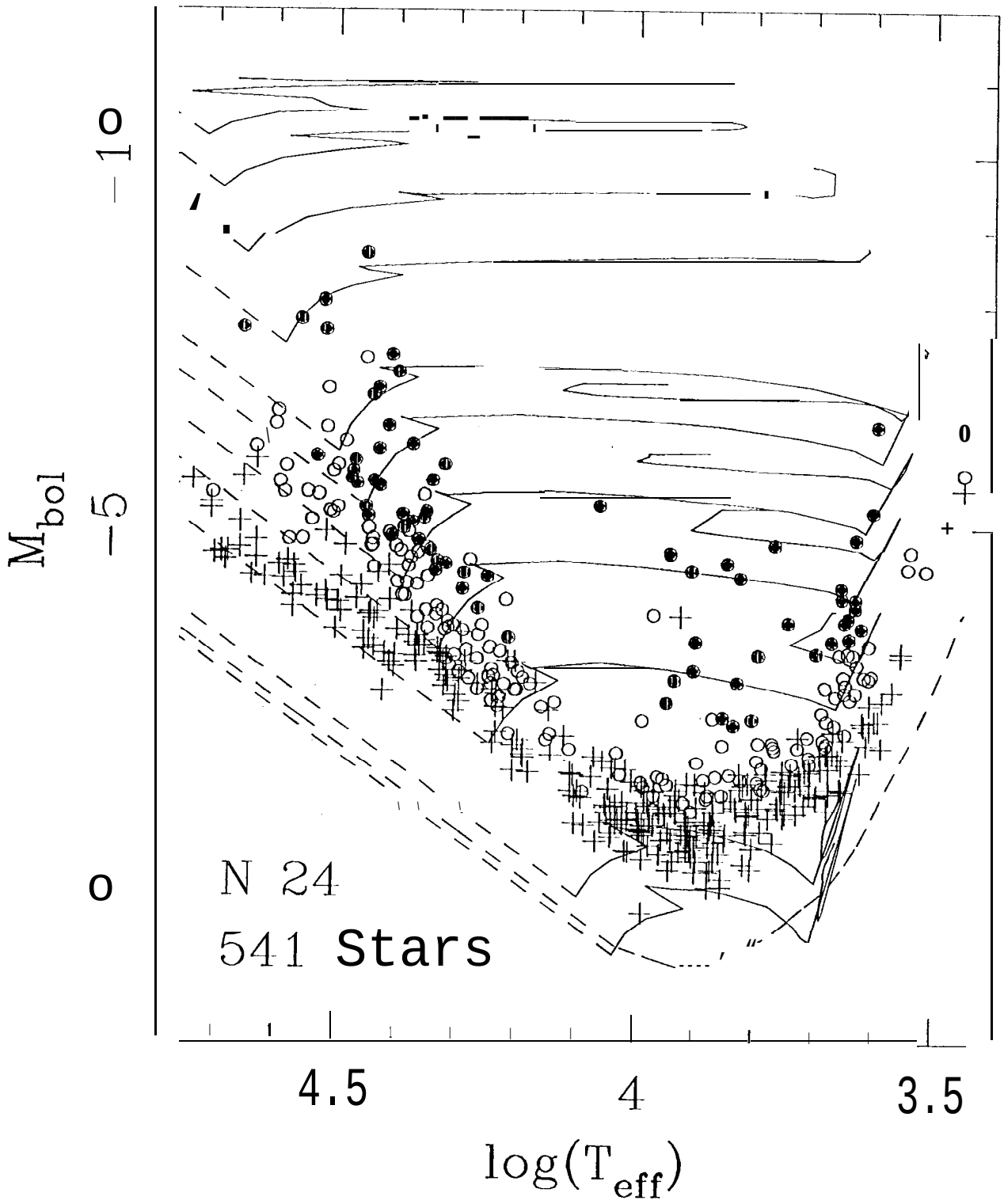

Figure 25

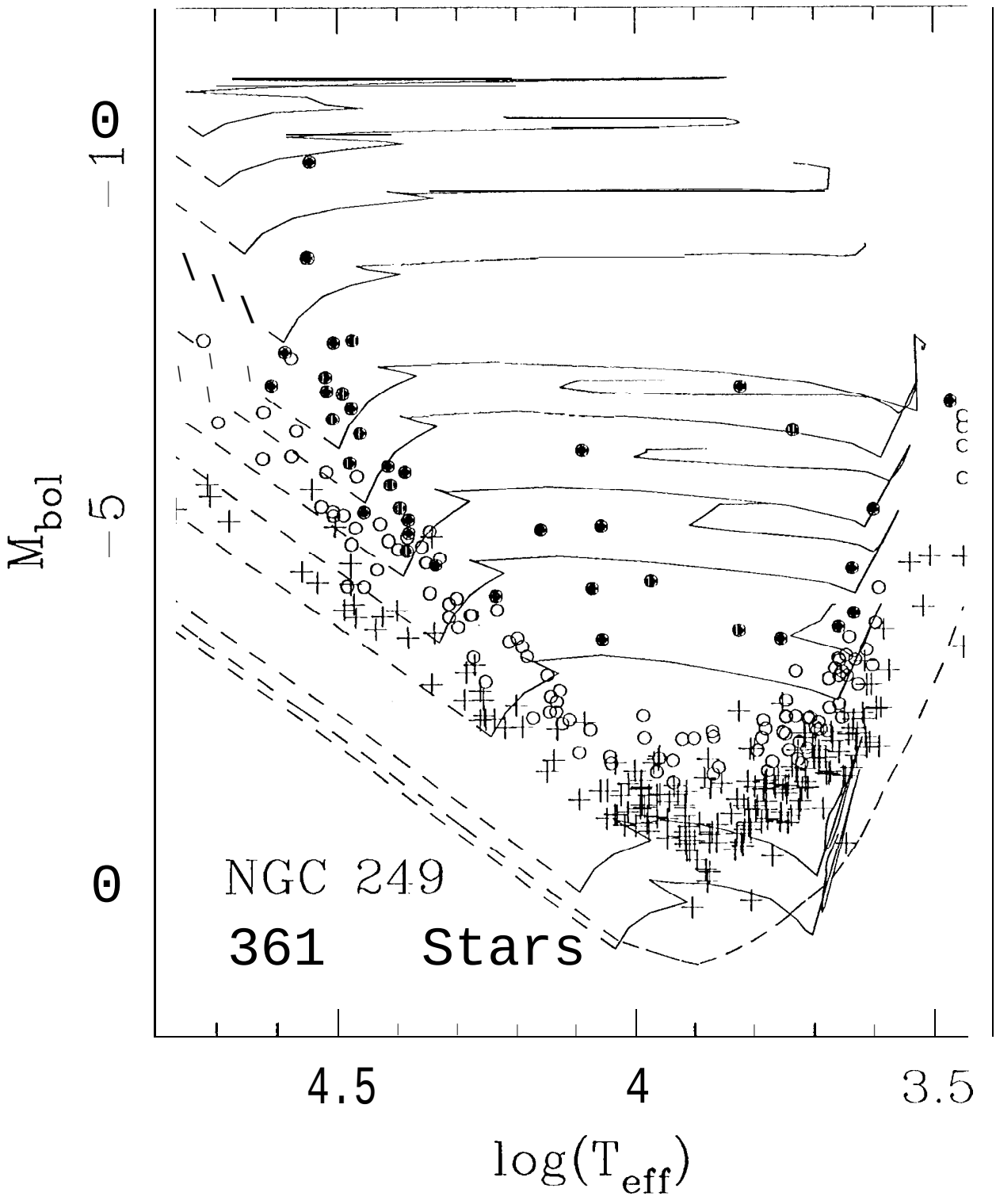

Figure 26

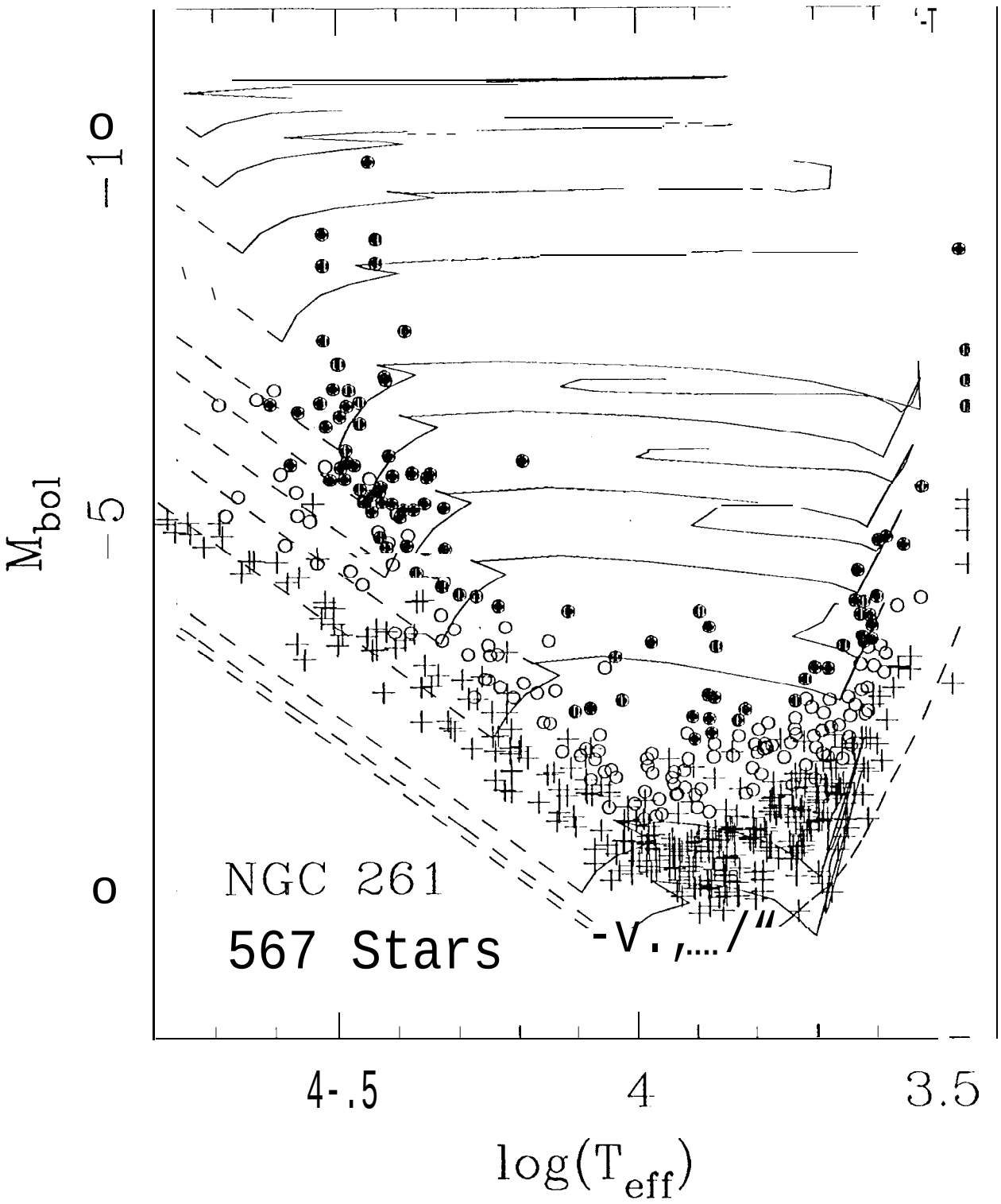

Figure 27

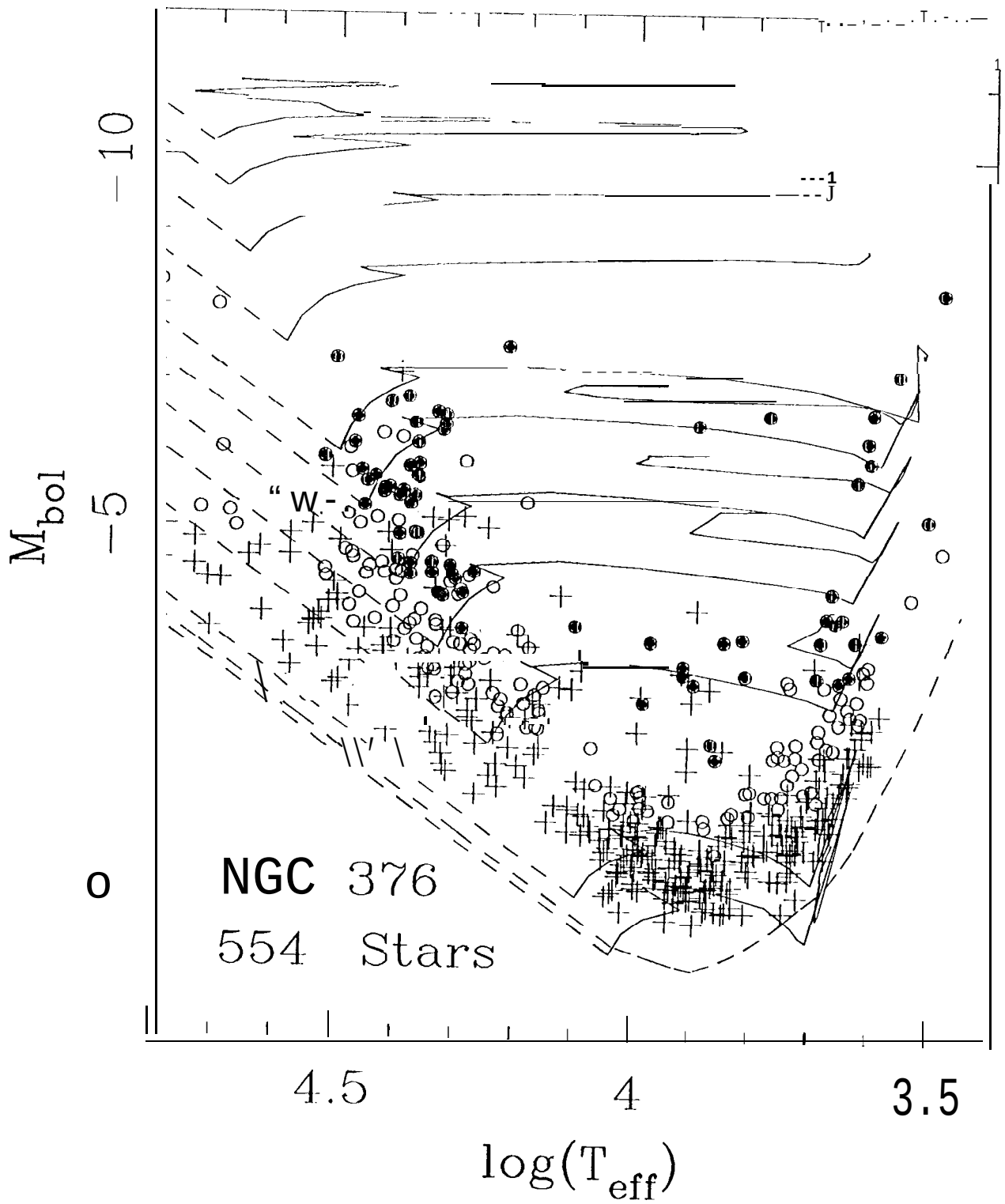

Figure 28

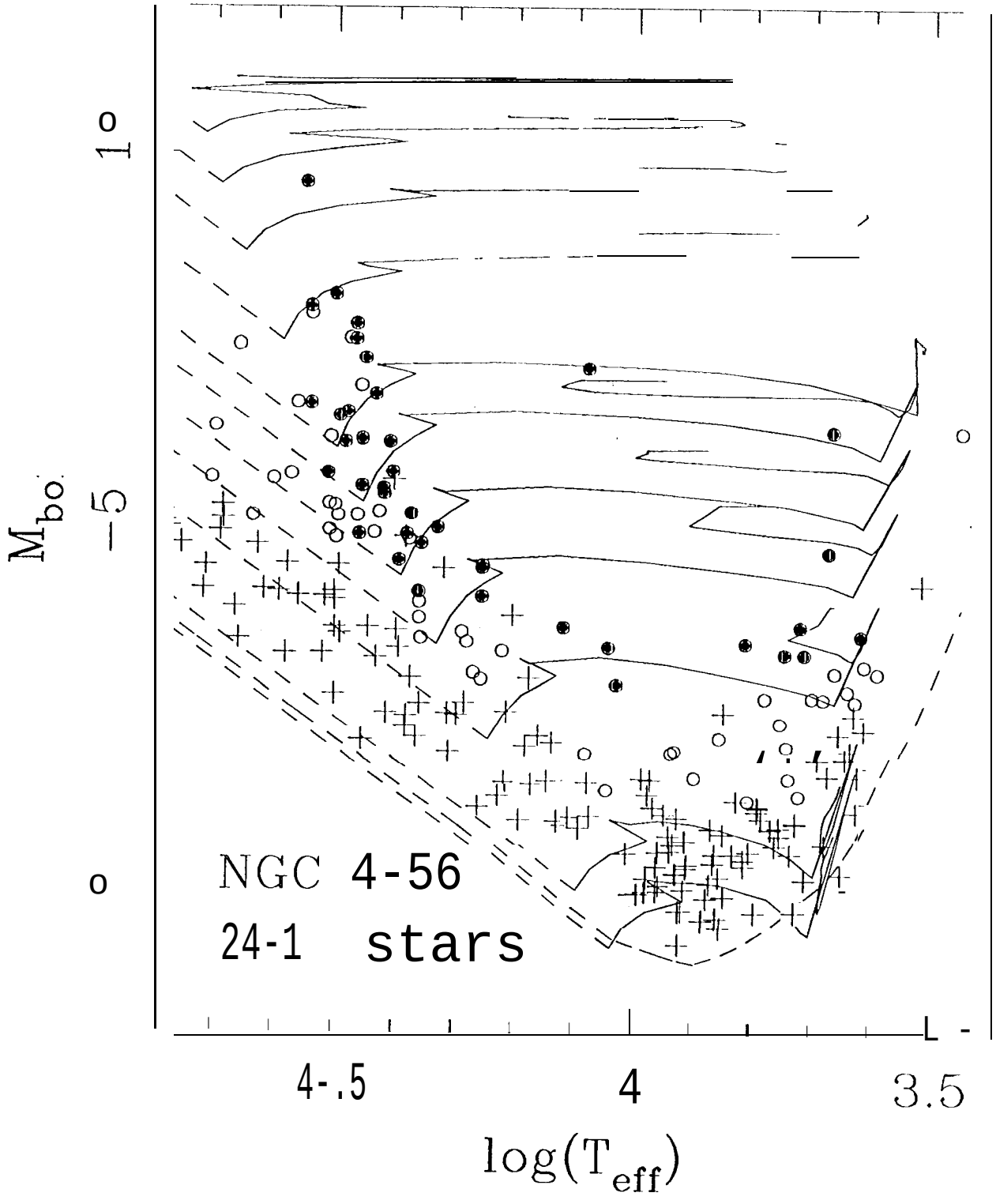

Figure 29

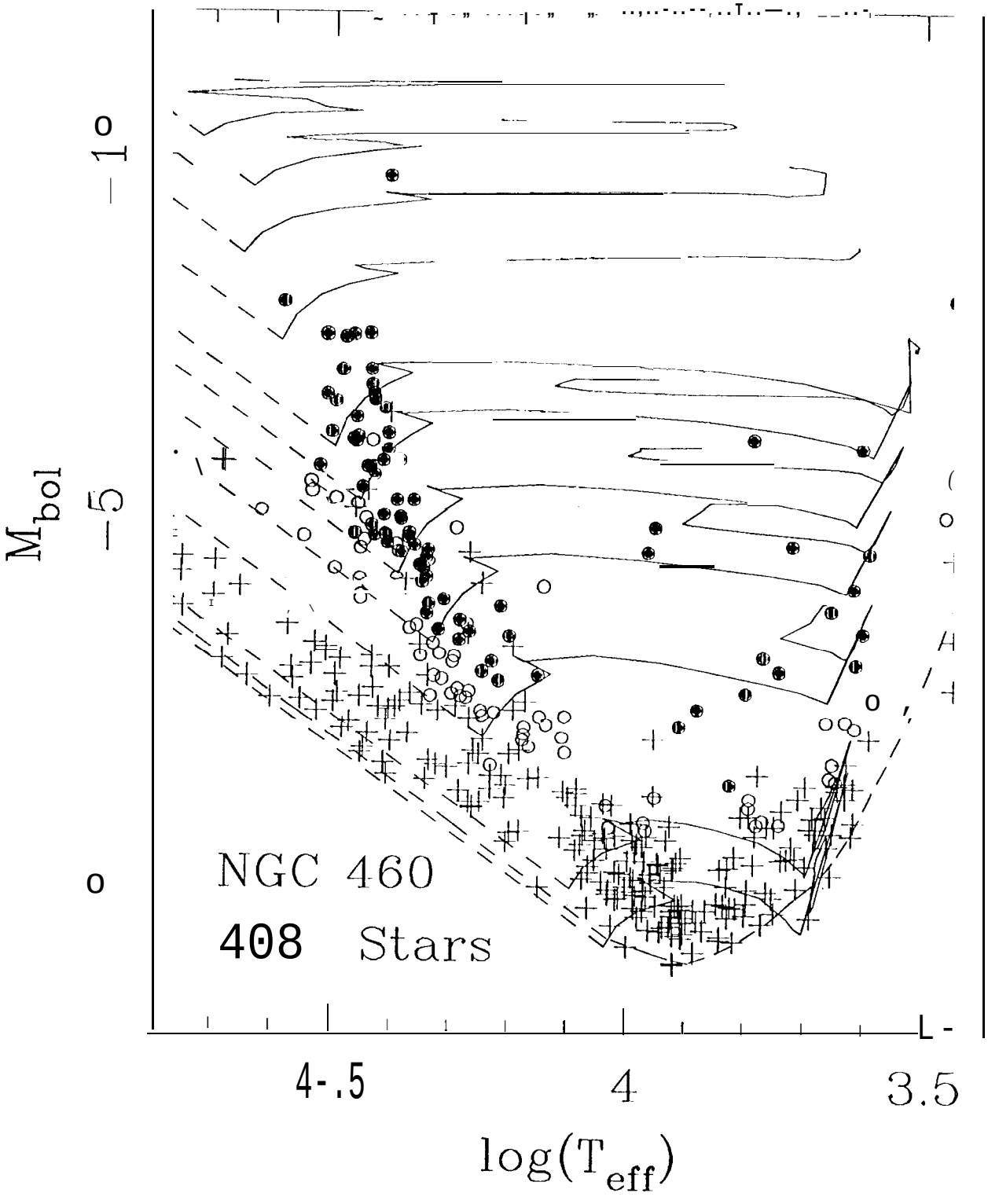

Figure 30

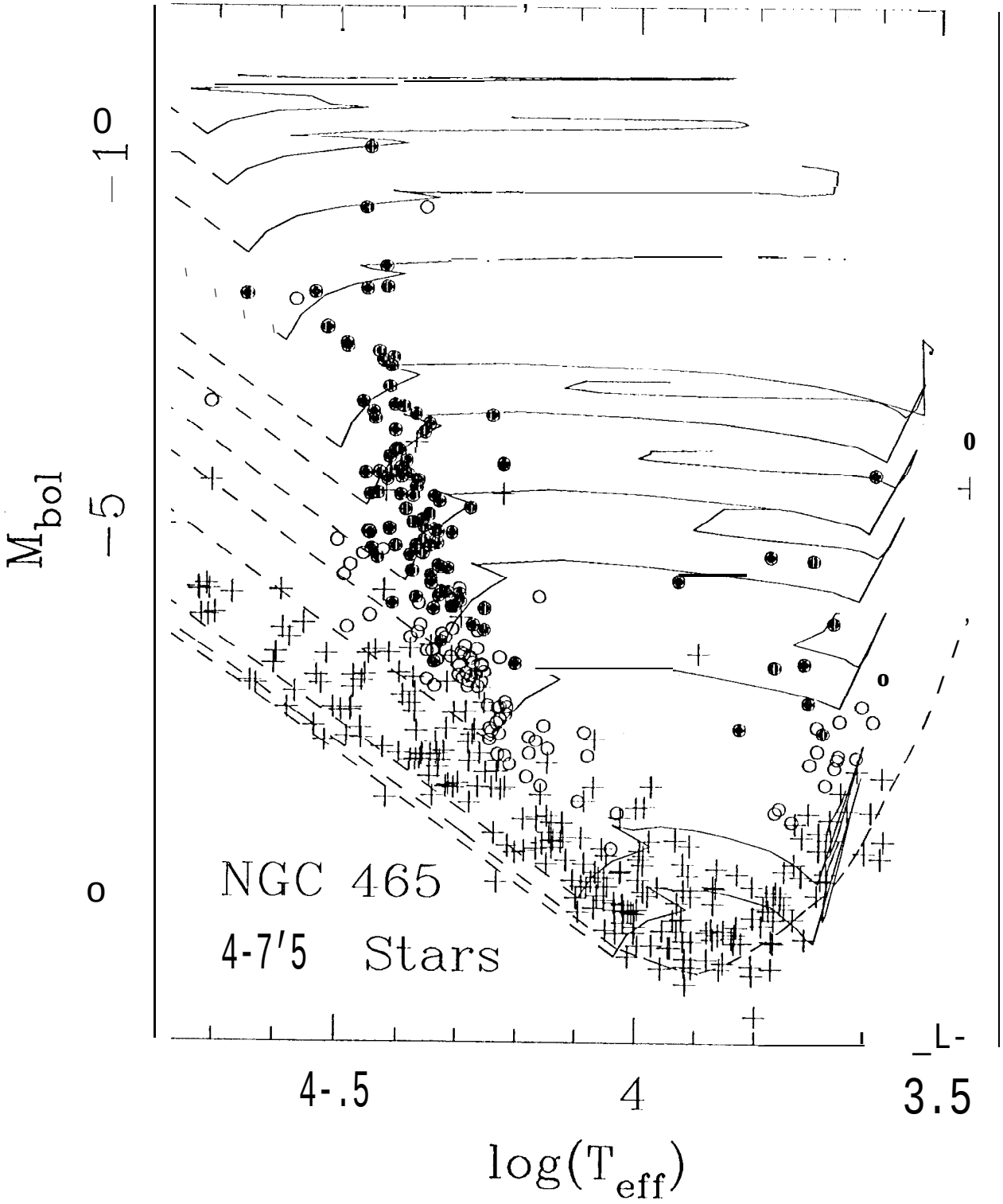

Figure 31

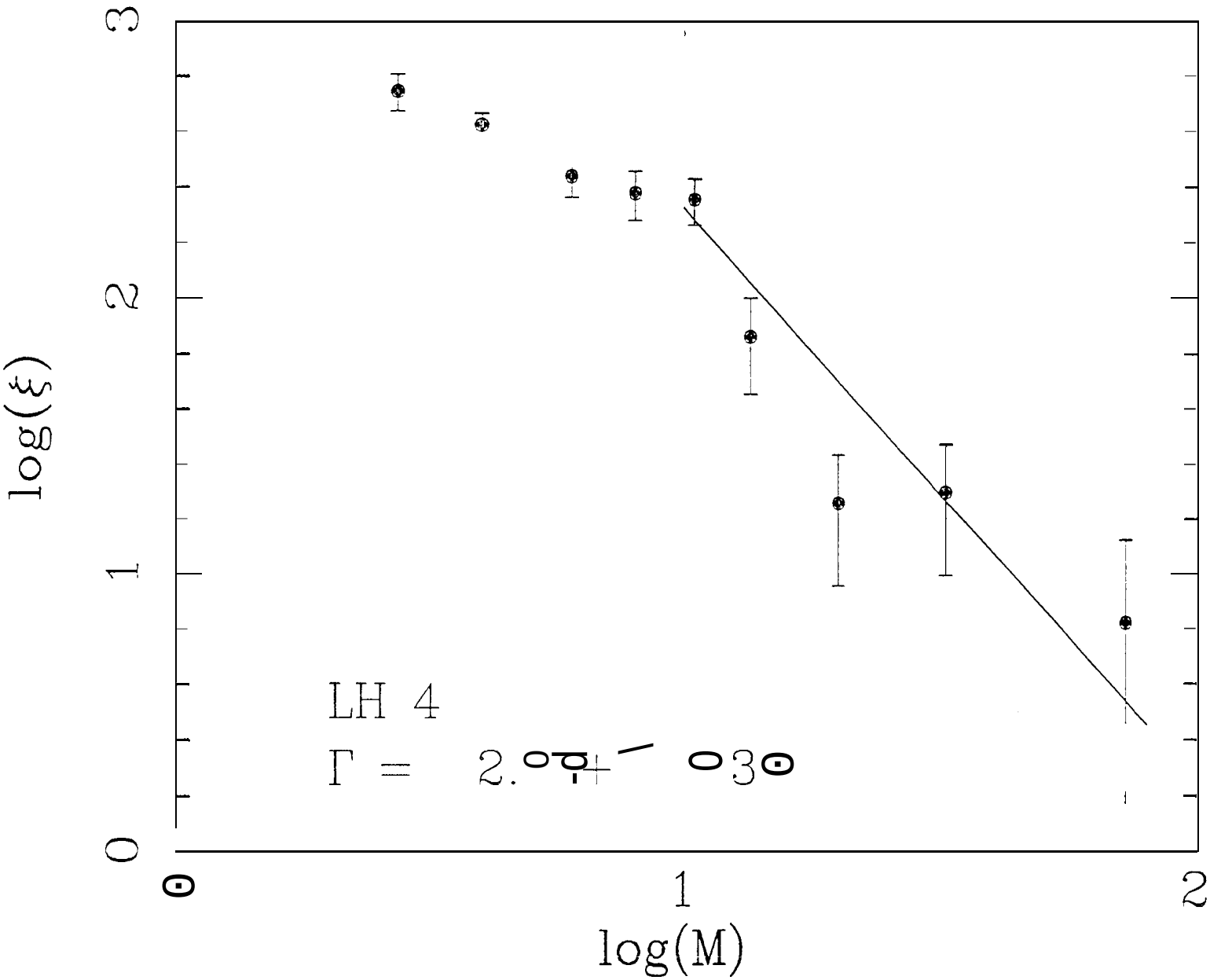

Figure 32

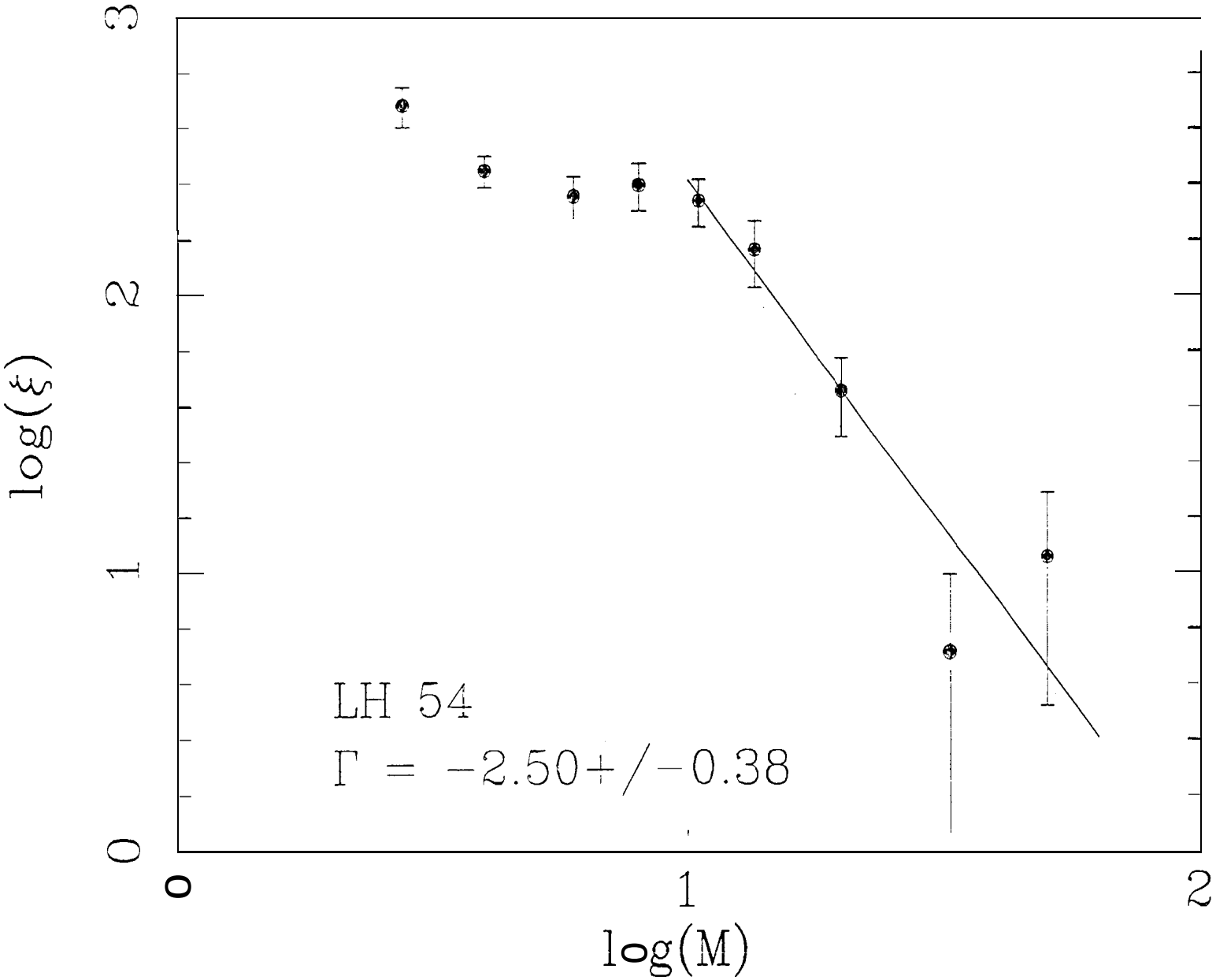

Figure 33

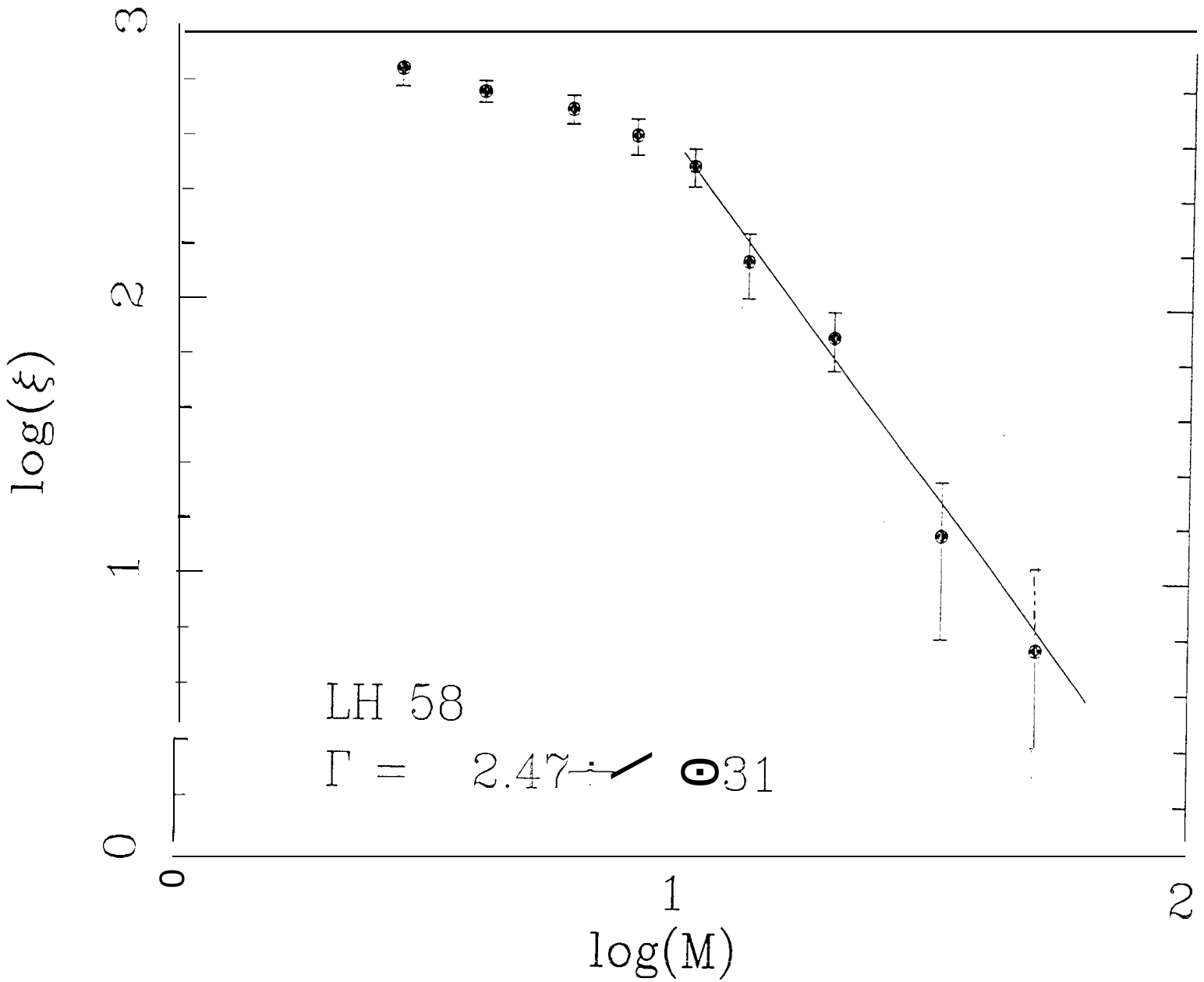

Figure 34

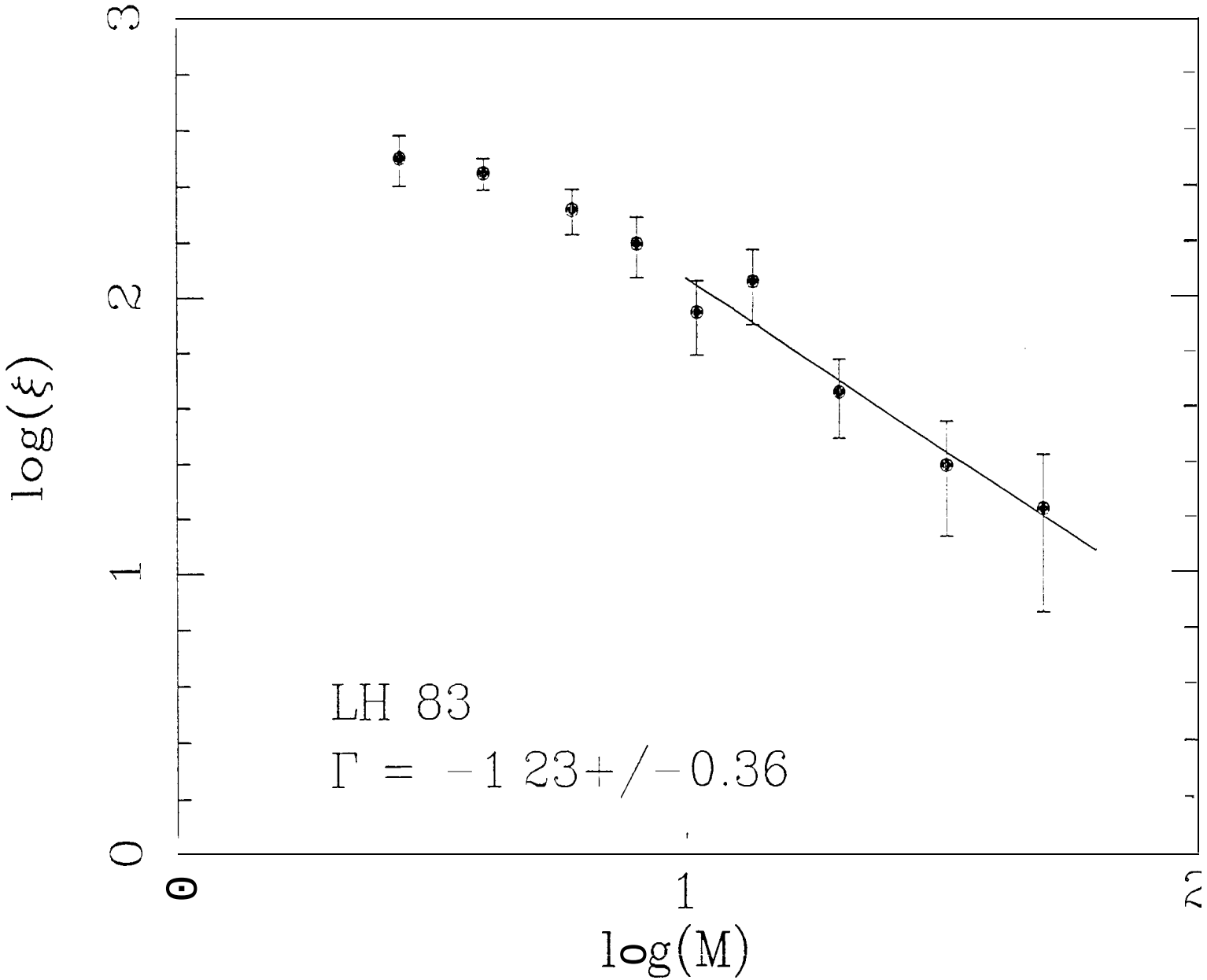

Figure 35

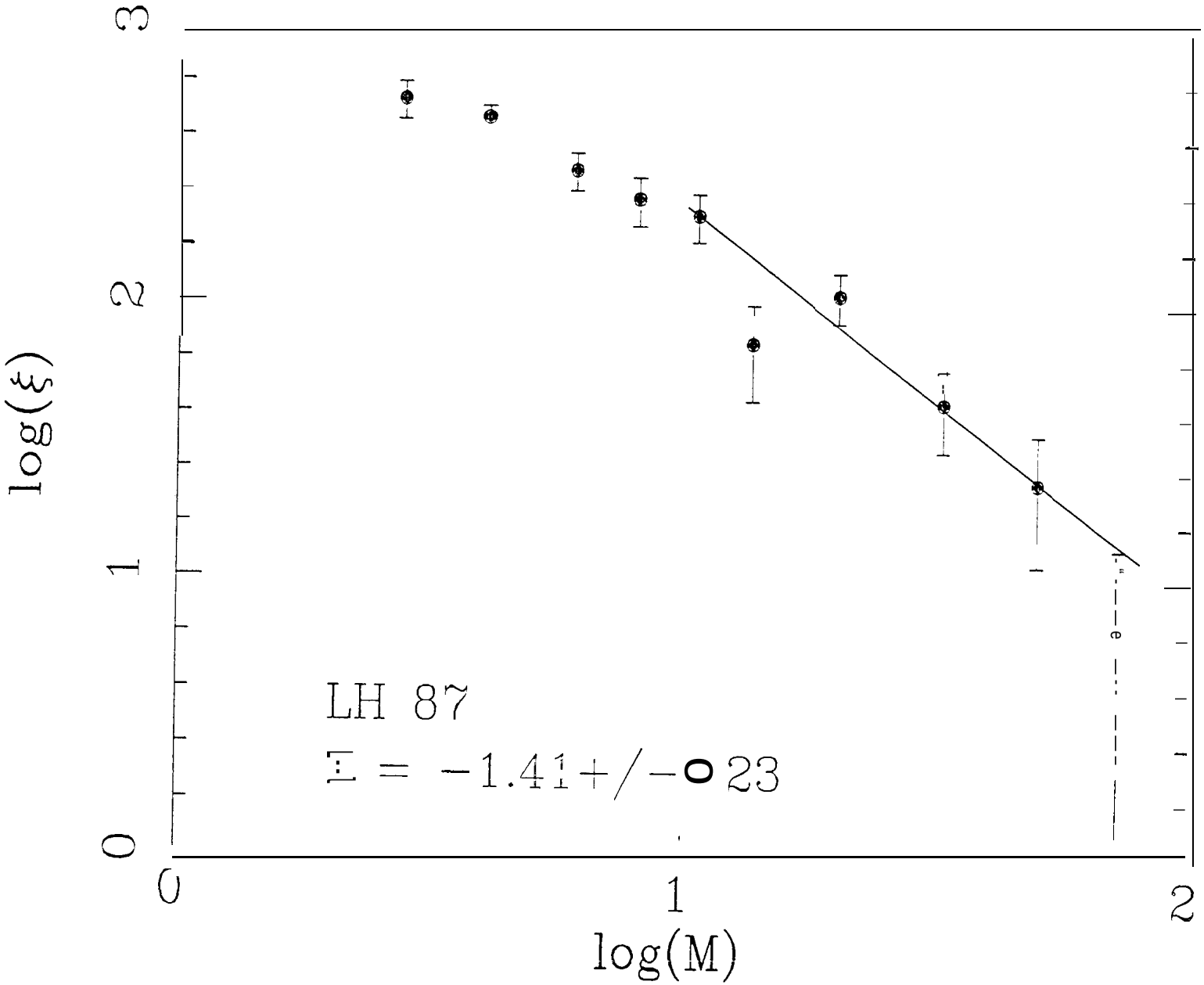

Figure 36

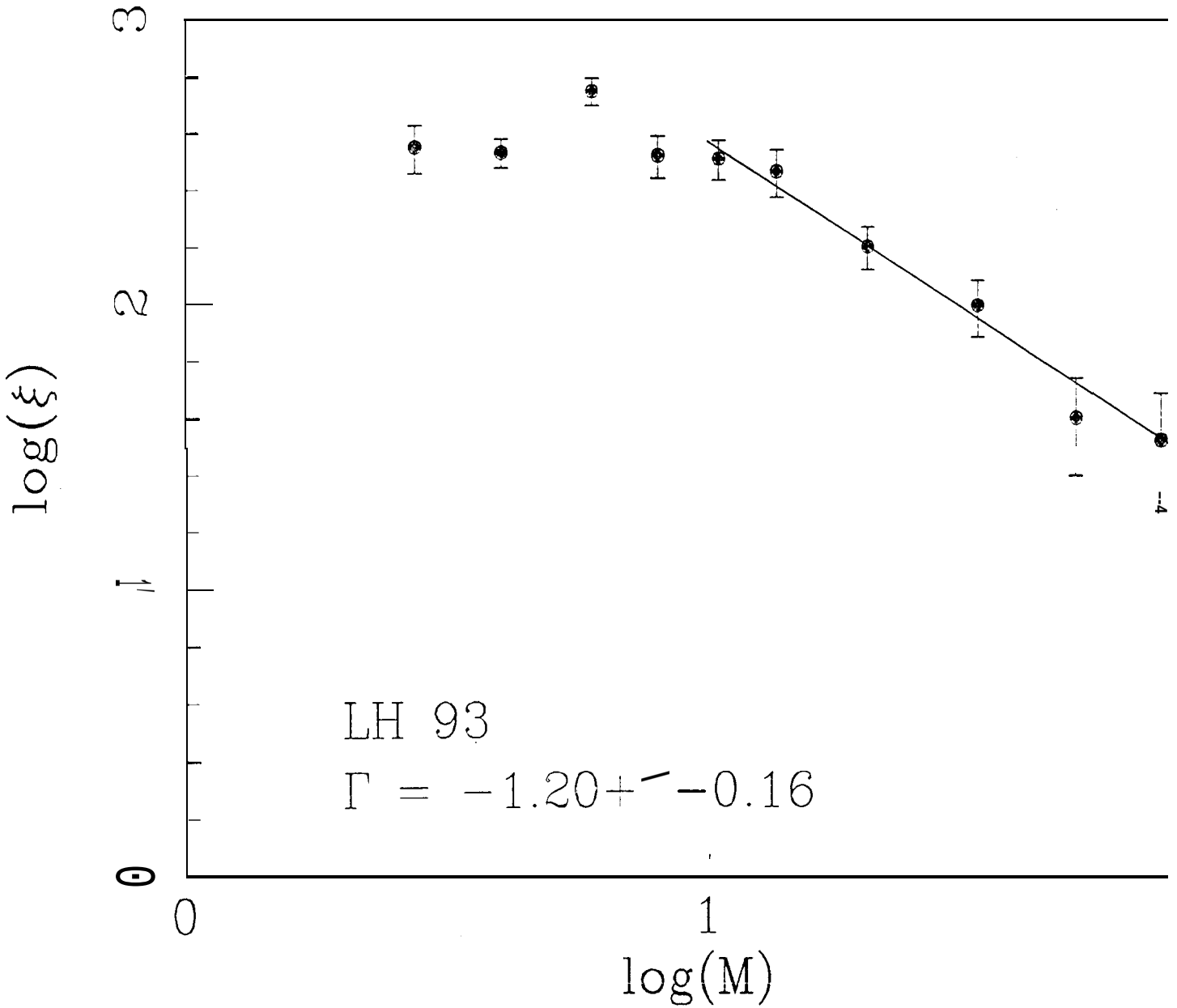

Figure 37

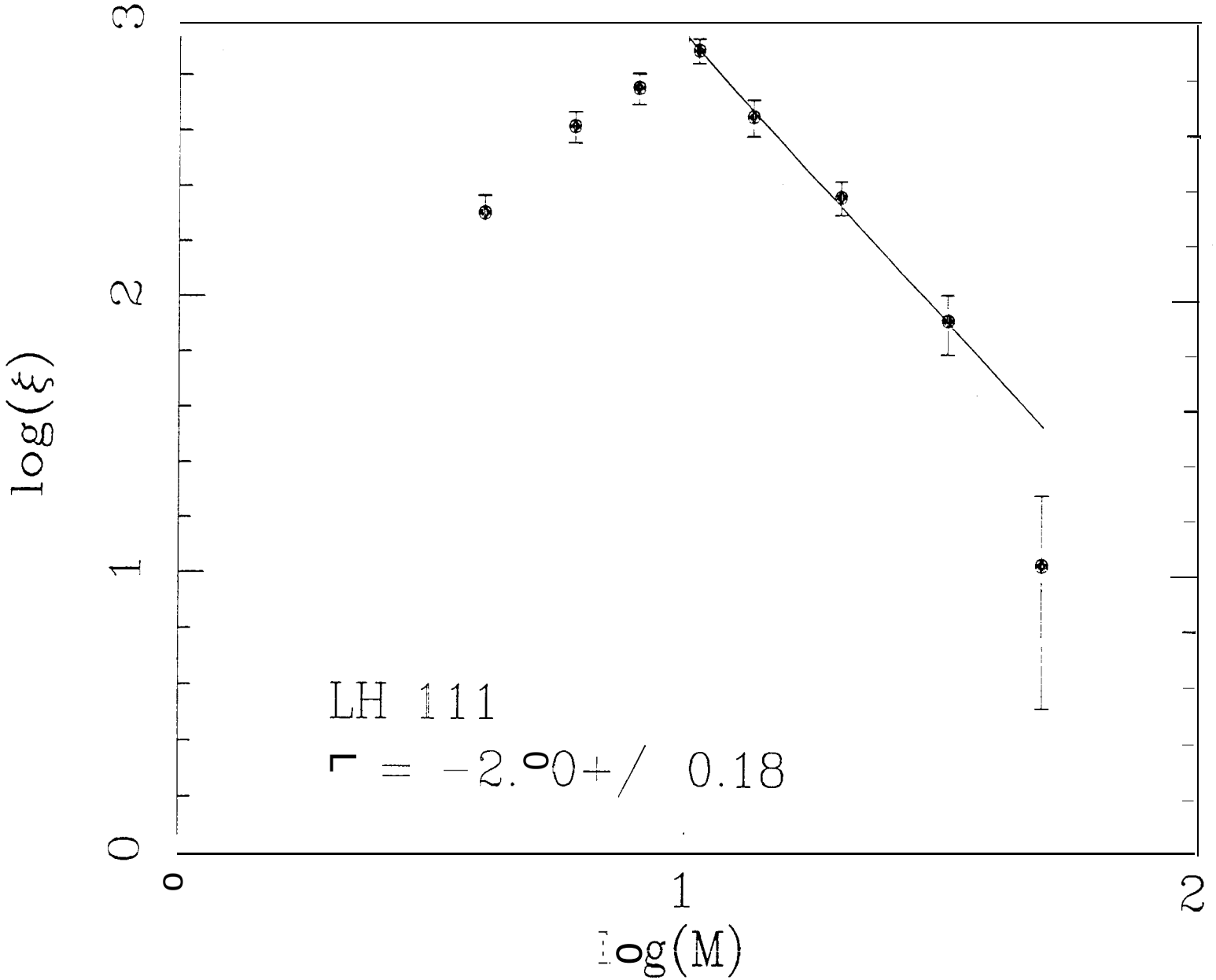

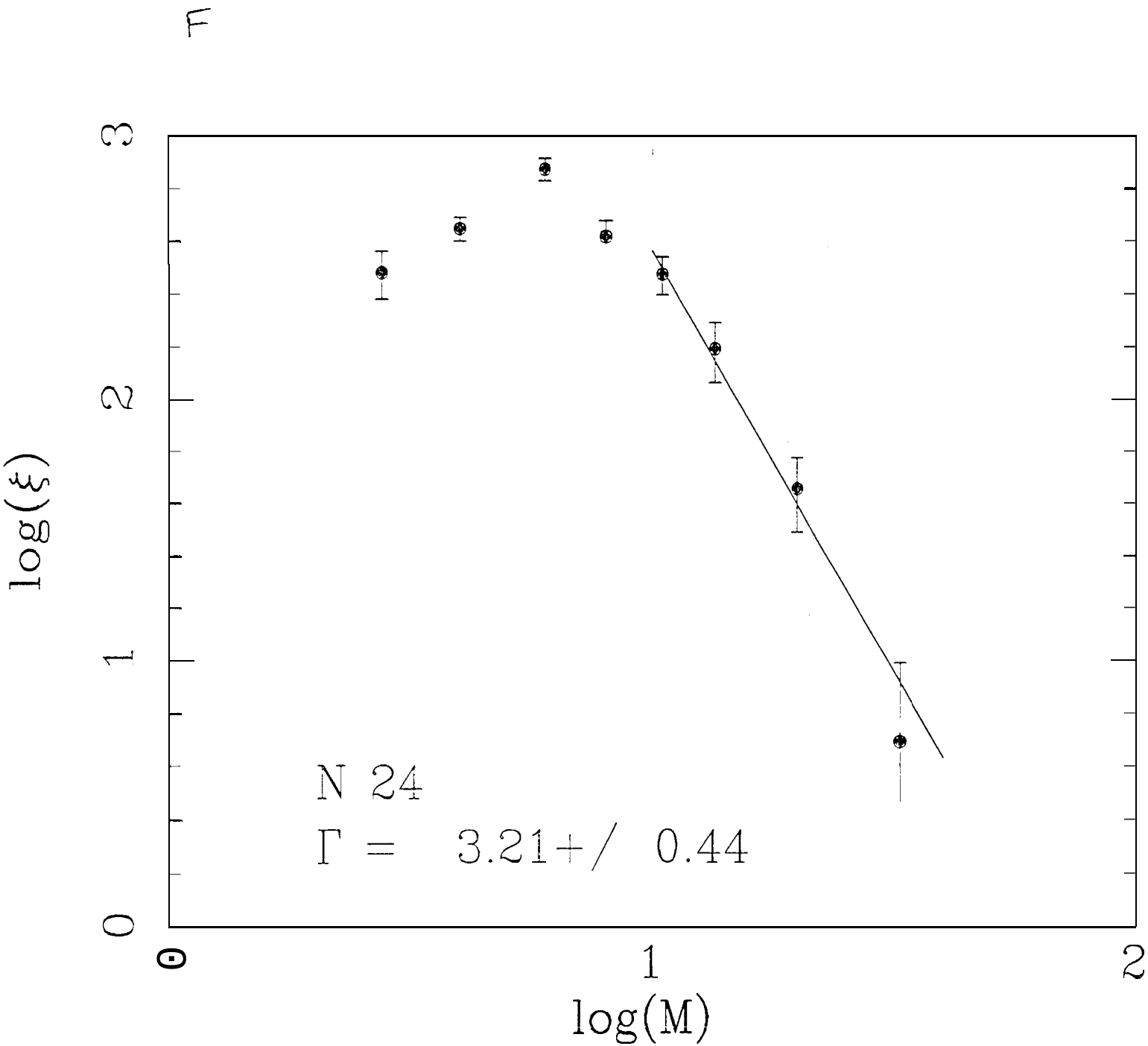
F
log(ξ)
log(M)
0
1
2
3
0
1
2
N 24
Γ = 3.21+/ 0.44

Figure 39

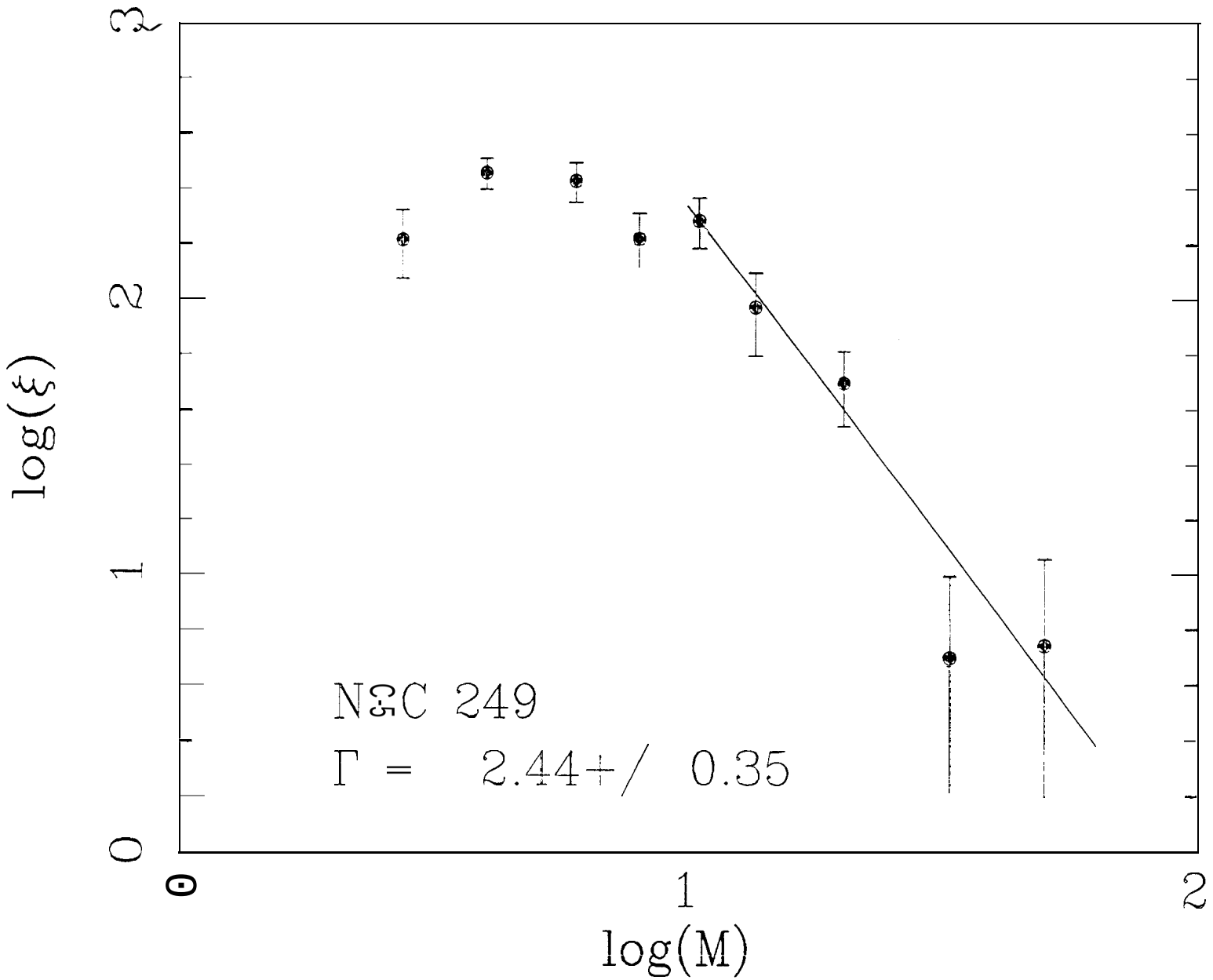

Figure 40

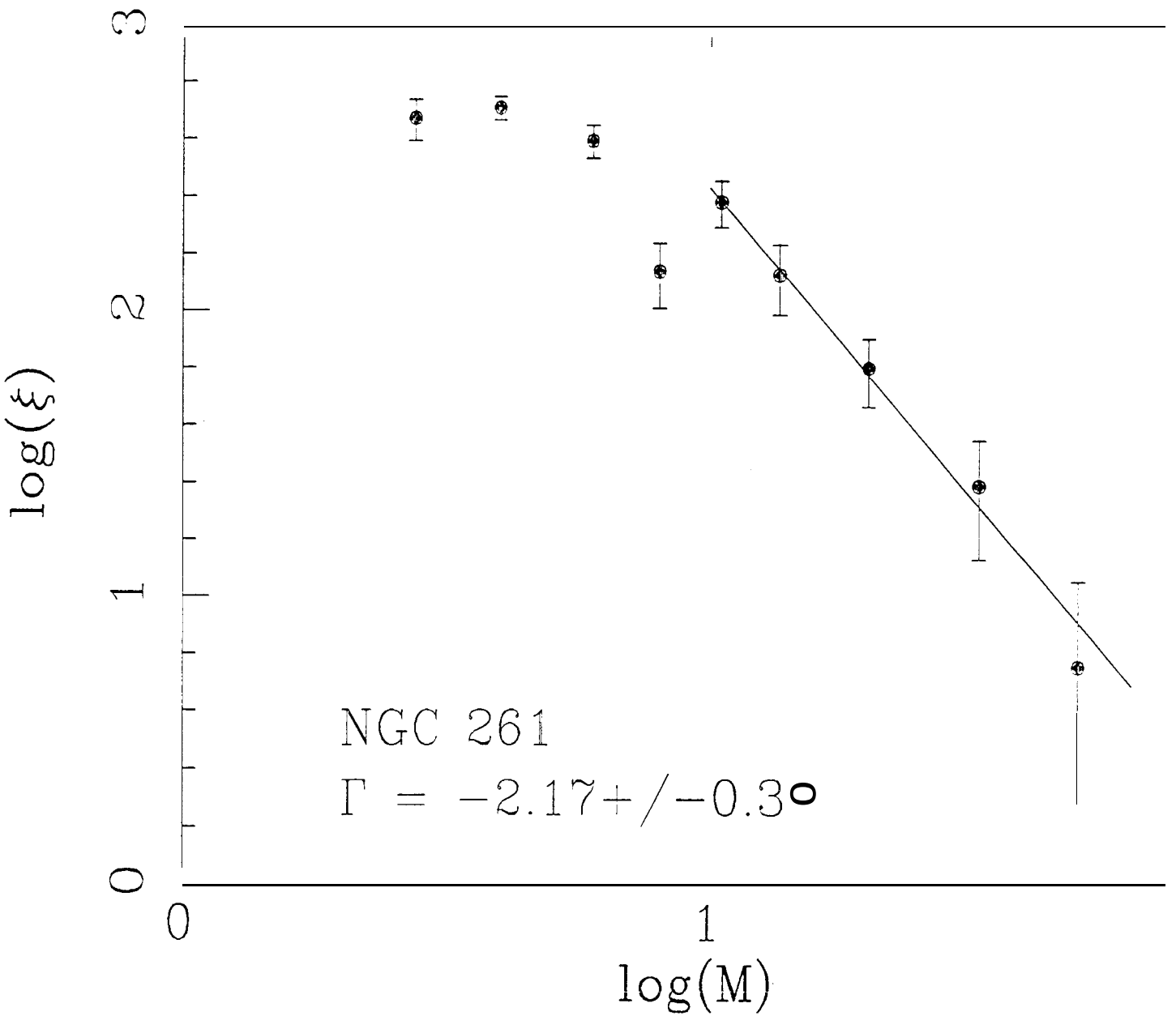

Figure 41

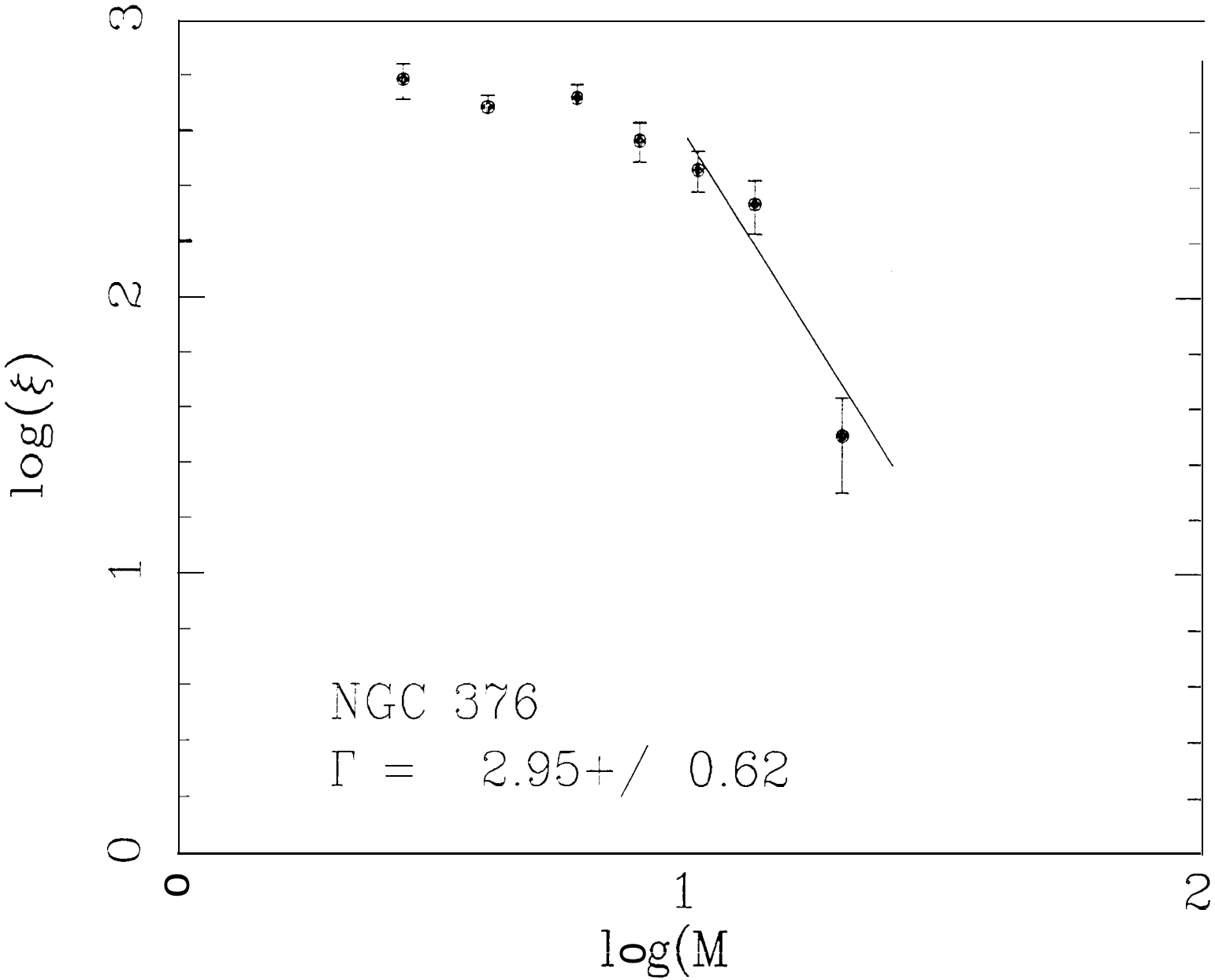

Figure 42

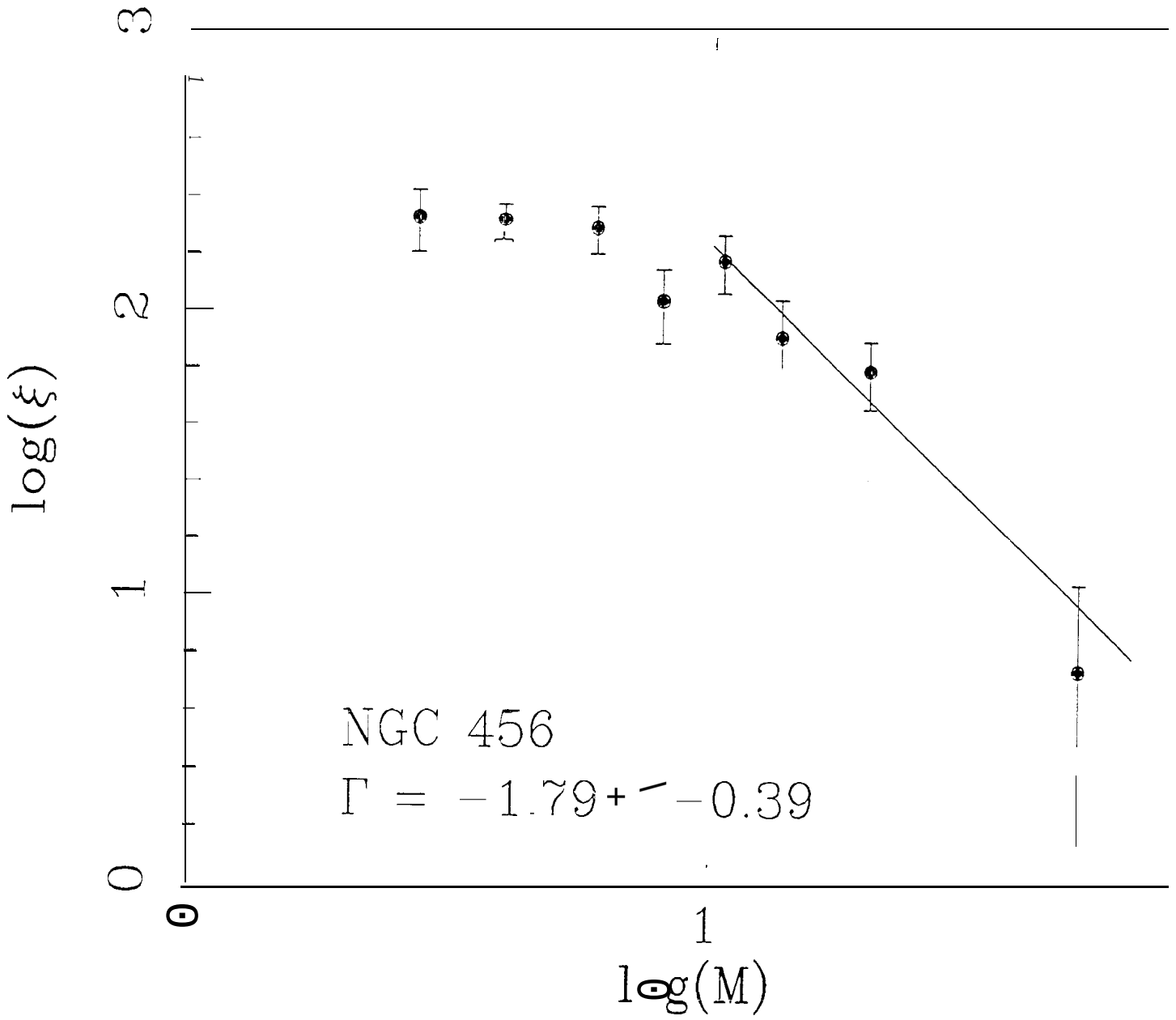

Figure 43

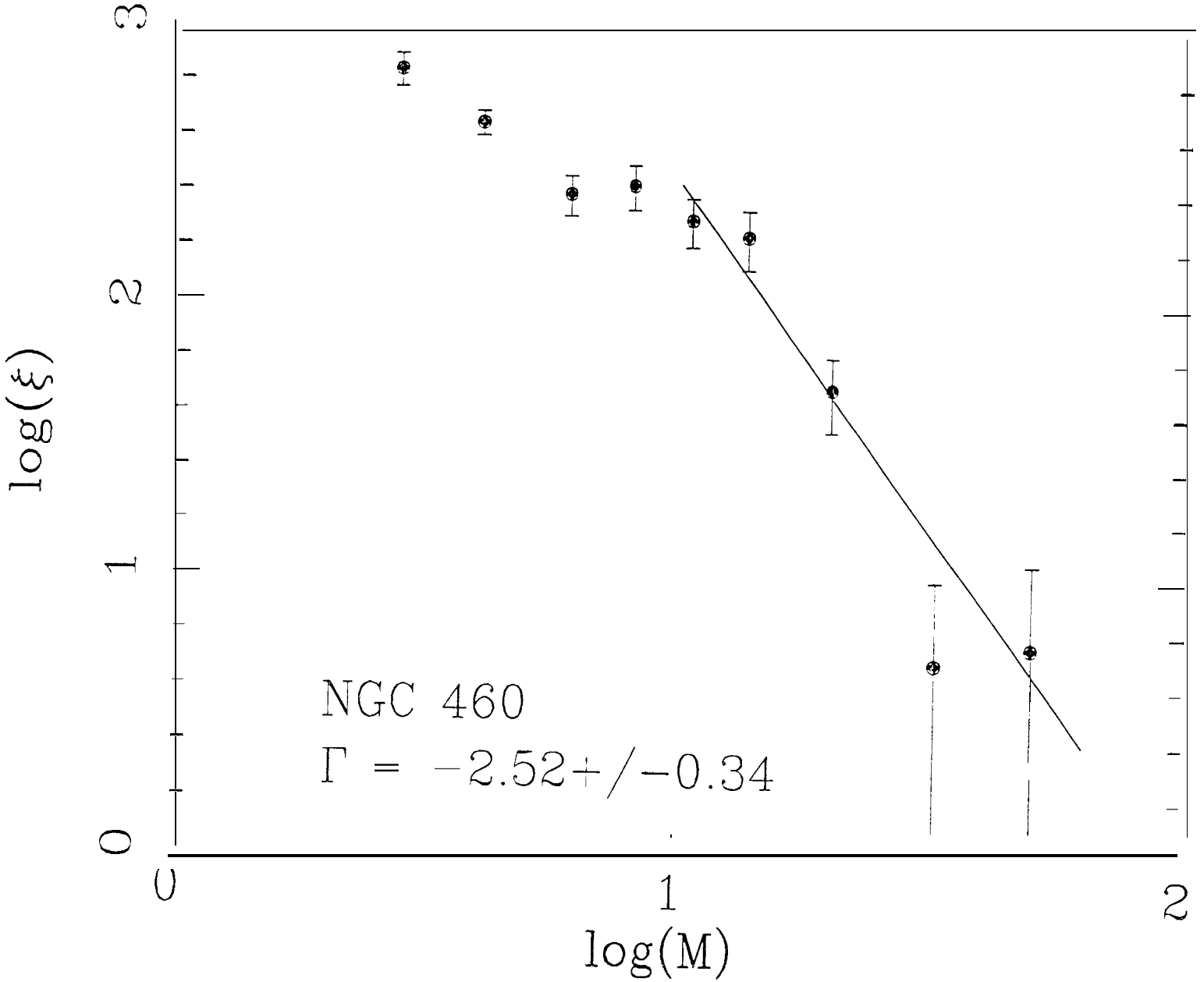

Figure 44